Detection and Quantification of Stenosis in Coronary Artery Disease (CAD) Using Image Processing Technique

A Thesis Presented

by

Gerabirhan Paulos Tumelsan

to

The Faculty of Informatics

of

St. Mary's University

In Partial Fulfillment of the Requirements
for the Degree of Master of Science

in

Computer Science

February 2020

ACCEPTANCE

Detection and Quantification of Stenosis in Coronary Artery Disease (CAD) Using Image Processing Technique

by

Gerabirhan Paulos Tumelsan

Accepted by the Faculty of Informatics, St. Mary's University, in partial fulfillment of the requirements for the degree of Master of Science in Computer Science

Thesis Examination Committee:

_____

Internal Examiner

_____

External Examiner

_____

Dean, Faculty of Informatics

February 07, 2020

DECLARATION

I, the undersigned, declare that this thesis work is my original work, has not been presented for a degree in this or any other universities, and all sources of materials used for the thesis work have been duly acknowledged.

<u>   Gerabirhan Paulos   </u>
Full Name of Student

_____
Signature

Addis Ababa

Ethiopia

This thesis has been submitted for examination with my approval as advisor.

<u>   Million Meshesha (PhD)   </u>
Full Name of Advisor

_____
Signature

Addis Ababa

Ethiopia

February 07, 2020

Abstract

Coronary Artery Disease (CAD) is the most common killer disease worldwide. To diagnosis and follow-up process of CAD is an essential requirement to control and cure the disease. Currently, Doctors perform most of the diagnoses after manual inspection of real-time coronary Computed Tomography Angiography (CTA) frame medical imaging systems. Such images investigation is tedious, time-consuming, and subject to error task for physicians. Computer-assisted CAD detection and quantification improve accuracy, save time, and minimizes human errors. Dealing with this, many pieces of research have proposed different algorithms to solve the problem. However, stenosis detection and quantification in CAD is still regarded as a challenging task. Hence, in this research, a better technique to address stenosis detection and quantification has been proposed.

In the proposed research, for detecting and quantifying stenosis (the narrow blood vessel) from the coronary artery we use CTA images. The image is first pre-processed to remove noise and enhance the contrast of the image. In the pre-processing, four alternative combinations of filtering, enhancement, and binarization have experimented; out of which image enhancement and filtering image preprocessing outperform with quality metrics parameters estimation and classification performance. Next, segmentation is used to obtain the Region of Interests (ROIs). Then, extract features using statistical and CNN based feature extraction, such as pre-trained CNN model *ResNet-50* using the *add-16* features layer, *DenseNet-201* using *fc1000* features layers, and a bag of features. The SVM and CNN classification techniques are used to identify, coronary artery stenosis presence in the CTA images. Finally, if the stenosis is present, then the stenosis quantification process to be used. The stenosis quantification is used to quantify the area of stenosis attributes. The stenosis attribute has a significant need for and importance of when determining the stent attributes to achieve the different requirements of the physiological vessels.

The performance of the proposed methods is compared with the Doctor's opinion that can be considered a subjective score. Experimental results show that 72.7% overall accuracy achieved using an SVM classifier. The accuracy of the proposed stenosis quantification algorithm also tested and achieved 97% of overall accuracy. The mean percentage error to stenosis quantification was 1.32 from the ground truth. The result thus obtained in this study is promising to apply image processing for coronary artery stenosis detection and quantification.

Keywords: *Medical image processing, Coronary Artery Diseases, Coronary Computed Tomography Angiography*

Acknowledgments

Table of Contents

List of Acronyms

AHE	Adaptive Histogram Equalization
CAD	Coronary Artery Disease
CHD	Coronary Heart Disease
CNN	Convolutional Neural Network
CT	Computed Tomography
CTA	Computed Tomography Angiography
CTA	Computed Tomography Angiography
CVD	Cardiovascular Disease
DICOM	Digital Imaging and Communications in Medicine
DIP	Digital Image Processing
IVUS	Intravascular Ultrasound
LOI	Line of Interest
MRI	Magnetic Resonance Imaging
PET	Positron Emission Tomography
ROI	Region of Interest
SPECT	Signal Photon Emission Computed Tomography
SVM	Support Vector Machine
WHO	World Health Organization

List of Figures

List of Tables

List of Algorithms

Chapter One
Introduction

1.1 Background

Globally, Cardiovascular Diseases (CVDs) are a group of disorders of the heart and blood vessels, which includes mainly Coronary Heart Disease (CHD) and strokes. They are the leading cause of death and are a major disease burden [1]. Coronary Artery Disease (CAD) is often used interchangeably with CHD which is generally used to refer to the pathological process affecting the coronary artery (usually, atherosclerosis) [2]. CAD, a disease of the blood vessels supplying the heart muscle, is causing heart attacks [3]. Imaging investigations are a basic step of the CAD diagnosis.

Medical imaging is a mechanism used to create the visual representation of the internal parts of the body [4]; that is, any organs or tissues, mainly for clinical analysis such as to diagnose or to treat disease. For better diagnostic, prognostic, and follow-up processes of heart diseases, the obtained images should be very effective [4].

Medical image acquisitions are the process of capturing an image in the medical field mostly depends on the requirements of the Doctor, type of disease or abnormalities and the area, where the disease or abnormalities is caused [4]. There are varieties of image acquisition devices that are available for capturing images of a particular region either, inside or outside the human body; namely, Magnetic Resonance Imaging (MRI), Computed Tomography (CT), X-Rays, Ultrasound, Positron Emission Tomography (PET), Signal Photon Emission Computed Tomography (SPECT), etc. [4]. Tomographic cardiovascular imaging tests, such as Intravascular Ultrasonography, coronary CTA, and MRI, can be used to assess atherosclerotic plaques for the characterization and early staging of CAD [5] [4]. Coronary CTA is one of the imaging methods and increasingly widespread use for diagnosing CAD [6] [7]. Coronary CTA can access cardiovascular pathology through visualization of gross anatomic abnormalities, characterization of tissue attenuation, and cardiac function analysis. As cardiac structures are in constant motion, special attention to the methodology of image acquisition is essential to capturing high-quality images during the most quiescent (not active or activated) stage of cardiac and coronary artery motion [8].

In the medical field nowadays, medical imaging and processing tools are playing crucial roles in many applications [9]. Medical image processing deals with the development of problem-specific approaches to the enhancement of raw medical image data for the purposes of selective visualization as well as further analysis. There are many topics in medical image processing: some emphasize on generally applicable theory and some focus on specific applications [10].

An image may be defined as a two-dimensional function, $f(x, y)$, where x and y are *spatial* (plane) coordinates, and the value of f at (x, y) is proportional to the brightness of the scene at that point [11]. The digested brightness value is called the gray level. A digital image is composed of a finite number of elements, which has a particular location and value. These elements are called *picture elements, image elements, pixels (pels). A pixel* is a term used most widely to denote the elements of a digital image [11], [12].

Once the image is acquired, which involves various imaging modalities based on the body parts that are under investigation, the next step is improving the image content. In order to enhance the visual interpretation, the various image-processing techniques are used [4]. Image processing is the study of an algorithm that takes an image as an input and in turn returns another image as an output. Image processing techniques help to improve the visual value of the images that are synthesized [13]. Image processing techniques usually process images as 2D signals and apply standard signal processing techniques to them [9]. Digital image processing refers to processing digital images by means of a digital computer [11]. Image processing is not a single-step process. Generally, a number of steps will need to be performed one after the other in order to extract the data of interest from the observed scene and a hierarchy in the processing steps will be evident, such as image pre-processing especially image filtering, image enhancement, and image binarization [14].

The poor quality of the image and the effect of noise are the most common degradations of the medical images when compared to normal images. The image filtering techniques are used to improve its quality and it is used prior to every other stage in medical image analysis. Image feature like edges is sharpened or accentuated during enhancement to make a resultant graphic display more suitable for analysis [4].

Image analyses involve taking measurements of objects within an image, preferably automatically, and assigning them to groups or classes. Image analyses begin with isolating the objects of interest from the rest (known as *segmentation* of the image) [14]. Image segmentation techniques are the most significant stage in medical image analysis, as it is used for extracting the ROI for further analysis [4].

Medical image feature extraction and selection methods are used to increase the diagnostic accuracy and work efficiency of Doctors. Generally, this is categorized based on the level of features used in low-level and high-level features [4].

- The low-level feature, features such as color, size, and texture which can be extracted automatically from an image without any shape information. These are divided into first-order edge detection, second-order edge detection, and localized feature extraction [4].
- High-level feature extraction concerns finding shapes in images. These are mainly divided into thresholding and subtraction; template matching and Hough transform etc. [4].

Image understanding is the information to experience to interpret the picture. Image understands information help to make decisions about what targets are present, their shape, and their positioning. A computer vision goes hand in hand with image understanding. The major task is classifying the object into a group according to its belonging, depending on whether its features fall inside or outside the tolerance of that group, respectively using a *classification* algorithm [14].

There are a number of challenges in image processing. Some of these challenging problems include image enhancement or restoration, image recognition, image classification, and image visualization.

In image *enhancement*, it aims to process images to improve their quality. An image may be of poor quality because its contrast is low, or it is noisy, or it is blurred, etc. Many algorithms have been devised to remove these degradations [15]. The challenging problem is how to remove degradations without hurting the signal [15].

A *recognition* system needs to classify an unknown input pattern into one of a set of pre-specified classes [15].

Image *classification* is a big challenge doing image analysis tasks, especially the selection of methods and techniques in exploiting the result of image processing and pattern recognition, classification methods, subsequently validating the classification result into expert knowledge [16].

Image *visualization* is considered as a part of computer graphics. The main task is to generate images or image sequences based on three-dimensional object and scene models [15].

Hence, in this study, an attempt is made to apply the image processing technique in the medical domain so as to provide its significance in the detection and quantification of stenosis in CAD.

1.2 Statement of the Problem

Cardiovascular diseases (CVDs) are the number one cause of death globally. In 2016, the World Health Organization (WHO) estimated that 17.9 million people lose life due to CVDs, which accounts for 31% of all global deaths. Of these deaths, 85% are due to a heart attack and stroke [17]. CAD is one of the leading causes of morbidity and mortality in most developed countries and its prevalence is increasing in developing countries [18]. Coronary heart disease is the commonest cardiovascular disease in Ethiopian patients; the artery heart disease has dramatically increased over the years [19]. WHO in 2017 reported that CAD deaths in Ethiopia reached 46,943 or 7.38% of total deaths [20]. In order to decrease mortality from CAD, accurate CAD diagnosis is very important.

The diagnosis of CAD is a relatively complicated procedure. Many tests are available for this purpose (e.g., exercise testing, echocardiography, and MRI) [21]. The choice of these tests and how many to perform depends on the patient's risk factors, history of heart problems, and current symptoms. Usually, the tests begin with the simplest and may progress to ones that are more complicated. Medical imaging is to acquire useful information about the organs of the body as well as the ongoing physiological and pathological processes by using an external or internal source of energy [22]. Manual analysis and estimation are usually subjective, inconsistent and prone to error. Image investigations are a basic step of the diagnostic, predict

4

and follow-up processes of CAD, which images are used to determine the compressibility along the entire course of the veins (blood vessel). Plaque imaging diagnostic gives the images of contrasted-filled veins, which can be used for estimating the stenosis caused by plaques. In a vessel with stenosis involvement, the challenge to the clinician is to define and properly specify the degree of vessel reduction. On the other hand, with the extraordinary contrast resolution of images, physicians can closely investigate the composition of plaques and perform quantitative measurements on them [22]–[25].

Cardiac imaging is an invaluable tool for the diagnosis and treatment of CAD. Coronary CTA has been used extensively for physiologic understanding and diagnostic purposes in cardiology [26]. Moreover, coronary CTA allows the detection of the coronary tree and quantification of coronary artery stenosis. These imaging technologies have greatly increased the understanding of normal and diseased anatomy [26]. Virtually all previously performed studies on the diagnostic accuracy of coronary CTA have shown a high sensitivity and high negative predictive value indicating CAD [27].

To achieve high accuracy and efficiency in evaluating the CAD, proper visualization techniques are needed. The accuracy of the final diagnosis ultimately depends on the skills and experience of the technician and the time spent studying each coronary CTA frame. The implementation of coronary artery stenosis detection and quantification using image processing techniques is important and useful in computer-aided diagnosis, treatment planning, reduces the time the physicians spent on the diagnostic settings, and in the area of preparation carrying out an evaluation before surgical operations.

The main concern in CAD is about the detection and measurements of vessel attribute that can be somehow obtained from the images and used as a basis for the diagnosis of CAD [28]. Stenosis attributes such as length, stenosis percentage are used for determining the stent attributes to achieve the different requirements of the physiological vessels. According to Zheng *et al.* [29], stents are common implantable devices that can be placed in the critical stenotic narrowing or radiation-induced arterial structure of physiology vessels to support the walls and assure the potency (openness) of a contracted artery.

In order to diagnose CAD, there should be a fast and effective CAD detection and quantification method, especially in developing countries where there is a shortage of

specialists and wrongly diagnosed cases are high. Image processing can be a convenient technique to assist physicians in detecting and quantifying the CAD by obtaining the ROI and extract information of interest from the patient's coronary CTA images.

So far, in order to improve diagnosis accuracy, different CAD diagnostic researchers realized the advent of detecting and quantifying CAD using image processing. Some research works [3], [30]–[32] have been devised to accept as a challenge this problem and a promising result were found though challenged back by the following key tasks.

- The difficulty of visualization of the coronary arteries, the contrast agent in surrounding structure structures, such as the pulmonary vessels, the bone, and the left ventricle. Thus, in the noisy structure abatement, resulting in coronary CTA machine.
- Highly challenging when developing accurate vessel segmentation algorithms because coronary arteries are vessel structures surrounding by blood-filled objects, such as the aorta and the heart chambers, which share the same intensity regions with the coronary arteries.
- Accurate detection and quantification of stenosis under coronary CTA images of CAD pose significant challenges.

Due to the above limitations, this study aims to experiment with image-based stenosis detection and quantification techniques that allow advancement in computer-assisted diagnostics, treatment, and follow-up of CAD. The outcome of the proposed study is believed to improve the detection and quantification of stenosis through image analysis.

Towards solving this problem, this study attempts to answer the following basic research questions:

- What are the suitable image pre-processing techniques for coronary CTA image filtering to remove noise and enhance the image quality?
- Which classification algorithm is suitable for coronary artery stenosis detection in the CAD from the coronary CTA image?
- To what extent the proposed approach performs in detecting and quantifying stenosis in the CAD?

1.3 Objectives of the Study

1.3.1 General Objective

The general objective of this study is to develop coronary artery stenosis detection and quantification system using image processing techniques in the general process of care, by means of assisting radiologists and cardiologists in their coronary CTA image analyses.

1.3.2 Specific Objectives

In order to achieve the above general objective, the following specific objectives are dealt with.

- To review the previous related works on CAD detection and quantification so as to understand the domain area and identify different detection and quantification methods.
- To study symptoms, perform a clinical validation, robustness, and speed of the developed methods in coronary stenosis detection of CAD events, to ensure that can be used in clinical practice.
- To collect and enhance the quality of a computing tomography angiography image by reducing errors using image pre-processing algorithms.
- To select suitable image segmentation, feature extraction and classification algorithms that result in a better CAD detection and quantification.
- To develop a prototype for the proposed approach in the detection and quantification of stenosis using the MATLAB environment.
- To evaluate the performance of the model in terms of coronary artery disease detection and quantification using sample data.

1.4 Scope and Limitation of the Study

This study focuses on developing a model for CAD coronary CTA image-based detection as a normal and stenosis present coronary artery stenosis and quantifies coronary artery stenosis attributes using image analysis techniques.

The proposed work is explored on the available local dataset (246 coronary CTA images) which are collected from MCM General Hospital, Gesund Cardiac and Medical Center, and

St. Peter Specialized Hospital, which was a limited dataset. Therefore, to generalize the results for larger groups, the study should have involved more datasets.

1.5 Contributions of the Study

It is intended that the findings of this study will set a state of the art through an extensive review of coronary artery image processing, artery morphology, artery imaging CTA modalities, techniques for coronary artery disease detection and quantification from these images. The outcome of the research brings a good opportunity in simplifying the challenge behind CAD diagnosis. It saves both the time and efforts of patients and physicians by fasting diagnosis, reduces medical errors, enhances diagnostic accuracy, and reduces the mortality rate from heart disease. In addition, the contribution of this study will provide valuable information for physicians when computer-assisted surgery planning and navigation, both avoid damaging vital structures and use an artery as an anatomical location. Furthermore, the result of this study will come up with better solutions to the problems facing heart disease diagnosis using coronary CTA images.

1.6 Research Methodology

The methodology applied by the study has been chosen in order to detect and quantify stenosis in CAD.

In order to summarize the current state of knowledge in the area to serve as a background for the study, a literature review was conducted from various books, journals, conference preceding, research papers, and the internet.

1.6.1 Research Design

This study follows the experimental research method for the detection and quantification of coronary artery stenosis by developing and investigating the utility of the proposed solution artifacts. The experimental research method is a systematic and scientific approach to research in which the researcher manipulates one or more variables, and controls and measures any change in other variables [33]. It is the collection of research design, which uses manipulation and controlled testing to understand causal processes [34].

Experimental research methods mean that an experiment in order to extract results from real-world implementations [35]. Experimental methods comprise the set of skills and techniques

for minimizing error in acquiring and communicating measurement and is a way of gaining knowledge by means of direct and indirect observation or experience [36].

1.6.2 Dataset Preparation

The process of capturing an image in the medical field mostly depends on the requirements of the Doctor, type of disease or abnormalities and the area, where the disease or abnormalities is caused [4]. Using CTA can visualization of all coronary artery branches with high sensitivity and specificity achieved. Coronary CTA is applied to diagnose the degree of coronary stenosis and assess the myocardium, detect and quantify the coronary artery calcifications, and also is used to image the coronary vasculature [18]. For this study, the sample data of 57 patients suspected of CAD who underwent coronary CTA, we have collected 246 images. These images are collected from the MCM General Hospital, Gesund Cardiac and Medical Center, and St. Peter Specialized Hospital, which are found in Addis Ababa, Ethiopia. For each patient, different images were considered, thus, contains digitized images from scanned coronary CTA films. For each patient 4 to 6 different projection images were considered. These images include those with a high degree of stenosis, low degree of stenosis and also images without stenosis. All the sampled data were up-to-date and they are taken in the year of 2017, 2018, and 2019 GC.

These coronary CTA films undergoing the data-preprocessing task to take the images from Digital Imaging and Communications in Medicine (DICOM). The DICOM images ware converted by saved as to have 96×96 resolution in "jpg" format using Philips DICOM viewer. Then, physician reading and labels each image as stenosis present and normal and quantify the stenosis attributes took 10 sample images randomly from a few patients.

1.6.3 Implementation Tools

To undertake the experiment of the proposed method tools and application development environments are required for image processing, analysis, and classification. Hence, MATLAB R2019a was used to implement the prototype of the system. MATLAB is a handy language for technical computing as well as data visualization which is designed for finding solutions to scientific as well as mathematical problems developed by Math Works [37]. For the data preprocessing purpose of incoherent frame (image) subtraction, Philips DICOM Viewer version 3.0 file descriptor is used.

1.6.4 Experimental Evaluations

The proposed work was evaluated by comparing the output against the manually observed phenomena using a confusion matrix and also by conducting a comparison with other algorithms that are frequently used by previous works. The confusion matrix is a 2 by 2 table with 4 outcomes, which is true positive (TP), true negative (TN), false positive (FP), and false-negative (FN) These outcome measures are used to describe the performance of a classification model on a set of data.

1.7 Organization of the Rest of the Thesis

The remaining of this thesis report organized as follows. The second Chapter presents a brief review of coronary artery disease and CAD detection and quantification using digital image processing. Basic theory and concepts of medical image analysis are also present. Finally, the chapter reviews related research works. Following the literature review chapter, the proposed algorithm is presented in Chapter three so that discussing research methods and techniques of stenosis detection and quantification based on coronary CTA image.

In Chapter four, the proposed algorithm is investigated extensively with the help of experiments, which test the robustness and performance of the algorithm to different conditions. Finally, in Chapter five we present our conclusions based on the experimental results and suggest the way forward.

Chapter Two
Literature Review

2.1 Overview

In this chapter, we present the research background information based on the context of the study. The chapter begins with a brief introduction to CAD and diagnosed with this the coronary CTA image-based CAD diagnosis is discussed. Then the overview of approaches to CAD detection and quantification is also presented. Finally, related works, that contributed towards the detection and quantification of CAD from the images of coronary CTA films and intravascular ultrasound (IVUS), both are broadly accepted diagnostic modality in CAD imaging are presented.

This chapter is organized into five main sections: Overview of Coronary Artery Disease, CAD diagnosis, CAD detection and quantification using digital image processing, medical imaging analysis, and related works.

2.2 Coronary Artery Disease

Coronary artery disease (CAD) is mainly caused by a blockage that prevents blood from flowing to the heart. Coronary arteries supply oxygen-rich blood to the heart [3]. CAD occurs when the coronary arteries supplying oxygen-rich blood to the myocardium (heart muscle) become narrow, which is usually happens due to the deposits of fatty material within their inner walls of the blood vessels that supply the heart. The narrowing of the arteries is known as stenosis [3]. The fatty material is known as atherosclerotic plaque. Plaques are made up of fat, cholesterol, and calcium found in the blood. This plaque (fatty material) prevents the supply of blood of the heart and thereby making blood clots. In turn, the blood clots completely block the blood flow to the heart, causing a heart attack. The cause of CAD is usually the presence of a combination of risk factors, such as tobacco use, unhealthy diet and obesity, physical inactivity and harmful use of alcohol, hypertension, diabetes, and hyperlipidemia [3] [13] [18] [30].

In the normal heart, the oxygen requirement of the myocardium is continuously matched by the coronary arterial supply. The myocardial ischemia in CAD results from fixed atherosclerotic plaques that narrow the vessel's lumen and limit myocardial blood supply.

However, the combination of fixed vessel narrowing and abnormal vascular tone contributed to by atherosclerosis-induced endothelial cell dysfunction. The hemodynamic significance of fixed atherosclerotic coronary artery stenosis relates to both fluid mechanics and the anatomy of the vascular supply [39].

2.2.1 Clinical Anatomy of Coronary

Knowledge of normal structure and function of the heart is crucial to understanding disease that affects the coronary artery. Figure 2.1 shows that there are right and left coronary arteries. The American heart association divides the coronary tree into 16 segments.

The right coronary artery (RCA) takes origin from the right aortic sinus of Valsalva and then divides to form two terminal branches, the posterior descending artery (PDA) and the posterolateral (PLV) branches: the sinus node artery, right ventricular (RV) branches, acute marginal (AM) branch, and the atrioventricular node artery [23].
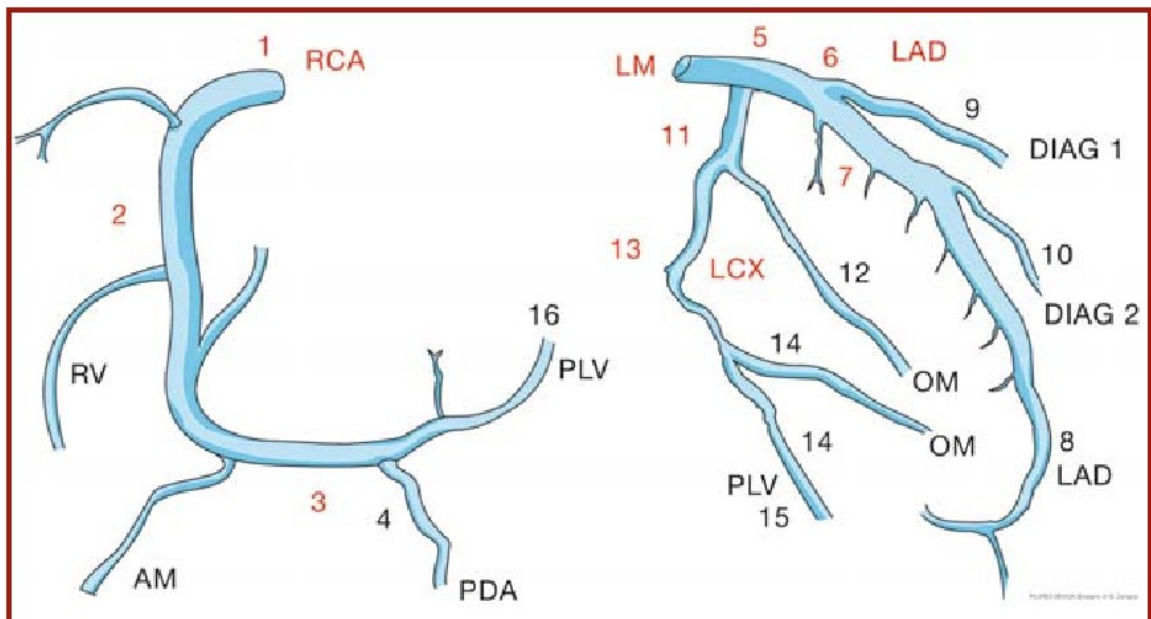
Figure 2.1: Division of right and left coronary arteries into segments [23].

The left coronary artery (LCA) arises from the left aortic sinus of Valsalva; the left main (LM) branch of the LCA ends in a bifurcation, giving rise to the left anterior descending artery (LAD) and left circumflex artery (LCX). The LDA gives off septal (SP) and diagonal (DIAG) branches and ends at the apex of the heart, sometimes reaching the posterior interventricular groove. The LCX has two or three obtuse marginal branches (OM), before either terminating

or, in the case of left-dominant or balanced circulation, giving off a posterolateral branch or ending in the posterior atrioventricular groove [23].

2.3 Coronary Artery Disease (CAD) Diagnosis

Despite continuing technological advances in cardiovascular medicine, the history and physical examination remain vital to establish an accurate diagnosis of chronic CAD. Whereas many patients may describe typical angina, providers cannot rely on these symptoms alone to diagnose ischemia because silent (asymptomatic) ischemia remains a common presentation, estimated to affect almost half of the patients with CAD. Conversely, some patients may endorse symptoms that closely mimic typical angina in the absence of significant CAD [2].

There are many medical imaging modalities such as CT (Computer Tomography), MRI (Magnetic Resonance Imaging), Ultrasound, and X-Ray that are in use today to acquire anatomical, physiological, metabolic, and functional information from the human body [22]. Using a computer, multi-dimensional digital images of anatomical structures can be processed and manipulated to visualize the diagnostic features that are difficult or impossible to see with planar imaging methods. In many critical radiological applications, multi-dimensional visualization and quantitative analysis of physiological structures provide clinical information that is extremely valuable in diagnosis and treatment [22].

Despite progressive improvements in noninvasive techniques, cardiac catheterization remains a key clinical tool for assessing the anatomy and physiology of the heart and its associated vasculature. The findings of diagnostic cardiac catheterization characterize the extent and severity of cardiac disease and thereby it can help to determine the most appropriate plan for medical, surgical, or catheter-based treatment. Although the majority of patients with CAD or valvular disease can be managed medically using clinical and noninvasive data (e.g., exercise testing, echocardiography, and MRI) [21].

In order for the diagnosis of CAD, there is a clinical need for tools to enable early and accurate diagnosis of CAD. Coronary CTA image is most frequently used to visualize the coronary artery and provides a comprehensive anatomic evaluation of the heart. The next sections describe the basic concept of coronary CTA modalities such as coronary artery imaging, diagnosis, and coronary artery stent evaluation.

2.3.1 Coronary CTA

Coronary Computed Tomography Angiography (CTA) has become a broadly accepted diagnostic modality in CAD imaging [18]. By inserting a small catheter (iodine-containing contrast material) into the femoral (or radial) artery, a radiocontrast medium is injected into the coronary arteries. The coronary angiographic system produces high-resolution X-ray images from several angles aim to examine most of the arteries that supply blood to the heart [40] [41]. In addition, CTA can assess cardiovascular pathology through visualization of gross anatomic abnormalities, characterization of tissue attenuation, and cardiac function analysis [8].

As cardiac structures are in constant motion, special attention to the methodology of image acquisition is essential to capturing high-quality images during the most quiescent stage of cardiac and coronary artery motion [8]. CTA of the coronary arteries is very fast and the most advanced imaging technique currently available for clinical use. Based on a multi-slice imaging approach together with specialized and dedicated software, CTA "freezes" cardiac movement, thereby acquiring static images of the rapidly moving heart. In addition, the same approach produces contrast-enhanced images of the coronary arteries, by employing a three-dimensional technique with high spatial and temporal resolution [23]. Coronary CTA can demonstrate accurately for the evaluation of coronary stenosis. CTA has made many significant advancements in simplifying patient workflow, acquisition, post-processing, interpretation of images, and an accurate prediction of major adverse cardiac events.

2.3.2 CTA Based CAD Diagnosis

Briefly, coronary CTA begins with the appropriate patient selection with regard to the symptoms in combination with the clinical history and cardiovascular risk profile [27]. Once an atherosclerotic plaque has been identified and properly characterized by means of coronary CTA, the next step is defining the extent of atherosclerotic involvement, i.e., significant reduction of the lumen by stenosis or complete occlusion of the vessel. A reduction in the caliber of the vessel lumen is associated with a reduction in blood flow and may have significant hemodynamic consequences; thus, an exact definition of the extent of lumen reduction by means of coronary CTA is very important from a clinical point of view. In most cases, this diagnostic procedure is not employed in highly symptomatic patients (in patients with strong clinical suspicion of coronary disease, catheter angiography is directly

performed); then, depending on the results of the clinical examination, a decision is made as to whether a more invasive approach (catheter angiography) is required. This decision depends at least in part on the significance of the vessel stenosis. In this latter group, catheter coronary angiography may confirm the significance of the disease and define the therapeutic approach [23].

The direct evidence of arterial stenosis provided by coronary CTA yields additional information. As noted by Dowe et al. [23], for example, stenosis greater than 70% causes a significant hemodynamic reduction of vascular flow. In clinical practice, the stenosis is considered significant when the vessel caliber is reduced by more than 50%. Thus, the goal is to interpret coronary CTA images such that the level of stenotic vascular involvement is precisely determined. If the non-significance of the lumen reduction is established, no further procedure is necessary, as coronary CTA is by itself diagnostic, allowing identification and characterization of the plaque as well as the definition of the extent of lumen reduction [23].

Atherosclerotic plaques happen because of the fact that significant stenosis may be eccentric, marginally located, or concentric. Coronary CTA images are able to define the influence of the plaque on lumen caliber and identify patients with significant stenotic involvement [23].

2.3.3 Cardiac CTA in the Evaluation of Stents

The general agreement on the accuracy of coronary stent evaluation with the CTA has high sensitivity and specificity for greater than 50% stenosis in stents with a diameter of 3 mm or larger [42]. Essentially, deployment of a stent consists of a collapsed wire mesh that is expanded following ballooning of lesion (stenosis). CTA and evaluation of the stent consist of determining whether the stent was completely deployed across a plaque or there is a stenosis in the lumen of the stent. The lumen and density in the stent should be similar to that of the adjacent artery [42].

2.4 Medical Image Processing

Interest in digital image processing methods stems from two principal application areas: improvement of pictorial information from human interpretation; and processing of image data for storage, transmission, and representation of autonomous machine perception [11]. According to Petrou *et al.* [12], digital image processing has been developed in response to three major problems concerned with pictures:

- Picture digitization and coding to facilitate its transmission, printing and storing;
- Picture enhancement and restoration in order, for example, to interpret more easily pictures of the surface of other planets taken by various probes;
- Picture segmentation and description as an early stage of Machine Vision.

Hence, the field of digital image processing refers to preprocessing, analysis, and understanding of digital images by means of a digital computer [11].

| Medical Image Acquisition | → | Image Preprocessing | → | Image Segmentation | → | Feature Extraction | → | Image Classification |
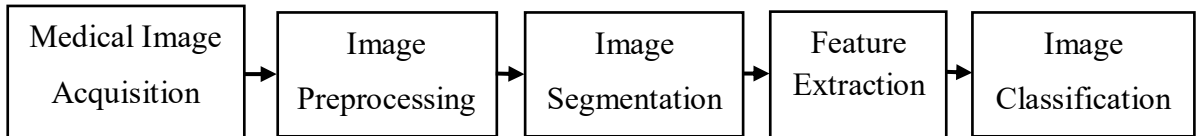
Figure 2.2: DIP processing techniques in medical image analysis [4].

As shown in Figure 2.2, the CAD detection model using image processing includes five main phases. In order to enhance the visual interpretation, the various image processing techniques are used in the hierarchy, for example, image enhancement precedes segmentation, which will precede feature extraction and selection. Finally, the analysis of medical images is performed in order to determine the abnormalities present [4].

2.4.1 Medical Digital Image Acquisition

The medical image acquisition system usually converts a biomedical signal or radiation carrying the information of interest to a digital image. A digital image is represented by an array of digital numbers that can be read by the processing computer and displayed as a two-, three-, or multi-dimensional image. Medical image modalities use different image acquisition systems such as X-Ray Radiographs, MRI, and X-Ray Computed Tomography as a part of the imaging instrumentation. The design of the image acquisition system depends on the type of modality and detector requirements [43].

Coronary CTA Imaging Protocols

The image produced from coronary CTA is consisting of 300-500 slices of the image with 512*512 DPI [24]. Data interpretation is based on interactive manipulation of these datasets using an image processing workstation, enhanced by post-processing tools such as maximum intensity projections and multi-planar reconstructions. Three-dimensional renderings, although impressive for visualization of the heart and coronary arteries, are not accurate for stenosis detection and play no role in data interpretation [2][24][41]. In order to achieve high

accuracy and efficiency in evaluating the coronary artery system from such volume data, proper image processing, and visualization techniques are required.

2.4.2 Image Pre-processing

Different medical imaging modalities provide specific information about internal organs or biological tissues. Medical images are affected by noise, blurriness and may suffer due to poor contrast and sharpness that may result in false diagnosis. Thus, the purpose of image filtering methods is to process an acquired image for better contrast and visibility of the feature of interest for visual examination as well as subsequent computer-aided analysis and diagnosis. Image enhancement and restoration is the crucial task of medical image processing. The process of image filtering does not raise the inbuilt information content of the data but can highlight the feature of interest to detect the objects in a simple and efficient manner [43] [44].

Image Filtering

Noise reduction in image processing is done, not only for producing results for human viewing but also to facilitate easier extraction of meaningful information in subsequent steps, such as in segmentation, and feature extraction. Gaussian filter, median filter, and mean filter are effectively performing low-pass filtering and thus remove high-frequency noise. Edge-preserving and smoothing filters in the sense that they change their smoothing behavior adaptively depending upon the local image structure [45].

Edge preserving filters can be classified into three types that are largely based on different strategies. The *Kuwahara* filters partition the filter kernel into smaller sub-kernels and the filter's result. In contrast, the *Bilateral* filter uses the differences between pixel values to the local average. Finally, the *anisotropic diffusion* filters interactively smooth the image similar to the process of thermal diffusion, using the gradient to block the local diffusion at edges and similar structures [45].

Kuwahara Filters

The *Kuwahara-type* filters partition the kernel into smaller sub-kernels and select the most "homogeneous" of the underlying image regions for calculating the filter's result [45]. Algorithm 2.1 presents how the Kuwahara filter works.

```
Kuwahara Filter (I, r)
        Input: I, a grayscale image of size M × N; r, filter radius (r ≥ 1).
        Returns a new (filtered) image of size M × N.
        R̄ ← [−r, r]                        ▷ comp. filter region of size (2r + 1) + (2r + 1)
        for k = 1 to K do                           ▷ define K sub-regions R₁, … , R_K
                R_K ← {p_{K,1}, … , p_{k,n_K}}, with P_{k,j} ∈ R̄
        (M, N) ← Size (I)
        I' ← Duplicate (I)
        for all image coordinates (u, v) ∈ M × N do
                σ²_min ← ∞, μ_min ← 0
                for k = 1 to K do
                        (σ², μ) ← EvalSubregion (I, R_K, u, v)
                        if σ² < σ²_min then
                                σ²_min ← σ²
                                μ_min ← μ
                I' (u, v) ← μ_min
        return I'.
```

Algorithm 2.1: The Kuwahara filter for arbitrary filter size and sub-region structure [45].

Bilateral Filter

In contrast with the Kuwahara filter, the *Bilateral* filter uses the differences between pixel *values* to control how much each individual pixel in the filter region contributes to the local average. Pixels that are similar to the current center pixel contribute strongly, while highly different pixels add little to the result. Thus, in a sense, the Bilateral filter is a non-homogeneous linear filter with a convolution kernel that is adaptively controlled by the local image content [45].

Anisotropic Diffusion Filters

The anisotropic diffusion filters iteratively smooth the image similar to the process of thermal diffusion, using the image gradient to block the local diffusion at edges and similar structures [45]. Algorithm 2.3 below shows details of anisotropic diffusion filters for grayscale images.

```
Perona-Malik Gray (I, α, k, T)
        Input: I, a grayscale image of size M × N; a, update rate; k, smoothness
parameter; T, number of iterations.
        Returns the modified image I.
        Specify the conductivity function:
        g(d) ≔ e^{-(d/k)^2}
        (M, N) ← Size(I)
        Create maps D_x, D_y: M × N → ℝ
        for n ← 1, …, T do                          ▷ perform T iterations
           for all coordinates (u, v) ∈ M × N do    ▷ re-calculate gradients
             D_x(u, v) ← {I(u+1,v)-I(u,v) if u<M-1
                         {0 otherwise
             D_y(u, v) ← {I(u,v+1)-I(u,v) if u<N-1
                         {0 otherwise
           for all coordinates (u, v) ∈ M × N do    ▷ update the image
             δ_0 ← D_x(u, v)
             δ_1 ← D_x(u, v)
             δ_2 ← {-D_x(u-1,v)   if u>0
                   {0            otherwise
             δ_3 ← {-D_y(u,v-1)   if v>0
                   {0            otherwise
             I(u, v) ← I(u, v) + a · Σ_{k=0}^{3} g(|δ_k|) · δ_k
        return I.
```

$$g(d) \coloneqq e^{-(d/k)^2}$$

$$(M, N) \leftarrow Size(I)$$

$$D_x(u,v) \leftarrow \begin{cases} I(u+1,v)-I(u,v) & \text{if } u<M-1 \\ 0 & \text{otherwise} \end{cases}$$

$$D_y(u,v) \leftarrow \begin{cases} I(u,v+1)-I(u,v) & \text{if } u<N-1 \\ 0 & \text{otherwise} \end{cases}$$

$$\delta_2 \leftarrow \begin{cases} -D_x(u-1,v) & \text{if } u>0 \\ 0 & \text{otherwise} \end{cases}$$

$$\delta_3 \leftarrow \begin{cases} -D_y(u,v-1) & \text{if } v>0 \\ 0 & \text{otherwise} \end{cases}$$

$$I(u,v) \leftarrow I(u,v) + a \cdot \sum_{k=0}^{3} g(|\delta_k|) \cdot \delta_k$$

Algorithm 2.2: Perona-Malik anisotropic diffusion filter for scalar images [45].

Image Enhancement

Image enhancement is a crucial task of medical image pre-processing. It is used in improving the visual quality of images. Image enhancement is the process by which we improve an image so that it looks subjectively better. We do not really know what the image should look like, but we can tell whether it has been improved or not, by considering, for example, whether more detail can be seen, or whether unwanted flickering has been removed, or the contrast is better [12]. Image enhancement techniques can be divided into two broad categories spatial domain enhancement method and frequency domain enhancement method [44].

- **Spatial Domain Enhancement Method**

Spatial domain techniques are used to denote techniques that perform manipulation operation of pixels in an image. It includes point arithmetic operations and neighborhood enhancement algorithms [12] [45]. Point arithmetic operations include gray-level transformation and histogram equalization. Gray-level transform includes linear, logarithmic and power-law transformation [44]. The linear transformation may result in the identity or negative

transformation of an image. Logarithmic transformation may expand the darker pixels of an image and higher values are compressed with yields an enhanced image. Power law transformation may include the nth root or n^{th} power transformation. The degree of enhancement may be adjusted depending on the value of n [44].

Histograms are the basis for numerous spatial domain processing techniques. Histogram manipulation can be used for image enhancement [11]. Histogram equalization may ensure the uniform distribution of gray levels [44].

- **Frequency Domain Enhancement Method**

This method considers the frequency components of the Fourier transform and spatial features of an image [11]. For instance, since the frequency is directly related to spatial rates of change, it is not difficult intuitively to associate frequencies in the Fourier transform with patterns of intensity variations in an image [11].

Image Binarization

Based on binary image regions that have been used for a very long time, they still play a major role in many practical image-processing applications because of their simplicity and efficiency. To obtain a binary image, the first and perhaps most critical step is to convert the initial color image to a grayscale image and then to a binary image, in most cases by performing thresholding operation [45].

Thresholding is used in image processing to separate an object's pixels from the background pixels [46].

2.4.3 Image Segmentation

Image segmentation refers to the process of partitioning an image into its constituent regions or objects by grouping together neighborhood pixels based on a predefined similarity creation [47]. The level of detail to which the partition is carried depends on the problem being solved. It is important to analyze the image for the extraction of features of interest involving edges, regions, texture, etc. for further analysis. Thus, image segmentation can also be considered as a pixel classification technique that allows an edge or region-based representation towards the formation of regions of similarities in the image. Edge detectors are local image processing methods designed to detect edge pixels. A line may be viewed as an edge segment in which

the intensity of the background on either side of the line is either much higher or much lower than the intensity of the line pixels [47] [11].

Medical image segmentation is about partitioning a medical image into multiple segments or regions correspond to the different organs, tissue classes, pathologies or the other biological structures, each segmentation or region composed of a set of pixels or voxels. Thus, its concern is finding the exact boundary of the object in a medical image. The region criterion can be determined using specific properties or features of pixels representing objects in the image. Often, segments correspond to semantically meaningful anatomical objects [43] [48].

Image segmentation methods can be broadly classified into three categories including edge-based methods, pixel-based methods, and region-based methods [36] [39].

Edge-based Methods

In Edge-based Methods, the edge information is used to determine the boundaries of objects. The boundaries are then analyzed and modified as needed to form closed regions belonging to the objects in the image [43]. Edge-based segmentation relies on edges found in an image by edge detecting operators, these edges mark image locations of discontinuities in grey level, color, context, etc. [49]. Edge-based approaches use special filtering methods to compute the first-order or second-order gradient information of the image [47]. Algorithm 2.4 shows edge-based image segmentation for edge detection.

---

1. *Evaluate a confidence $c^{(1)}(e)$ for all crack edge e in the image.*
2. *Find the edge type of each edge based on edge confidences in its neighborhood.*
3. *Update the confidence $c^{(k+1)}(e)$ of each edge e according to its type and its previous confidence $c^{(k)}(e)$.*
4. *Repeat steps (2) and (3) until all edge confidences have converged either to 0 or 1.*

Algorithm 2.3: Edge-based Segmentation Method (Edge relaxation) [49].

Pixel-based Methods

Pixel-based Methods in which heuristics or estimation methods derived from the histogram statistics of the image are used to form closed regions belonging to the objects in the image [43]. The pixel-based direct classification methods use histogram statistics to define single or multiple thresholds to classify an image pixel-by-pixel. The threshold for classifying pixels into classes is obtained from the analysis of the histogram of the image [47].

Thresholding at the median segment the image into the approximately equalized background and foreground sets, i.e., $|C_0| \approx |C_1|$, which assumes that the "interesting" (foreground) pixels cover about half of the image. If the approximate fraction b $(0 < b < 1)$ of expected background pixels is known in advance, the threshold could be set to that *quantile* instead. In this case, q is simply chosen using equation 2.1 [45]:

$$q = \underset{j}{argmin} \sum_{i=0}^{j} h(i) \geq N \cdot b, \qquad (2.1)$$

Where N is the total number of pixels. The optimal threshold value $q \in [0, K-2]$ is returned, or one if no valid threshold was found is summarized in Algorithm 2.5 below.

Quantile Threshold (h, b)
> *Input: h: $[0, k-1] \to \mathbb{N}$, a grayscale histogram.*
>   *b, the proportion of expected background pixels (0<b<1).*
> *Output: Returns the optimal threshold value or -1 if no threshold is found.*
> *$K \leftarrow Size(h)$*   ▷ *number of intensity levels*
> *$N \leftarrow \sum_{i=0}^{k-1} h(i)$*   ▷ *number of image pixels*
> *$j \leftarrow 0$*
> *$c \leftarrow h(0)$*
> ***while** $(j < K)\,(c < N \cdot b)$ **do***   ▷ *quantile calculation (equation (2.1))*
>   *$j \leftarrow j + 1$*
>   *$c \leftarrow c + h(j)$*
> ***if** $c < N$ **then***   ▷ *foreground is non-empty*
>   *$q \leftarrow j$*
> ***else***   ▷ *foreground is empty, all pixels are background*
>   *$q \leftarrow -1$*
> ***return** q.*

Algorithm 2.4: Quantile thresholding [45].

Region-based Methods

Region-based Methods in which pixels are analyzed directly for a region expansion process based on a predefined similarity criterion to form closed regions belonging to the objects in the image [43]. Region-growing based segmentation algorithms examine pixels in the neighborhood based on a predefined similarity criterion and then assign pixels into groups to form regions. The neighborhood pixels with similar properties are merged to form closed regions for segmentation. The Region growing approach can be extended to merging regions instead of merging pixels to form larger meaningful regions of similar properties. Such a region merging approach is quite effective when the original image is segmented into a large

number of regions in the preprocessing phase. Once the regions are defined, statistical and other features can be computed to represent regions for characterization, analysis, and classification [47]. Region growing assumes that the neighboring pixels (voxels) within one region share similar values. Starting from a set of seed pixels, the regions are iteratively grown, merging new unallocated neighboring pixels into the region if the unallocated pixel is close enough to those in the region [48].

The segmentation resulting from edge-based methods and region growing methods are not usually exactly the same. Region growing technique is generally better in noisy images where edges are extremely difficult to detect [49].

The most natural method of region growing is to begin the growth in raw image data, each pixel representing a single region. These regions almost certainly do not satisfy the condition of equation 2.3, and so regions will be merged as long as equation 2.2 remains satisfied. An algorithm is a general approach to region merging segmentation [49]. Algorithm 2.5 shows the region merging procedure.

$$H(R_i) = TRUE \qquad i = 1,2,\dots,S \tag{2.2}$$

$$H(R_i \cup R_j) = FALSE \quad i \neq j, \; R_i \; adjacent \; to \; R_j \tag{2.3}$$

Where S is the total number of regions in an image and $H(R_i)$ is a binary homogeneity evaluation of the region R_i. Resulting regions of the segmented image must be both homogeneous and maximal whereby 'maximal' we mean that the homogeneity criterion would not be true after merging a region with any adjacent region.

β: the set of points belonging to the background
N_m: Number of merges that have been made
>
> **for** *each contour* $c \in C$ **do**
>
> > **do**
> >
> > > $N_m \leftarrow 0$
> > > **if** $(\exists_{ri} \in C \mid A(r_i) \leq T \times H(c))$ **then**
> > > > *Find* r_n: *nearest region to* r_i
> > > > *Compute l: shortest segment between* r_n *and* r_i
> > > > **if** $(l \cap B) = \emptyset$ **then**
> > > > > *Merge* r_i *and* $r_n : r_i \cup l \cup r_n$
> > > > > $N_m \leftarrow N_m + 1$
> > > > **end if**
> > > **end if**
> > **while** $N_m \neq 0$
> **end for**

Algorithm 2.5: Region merging [50]

2.4.4 Feature Extraction and Representation

Feature extraction, after segmentation, specific features representing the characteristics and properties of the segmented regions in the image need to be computed for object classification and understanding. Features are also important for measurements of parameters leading to direct image understanding [43]. The techniques for feature extraction and representation include statistical pixel-level features, shape, texture, and color features.

Statistical Pixel-Level (SPL) Features

These features provide quantitative information about the pixels within a segmented region. The SPL features may include mean, variance, and histogram of the gray values of pixels in the region. In addition, SPL features may include the area of the region and information about the contrast of pixels within the region and edge gradient of boundary pixels [43].

Once the region is segmented in the image, gray values of pixels within the region can be used for computing the following SPL features [47]:

1. *The histogram of the gray values of pixels in the image as*

$$histogram\ (I) = P(r_i)\frac{n(r_i)}{n} \hspace{4cm} (2.4)$$

   where $P(r_i)$ and $n(r_i)$ are, respectively, the probability and number of occurrences of a gray value r_i in the region and n is the total number of pixels in the region.
2. *Mean m of the gray values of the pixels in the image can be computed as*

24

$$m = \frac{1}{n}\sum_{i=0}^{L-1} r_i p(r_i) \qquad (2.5)$$

where L is the total number of gray values in the image with 0, 1, . . ., L – 1.

3. *Variance and central moments in the region can be computed as*

$$\mu_n = \sum_{i=0}^{L-1} p(r_i)(r_i - m)^n, \qquad (2.6)$$

where the second central moment μ_2 is the variance of the region. The third and fourth central moments can be computed, respectively, for n = 3 and n = 4. The third central moment is a measure of non-centrality while the fourth central moment is a measure of the flatness of the histogram.

4. *Energy: Total energy E of the gray values of pixels in the region is given by:*

$$E = \sum_{i=0}^{L-1}[p(r_i)]^2. \qquad (2.7)$$

5. *Entropy: The entropy Ent as a measure of information represented by the distribution of gray-values in the region is given by:*

$$Ent = \sum_{i=0}^{L-1} p(r_i)\ \log_2(r_i). \qquad (2.8)$$

6. *Local contrast corresponding to each pixel can be computed by the difference of the gray-value of the center pixel and the mean of the gray values of the neighborhood pixels. The normalization local contrast C (x, y) for the center pixel can also be computed as:*

$$C(x,y) = \frac{|P_c(x,y) - P_s(x,y)|}{\max\{P_c(x,y), P_s(x,y)\}}, \qquad (2.9)$$

Where $P_c(x,y)$ and $P_s(x,y)$ are the average gray-level values of the pixels corresponding to the "center" and the "surround" regions that are grown around the central pixel through a region growing method.

7. *Additional features such as maximum and minimum gray values can also be used for representing regions.*

8. *The features based on the statistical distribution of local contrast values in the region also provide useful characteristics information about the regions representing objects.*

9. *Features based on the gradient information for the boundary pixels of the region are also an important consideration in defining the nature of edges* [47].

Shape Feature

The features provide information about the characteristic shape of the region boundary. The shape-based features may include circularity, compactness, moments, chain-codes, and Hough transform. Recently, morphological processing methods have also been used for shape description [43].

Mathematical morphology is based on set theory. It provides basic tools to process images for filtering, thinning, and pruning operations. These tools are useful in the description of region shape, involving boundary and skeleton representations [43].

For example, Figure 2.3 shows a segmented region and its minimum bounded rectangle ABCD.
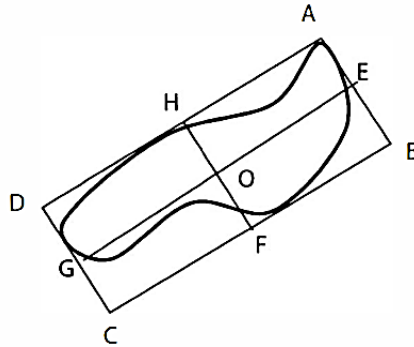
Figure 2.3: A segmented region with a minimum bounded region [43].

Several shape features using the boundary pixels of the segmented region can be computed [47]:

1. *Longest axis GE.*
2. *Shortest axis HF.*
3. *Perimeter and area of the minimum bounded rectangle ABCD.*
4. *Elongation ration: GE/HF*
5. *Perimeter p and area A of the segmented region.*
6. *Hough transform of the region using the gradient information of the boundary pixels of the region.*
7. *Circularity (C = 1 for a circle) of the region computed as:*

$$C = \frac{4\pi A}{p^2}. \tag{2.10}$$

8. *Compactness C_p of the region computed as:*

$$C_p = \frac{p^2}{A}. \tag{2.11}$$

9. *Chain code for boundary contour as obtained using a set of orientation primitives on the boundary segments derived from a piecewise linear approximation.*
10. *Fourier descriptors of boundary contours as obtained using the Fourier transform of the sequence of boundary segments derived from a piecewise linear approximation.*
11. *Center moment-based shape features for the segmented region.*
12. *Morphological shape descriptors as obtained through the morphological processing of the segmented region* [47].

Texture Features

These features provide information about the local texture within the region or the corresponding part of the image. The texture features may be computed using the second-

26

order histogram statistics or co-occurrence matrices. In addition, wavelet processing methods for spatial-frequency analysis have been used to represent local texture information [43].

Using spectral analysis, the texture is represented by a group of specific spatial-frequency components. The gray-level co-occurrence matrix (GLCM) exploits the higher-order distribution of gray values of pixels that are defined with a specific distance or neighborhood criterion. In the simplest form, the GLCM $p(i,j)$ is the distribution of the number of occurrences of a pair of gray values i and j separated by a distance-vector $d = [dx, dy]$ [43].

Color Features

The color feature extraction method divides the total color space into the fixed number of a set called bins. Each bin representing some color and each pixel is put into the nearest colored bin and the size of the bin is then represented in terms of percentage of color in that image [51].

2.4.5 Classification Techniques

The selected features of image representation that are generated from feature selection are used in object recognition and characterization. In the medical image analysis, features and measurements can also be used for region segmentation to extract meaningful structures, subsequently, interpret the result using knowledge-based model and classification methods [16]. Image classification is one of the classical problems of concern in image processing. The goal of image classification is to predict the categories of the input image using its features [52].

There are two main types of classification tasks: supervised, and unsupervised. The supervised learning is done using **ground truth**, or in other words, we have prior knowledge of what the output values for our samples should be [53]. Therefore, the goal of supervised learning is to learn a function that, given a sample of data and desired outputs, best approximates the relationship between input and output observable in the data. Unsupervised learning, on the other hand, does not have labeled outputs, so its goal is to infer the natural structure present within a set of data points [53].

There are various approaches for image classification techniques, such as statistical classification methods, Rule-based systems, the Convolutional Neural network classifier, and the Support vector machine (SVM) for classification [16] [54].

Statistical Classification Methods

The categories of these methods are an unsupervised and supervised approach. The unsupervised methods cluster the data based on their separation in the feature space, such methods include K-means and fuzzy clustering. On the other hand, a supervised approach needs training data, test data, and class labels to classify the data using probabilistic methods like the nearest neighbor and Bayesian classifier [16].

Rule-based Systems

The decision-making process of classification can be implemented using a rule-based system [43]. A rule-based system analyzes the feature vector using multiple sets of rules that are designed to test specific conditions in the feature vector database to set off an action. The rules consist of two parts: condition premises and actions. They are based on expert knowledge to deduce the action when the conditions are satisfied. The action part of the rule could change the database state or label of a feature vector based on a specific state of analysis [16].

Support Vector Machines (SVM) for Classification

The Relevance Vector Machine (RVM) combines regression, classification, and a Bayesian probabilistic principle [16]. Support Vector Machine (SVM) is a supervised learning algorithm that can be used for classification and regression problems as support vector classification (SVC) and support vector regression (SVR). It is used for smaller datasets as it takes too long to process [55].

Support vector machine for binary classification problems.

Let us consider a linear binary classification task, as depicted in Figure 2.4 with m data points $x_i (i = 1, ..., m)$ in the n-dimensional input space R^n, having corresponding labels $y_i = \pm 1$ [56].
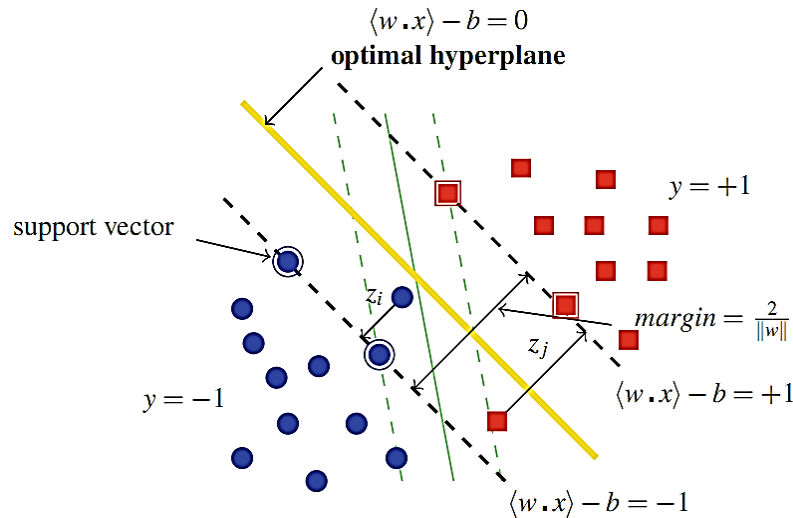
Figure 2.4: Linear separation of the data-points into two classes [56].

For the classification problem, the SVM algorithms try to find the best separating plane (denoted by the normal vector $\omega \epsilon R^n$ and the scalar $b \epsilon R$, i.e. furthest from both class +1 and class -1. It can simply maximize the distance or the margin between the supporting planes for each class($x.w - b = +1 \ for \ class + 1, x.w - b = -1 \ for \ class - 1$). The margin between these supporting planes is $2/||\omega||$ (where $||\omega||$ is the 2-norm of the vector ω). Any point x_i falling on the wrong side of its supporting plane is considered an error, denoted by $Z_i(Z_i \geq 0)$. Therefore, SVM has the ability to simultaneously maximize the margin and minimize the error [56].

Convolutional Neural Network (CNN) Classifier

CNN is one of the most popular categories of neural networks, especially for high-dimensional data (e.g., images and videos). CNN operates in a way that is very similar to standard neural networks. A key difference, however, is that each unit in a CNN layer is a two- (or high-) dimensional filter which is convolved with the input of the layer [54]. This is essential for cases where we want to learn patterns from high-dimensional input media, e.g., images or videos [54].

CNN's are a useful class of models for supervised learning paradigms. The supervised learning mechanism is the one where the input to the system and the desired outputs (true labels) are known and the model learns a mapping between the two. In the unsupervised mechanism, the true labels for a given set input are not known and the model aims to estimate the underlying distribution of the inputs data samples [54].

An example of a supervised learning task (image classification) is shown in Figure 2.5. The CNN learns to map a given image to its corresponding category by detecting a number of abstract feature representations, ranging from low-level features in the initial layers, followed by more complex intermediate and high-level feature representations that are used for a classification task. These discriminative features are then used in the network to predict the correct category of an input image [54].
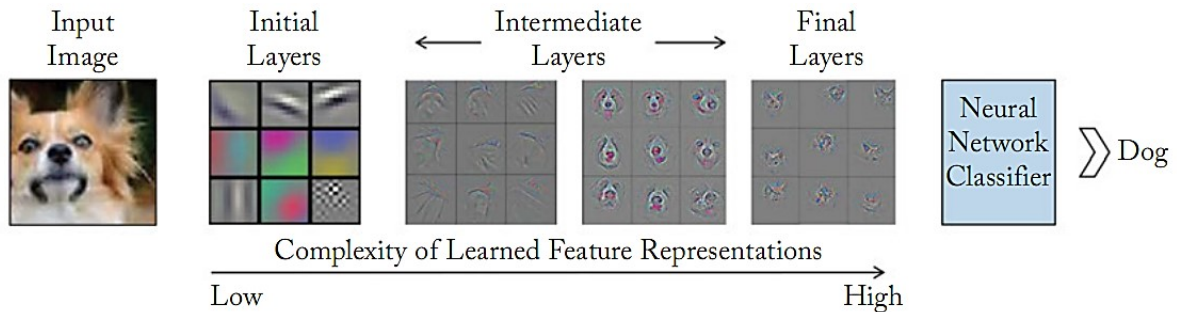
Figure 2.5: The learning process in the CNN framework [54].

The function of a CNN is similar to this pipeline, with the key difference being the automatic learning of a hierarchy of useful feature representations and its integration of the classification and feature extraction stages in a single pipeline which is trainable in an end-to-end manner [54].

2.4.6 Stenosis Shape Description

Image measurements aim at characterizing the objects of an image by some numerical values. The measurement is discriminant for a given criterion if the values obtained for objects satisfying this criterion are very different from those obtained for all other objects [57].

A shape description scheme is a *notational system* for expressing the shapes of objects, a way of writing the shape information symbolically to avoid both ambiguity and obscurity [58].

2.5 Medical Image Analysis

The accuracy of medical image analysis is determined mainly by the ability to set a precise boundary of the ROI in medical images. In order to perform objective or quantitative, consistent, and fast analysis, and to help the medical professionals in the decision-making process, image processing techniques are widely used for computer-aided diagnosis analysis of medical images. Computer-aided diagnosis is a concept established by taking into account

the roles of physicians and computers; the physicians use the computer output as a "second opinion" to make the final decision [22].

Medical imaging has undergone a major advancement. According to Zhou [48], medical image recognition, segmentation, and parsing are essential topics of medical imaging analysis. Medical image recognition is about recognizing which objects are inside a medical image. Object recognition often it is beneficial to associate object recognition with object detection or localization. Once the object is recognized or detected using, say, a boundary box, medical image segmentation further concerns finding the exact boundary of the object in a medical image. When there are multiple objects in the images, segmentation of multiple objects becomes medical image parsing that, in the most general form, assigns semantic labels to pixels in a 2D image or voxels in a 3D volume. By grouping the pixels or voxels with the same label, segmentation is realized.

Zhou [48] pointed out that, imaging has the following three components:

1) *Scanner*: Because the computed tomography (CT) or magnetic resonance imaging (MRI) scanner is equipped with configuration possibilities or imaging protocols, an ideal diagnostic CT scan should be personalized to image only target region of a given patient, no more (to reduce dose) or no less (to avoid missing information). Therefore, efficient detection of organs from a scout image enables personalized scanning at a reduced dose, saves exam time and cost, and increases the consistency and reproducibility of the exam [48].

2) *Image reading for diagnosis, therapy, and surgery planning*: During image reading, when searching for disease in a specific organ or body region, a radiologist needs to navigate the volume to the right location. Further, after a certain disease is found, he/she needs to report the finding. Medical image parsing enables structured reading and reporting for streamlined workflow, thereby improving image-reading outcomes in terms of accuracy, reproducibility, and efficiency. And also, in radiation therapy, intervention procedures, and orthopedic surgery, medical image parsing is a prerequisite in the planning phase [48].

3) *Advanced quantification and modeling*: Clinical measurements such as organ volumes are important for quantitative disease diagnosis. However, it is time-consuming for a physician to identify the target object especially in 3D and perform quantitative measurements without the

aid of an intelligent post-processing software system. Automatic image parsing overcomes the simulates biomechanical or hemodynamically process is feasible [48].

2.6 Challenges in Medical Image Processing

Many recent improvements have been occurring in various image processing techniques of the medical image analysis system. However, according to Chinmayi, *et al.* [4] still there are some existing challenges in image enhancement and restoration, automated and accurate segmentation of ROI, automated and accurate registration and fusion of image multimodality, classification of image features (namely characterization and typing of structures), quantitative measurement of image features and an interpretation of the measurements, and development of integrated systems for the clinical sector.

- The techniques available in the image enhancement field fails to preserve the weak texture on an image when the density of the noise is more.
- The available segmentation techniques are not convinced by the physician/radiologist because it fails to provide an accurate ROI, when there is more noise, requires high computational time, more information loss, no fully automated segmentation algorithm, and high implementation complexity.
- None of the existing feature extraction algorithms guaranteed the expected accuracy (i.e. 100%) with less computational time mainly in terms of features, as it is expected for better diagnosis.
- The demand for the unsupervised classifier still exists when there is no labeled training sample available to the classifier in advance.

2.7 Review of Related Works

The coronary artery disease (CAD) diagnosis is significant around the world and a number of researchers apply digital image processing techniques in order to detect and quantify the CAD from different image modality. In this section, previous related works of the image processing method for CAD detection and quantification are reviewed. These reviews help us to see different image analysis techniques and tools to detect, quantify and classify CAD.

Chi *et al.* [31] presented the panoramic Maximum Intensity Projection (MIP) of coronary arteries on coronary CTA images and assessed its performance on the detection and

quantification of coronary artery stenosis. The detected stenosis lesions with a diameter reduction of 50% or more were considered representative of anatomically significant stenosis. The heart region isolation donned by abating the bone and lung vessels by isolating the heart region and setting the rest background using thresholding operation, followed by morphological analysis such as dilation and erosion. The left ventricle extracted to start the region growing by image segmentation and set it as background. Then fix point ray casting was employed to image from various viewpoints. That employed to keep on rotating and rendering the visualized images on the screen. Finally, the study enhanced the image by histogram equalization and rendered. The method was tested in six CAD patients and the results achieved a sensitivity of 82% and a specificity of 95% result. In stenosis quantification, three images are provided and a better accuracy 89% achieved. The experimental results showed that the panoramic MIP provides a fast and accurate way for stenosis detection and quantification comparison with Invasive Coronary Angiography (ICA). However, the system to generate the panoramic MIP, on abate highly attenuating structure in that they used a semi-automatic method.

Mirunalini and Aravindan [32] designed an automatic segmentation of coronary arteries and detection of stenosis, using a CTA modality of diagnosing and treat CAD. The segmentation of the coronary artery is achieved by techniques such as image smoothing using a Gaussian filter, a vessel enhancement technique using a Sobel operator, localized threshold and connected component labeling. Stenosis detection by finding the discontinuities in the vessel by centerline extraction is achieved by the skeletonization technique, calculating the thickness and the intensity of the vessel. The study was carried out by collecting 2D projection images of 15 different patients, in DICOM format. For each patient 10 to 15 different projection images, ware is considered. These images include stenosis and images without stenosis. The experimental result showed that the compared outcome with the ground truth given by the experts and this provides an average recall measure of 97% result. The study presents stenosis in the segmented coronary arteries is detected based on the heuristics used in the centerline extraction algorithm. Thus, it achieved a reduction in false-negative responses by detecting out all suspected parts of the coronary arteries. They did focus only on through the segmentation detect the stenosis process. They stated that their proposed method was checked

on 11 stenosis patients of 34 sample images from 15 patients. The further improvement by using machine-learning techniques can be carried out as the future scope of the work.

Kang *et al.* [59] presented a knowledge-based algorithm that dose centerline extraction and vessel classification, vessel linearization, lumen segmentation, and lesion detection. It requires two user inputs: a point at the ostium of the right coronary artery and left main coronary artery, and placing a circular region over the aortic root. 3D thinning and graph theory perform the centerline extraction, followed by artery classification using Dijkstra's shortest path algorithm and anatomical knowledge. The vessel is then linearized using a plane perpendicular to the centerline and the lumen segmentation is done with specific threshold levels for lumen and plaque. The lumen is determined by using a recursive region-growing in the linearized volume, and the stenosis is calculated using a knowledge-based algorithm. The system was tested in a coronary CTA dataset of 42 patients. In the 45 images with stenosis $\geq$ 25%, 20 images were obstructive $\geq$ 50%. When the artery was divided into 15 coronary segments according to standard cardiology reporting guidelines, per-segment basis, sensitivity was 93% and pre-segment specificity was 81% using 10-fold cross-validation. The study result showed promising results in the detection of both obstructive and non-obstructive CCTA lesions. However, the authors focus only on the stenosis present images detection of coronary artery stenosis and they did not address the stenosis quantification.

Mohan and Vishnukumar [3], used digital imaging and communications in medicine (DICOM) images of the heart for detecting and localizing the stenosis regions in the artery. The ROI is considered as the coronary arteries and is segmented using a vessel enhancement diffusion filter along with the application of dilation and erosion morphological operations. After segmenting the vessels from the image, the image enhancement process is carried out to enhance the edges of the vessels. For enhancing the image, they use morphological operations. The centerlines of the segmented arteries are extracted using a fast-marching based method. It is mainly used in boundary value problems. Based on this approach a skeleton is built which consists of centerline points of the artery. In order to estimate the vessel diameter, calculate the expected diameter of each cross-section for every centerline point is calculated and actual diameter estimation is carried out using linear regression. The detection and localization were applied 15 images in which 86% accuracy achieved for detecting stenosis. The study showed a novel approach for the detection of coronary artery stenosis. The

algorithm can be modified for improving the accuracy of stenosis detection and also to reduce the execution time and user interaction. The blur and distortion removal can be carried out as future enhancement of the work. The quantification of the stenosis area can be carried out as the future scope of the work.

Goldenberg *et al.* [60], presented a CAD system for the interpretation of coronary from CTA images. The automatic software segments the coronary artery tree, label the major arteries and detects stenosis lesions with obstruction higher than 50%. The system also rejects low-quality images. The coronary tree segmentation is done by finding the mediastinum. The ascending aorta is identified by using a circular Hough transform. The remaining coronary tree is found by tracking tubular components using depth-first-search. The tree is then pruned to obtain only the coronary arteries. The labeling is based on a probabilistic anatomic model from a manually segmented training dataset. Finally, the detection of the stenosis lesions is performed by straightening the artery segments (curved planar reformation), and the boundary and lumen are delineated using an iterative, model-based, active contour approach. Calcified and non-calcified lesions are detected by the intensity of the voxels, and the final decision is made by a fuzzy logic system trained from manually classified images by physicians. The results achieved a sensitivity of 90% per patient and a specificity of 40-70% per patient. The study showed that clinically validated CAD system for fully automatic analysis of coronary CTA and detection of significant stenosis. However, it does not replace humans in making the final decision. A trained physician should verify the diagnosis.

In addition to this, as shown by much of the recent literature regarding CAD detection, the coronary artery plaque boundary is detected using an intravascular ultrasound (IVUS) images [30], [61], which has that imaging the underlying plaque as well as measuring the luminal cross-sectional area at the point of a borderline lesion. Sofian *et al.* [61], detect the calcification boundary and measure the calcification area in the tunica (the layer of body tissue) media coronary artery using an intravascular ultrasound image (IVUS). To detect the calcification boundary area, they adapt thresholding morphological operation and empirical thresholding. The first phase of the segmentation process is to select the pixel threshold of the entire image and smoothing out the calcification boundary where the image is closed, opened, eroded and dilated. Based on the setting of the empirical threshold parameter, all pixels below the threshold value is changed zeros, and all pixels above the threshold value is changed to

one. The resultant image is a binary image. In the final phase, the tunica adventitia region removes to get the calcification region.

The work in Sofian *et al.* [30], provides deep structured learning in the IVUS image for CAD. The central focus of Sofian *et al.* [30], also detect the calcification present and calcification absent in the CAD. The four types of images that are a Cartesian coordinate image, polar reconstructed coordinate image, Cartesian coordinates warp images with and polar constructed warp image was used as an input image. And they use three types of classifiers together (Decision Tree, K-nearest Neighbour, and Naïve Bayesian) for the detection of the calcification present and calcification absent.

2.8 Summary

In this chapter, a general background regarding CAD and its diagnosis process has been discussed. In addition to this, the digital image processing that is applied to CAD detection and quantification such as image pre-processing, segmentation, feature extraction, and classification are discussed. The image processing associated with the quantification of stenosis also discovered. Finally, reviewed the CAD detection and quantification system that is related to the study at hand. In general, the whole attempts CAD detection. The coronary CTA images difficult about visualization affected by blurring and noisy structure abatement of the image were not considered satisfactory. Besides, the quantification of stenosis needs to improve. By this, it is meant that further research is needed to complement the gap specified above.

Thus, this thesis applies digital image processing to come up with the detection and quantification of stenosis.

Chapter Three
Research Methods and Techniques

The purpose of this study is to develop and evaluate an algorithm for CAD detection and quantification of stenosis methods for processing coronary artery images. Image processing is the study of an algorithm that takes an image as input and returns an image as output. After visualizing the coronary artery, several image analysis techniques can be applied for coronary stenosis detection and vessel quantification. The main techniques are preprocessing, segmentation, feature extraction, and classification. In addition, the study gives attention to proposing a stenosis quantification method.

3.1 Proposed Architecture

The proposed architecture in this study is illustrated in Figure 3.1. The architecture shows the steps followed in the detection and quantification of stenosis from coronary CTA images, such as image preprocessing, segmentation, feature extraction, and classification once image instance is classified as stenosis present: they are further processed to detect and quantify stenosis.

In the proposed architecture, the patient's data were taken as input and stored in the dataset and this dataset contains the patient's data who are suffering from CAD. To validate the proposed method, we use the coronary CTA images. The input datasets of coronary CTA images undergo data preparation. The coronary CTA image selection forms the dataset, a process done by identification of lesions with any stenosis greater than or equal to 50% and normal images. These images are selected manually from different angles and approved by the physician.
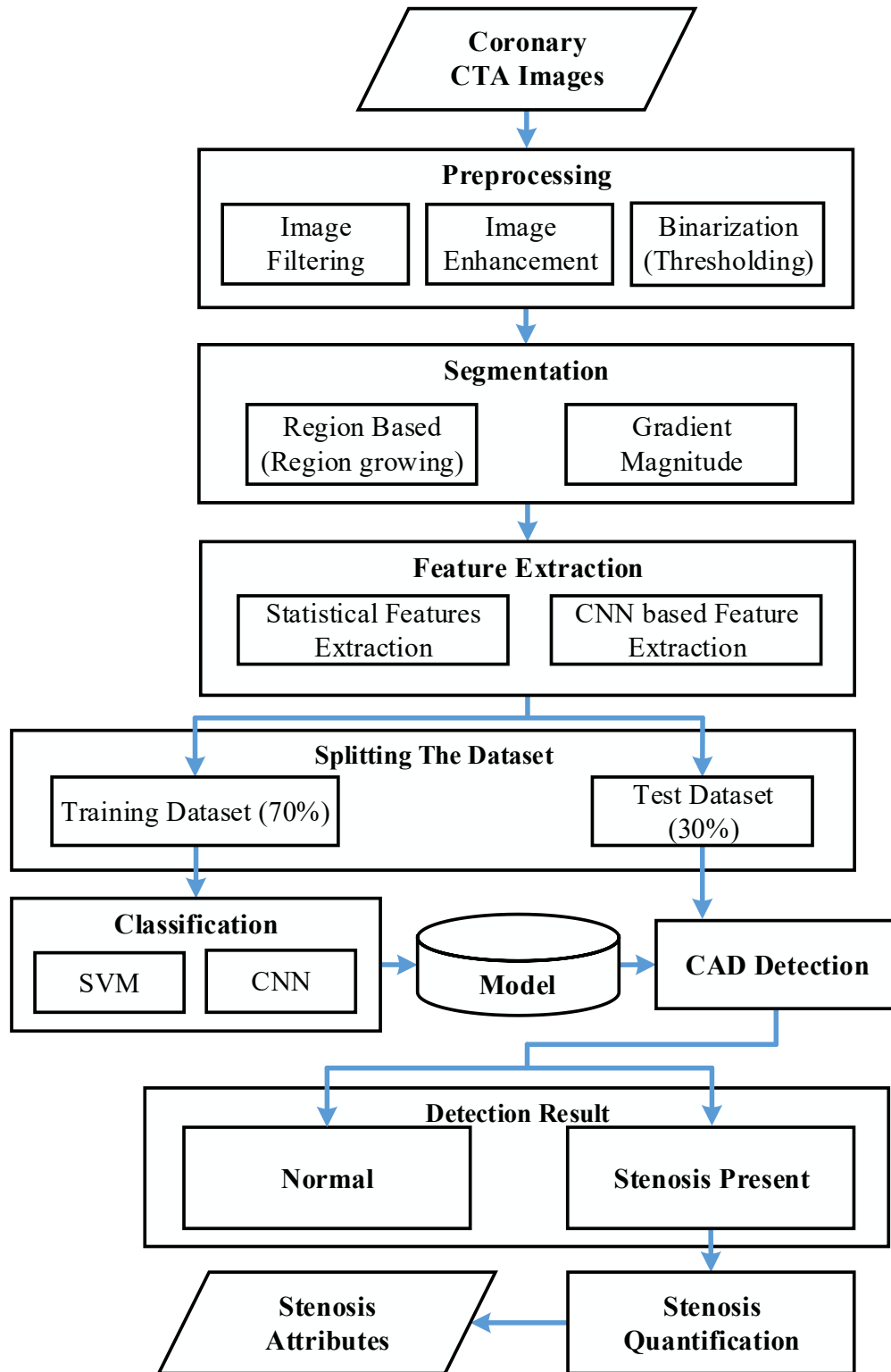
Figure 3.1: The Proposed Architecture

The proposed architecture passes through five main stages, namely, preprocessing, segmentation, feature extraction, classification, and finally CAD (Stenosis) detection of the ROI and stenosis quantification step. The preprocessing component does the job to suppress

38

noise and enhance the quality of images. The output of the preprocessing component fed into the segmentation and classification component. The segmentation component is responsible for isolating the ROI from the other part. The third component, feature extraction, computes discriminant properties of the image constitutes from the result of preprocessing and segmentation. Then the classification components use to classify the constituents of a coronary image into two class, normal or stenosis present. Finally, the stenosis detection and quantification component used to quantify the area of stenosis attributes.

3.2 Preprocessing

After coronary CTA image is acquired using save as image from DICOM viewer, it is essential to perform preprocessing. The aim of preprocessing in the proposed architecture is to improve the quality of a coronary CTA image by enhancing the quality of an image for further analysis. Thus, image pre-processing is processing the coronary CTA images to increase contrasts and suppress noise in order to make the input image ready for the segmentation component.

Preprocessing in the types of X-Ray is Computed Tomography (CT), Mammography, Fluoroscopy, and Angiography images generally denote the de-noising images. If enhancement algorithms are applied without de-noising then they may greatly amplify the noise and may cause loss of information in images. Thereby, they cannot highlight the edges of the image and cannot be applied to detection. Therefore de-noising may be performed using suitable filters [44].

The steps used for the preprocessing method such as image filtering, image enhancement, and image binarization are summarized as follows:

- Reduce the noise in the original coronary CTA image using the image filtering technique.
- After image filtering, enhance the image in order to adjust the contrast of an image by using image enhancement techniques.
- Convert the grayscale image into a binary image using the image binarization technique.

3.2.1 Image Filtering

There are many image-filtering algorithms used to isolate the heart from its surroundings to suppress noise from pulmonary vessels and improve the quality. For determining the ROI in the coronary CTA image, we use edge-preserving filters among which are the separable bilateral filter with Gaussian kernels, guided filtering, and non-local mean filtering algorithm.

Bilateral Filtering Method

Separable *approximation* of the bilateral filter is proposed that brings about a significant performance increase. In this implementation, a *one*-dimensional Bilateral filter is first applied in the horizontal direction only, which uses one dimension domain and range kernels H_d *and* H_r, respectively, and produces the intermediate image $I^\triangleright$ using equation 3.1 [45],

$$I^\triangleright(u,v) \leftarrow \frac{\sum_{m=-k}^{k} I(u+m,v) \cdot H_d(m) \cdot H_r\big(I(u+m,v)-I(u,v)\big)}{\sum_{m=-k}^{K} H_d(m) \cdot H_r\big(I(u+m,v)-I(u,v)\big)}. \qquad (3.1)$$

In the next (second) pass, the *same* filter is applied to the intermediate result $I^\triangleright$ in the vertical direction to obtain the result I' as shown below in equation 3.2.

$$I'(u,v) \leftarrow \frac{\sum_{n=-k}^{k} I^\triangleright(u,v+n) \cdot H_d(n) \cdot H_r\big(I^\triangleright(u,v+n)-I^\triangleright(u,v)\big)}{\sum_{m=-k}^{K} H_d(m) \cdot H_r\big(I(u+m,v)-I(u,v)\big)}, \qquad (3.2)$$

Separable Bilateral filter with Gaussian kernels presented below in Algorithm 3.1. The advantage of the separable filter is performance. For a given kernel radius K, the original (non-separable) requires $O(K^2)$ calculations for each pixel, while the separable version takes only $O(K)$ steps [45].

Bilateral Filter Gray Separable (I, σ_d, σ_r)
      Input: *I, a coronary artery image, the size of image $M \times N$; σ_d, width of the 2D Gaussian domain kernel; σ_r, width of the 1D Gaussian rang kernel;*
      Output: *returns a new filtered image of size $M \times N$.*
      Convert the RGB image into a grayscale image, I
      $(M,N) \leftarrow Size\ (I)$
      $K \leftarrow [3.5 \cdot \sigma_d]$ ▷ *width of domain filter kernel*
      $I^\triangleright \leftarrow Duplicate(I)$
      for all *coordinates* $(u,v) \in M \times N$ **do**   ▷ **Pass 1** *(horizontal)*
            $\alpha \leftarrow I(u,v)$
            $S \leftarrow 0, \quad W \leftarrow 0$

$$
\begin{aligned}
&\textbf{\textit{for }} m \leftarrow -K, \dots K \textbf{\textit{ do}} \\
&\quad b \leftarrow I(u+m, v) \\
&\quad w_d \leftarrow e^{-\frac{m^2}{2\sigma_r^2}} \qquad\qquad\qquad\qquad \triangleright \textit{ domain weight } H_d(m) \\
&\quad w_r \leftarrow e^{-\frac{(a-b)^2}{2\sigma_r^2}} \qquad\qquad\qquad\qquad \triangleright \textit{ range weight } H_r \\
&\quad w \leftarrow w_d \cdot w_r \qquad\qquad\qquad\qquad \triangleright \textit{ composed weight} \\
&\quad S \leftarrow S + w \cdot b \\
&\quad W \leftarrow W + w \\
&\quad I^{\triangleright}(u, v) \leftarrow \frac{1}{W} \cdot S \qquad\qquad\qquad \triangleright \textit{ see equation (3.1)} \\
&I^{\triangleright} \leftarrow Duplicate(I) \\
&\textbf{\textit{for all }} coordinates\ (u, v) \in M \times N \textbf{\textit{ do}} \qquad \triangleright \textbf{\textit{Pass 2}}\ \textit{(vertical)} \\
&\quad a \leftarrow I^{\triangleright}(u, v) \\
&\quad S \leftarrow 0, \qquad W \leftarrow 0 \\
&\quad \textbf{\textit{for }} n \leftarrow -K, \dots, K \textbf{\textit{ do}} \\
&\qquad b \leftarrow I^{\triangleright}(u, v+n) \\
&\qquad w_d \leftarrow e^{-\frac{n^2}{2\sigma_d^2}} \qquad\qquad\qquad \triangleright \textit{ domain weight } H_d(n) \\
&\qquad w_r \leftarrow e^{-\frac{(a-b)^2}{2\sigma_r^2}} \qquad\qquad\qquad \triangleright \textit{ range weight } H_r \\
&\qquad w \leftarrow w_d \cdot w_r \qquad\qquad\qquad \triangleright \textit{ composed weight} \\
&\qquad S \leftarrow S + w \cdot b \\
&\qquad W \leftarrow W + w \\
&\quad I'(u, v) \leftarrow \frac{1}{W} \cdot S \qquad\qquad\qquad \triangleright \textit{ see equation (3.2)} \\
&\textbf{\textit{return }} I'.
\end{aligned}
$$

Algorithm 3.1: Separable Bilateral filter with Gaussian kernels [45].

Guided Filtering Method

The guided image filtering is an image filter based on the local linear model. The guided image filtering can preserve the edge information of the image [62]. The filtering output is locally a linear transform of the guidance image. This filter has an edge-preserving smoothing property like the bilateral filter but does not suffer from the gradient reversal artifacts [63]. Algorithm 3.2 presents the steps followed in guided filtering.

Input: *filtering input image p, guidance image I, radius r, regularization ∈, mean filter* f_{mean}

Output: *filtering output q.*

$mean_I = f_{mean}(I)$

$mean_p = f_{mean}(p)$

$corr_I = f_{mean}(I.*I)$

$corr_{Ip} = f_{mean}(I.*p)$

$var_I = corr_I - mean_I. * mean_I$

$cov_{Ip} = corr_{Ip} - mean_I. * mean_p$

$a = cov_{Ip}./(var_{I+}∈)$

$b = mean_p - a.* mean_I$

$mean_a = f_{mean}(a)$

$mean_b = f_{mean}(b)$

$q = mean_a.*I + mean_b$

Algorithm 3.2: Guided filtering [64]

Non-local Means Filtering Method

The non-local means is a parametric filter highly dependent on the setting of its parameters. The non-local mean filter is an evolution of the filter which averages similar image pixels according to their intensity distance [65]. The non-local means-filtering algorithm estimates the de-noised values of pixel p using these steps. The detail of the non-local means filtering algorithm is presented in Algorithm 3.3.

Input: *a coronary artery image, the size of image M × N, search window size l, similar window size m, smooth parameter h*

Output: *filtered image*

for (i=1: M × N)

    for (j=1: l)

        for(k=1:m)

            Calculate the Euclidean distance within the similar window, and cumulate the sum of all the Euclidean distance;

        end for

        Calculate and cumulate the weight of the pixel within the search window;

        Cumulate the restored value;

    end for

    Normalize the restored value to the sum of weights;

end for

Algorithm 3.3: Non-local Mean filtering [66].

3.2.2 Image Enhancement

Histograms are the basis for numerous spatial domain-processing techniques [11]. Image enhancement gives better image quality that is given as input to various digital image processing applications. In this study, we compare three image enhancement techniques, namely, histogram equalization, adaptive histogram equalization, and Edge-aware local contrast enhancement.

Histogram Equalization

Histogram equalization uniformly redistributes the gray-level values of the pixels within an image so that the number of pixels at any one gray-level is about the same in order to adjust the contrast of an image by modifying the intensity distribution of the histogram [46]. The steps for implementing a general approach for histogram equalization is presented in Algorithm 3.4.

Input: A filtered image or original image, I
Output: Histogram equalized image
for(I=0, I<256, I++)
    number = histogram [I]
    if(number<target)
     moveRandPixels(I+1, I, target - number)
    else
     moveRandPixels(I, I+1, number - target)
end for

Algorithm 3.4: Image enhancement using histogram equalization [46]

Adaptive Histogram Equalization

Adaptive histogram equalization improves on this by transforming each pixel with a transformation function derived from a neighborhood region. When the image region containing a pixel's neighborhood is homogeneous, its histogram will be strongly peaked, and the transformation function will map a narrow range of pixel values to the whole range of the resulting image. This causes adaptive histogram equalization to over amplify small amounts of noise in largely homogeneous regions of the image. This method used to improve the contrast of the images [67]. Algorithm 3.5 shows the adaptive histogram equalization image enhancement.

Input: A filtered image
Output: Adaptive histogram equalized image
function AHE(I,win_size)
    for each pixel (x, y) in image, I do
        rank ← 0
        contextual_region* ← (win_size × win_size) window centered around (x,y)
        for each (i, j) in contextual_region do
          if im(x, y) > im(i, j) then
            rank ← rank + 1
        end for
        output (x, y) ← rank × 255/(win_size × win_size)
    end for
    return output

Algorithm 3.5: Image enhancement using Adaptive histogram equalization [68].

Edge-aware Local Contrast Image Enhance

Edge-aware local image enhancement flattens the local contrast of the image by increasing or smoothing details while leaving strong edges unchanged. The steps followed in image enhancement using edge-aware local contrast Laplacian filtering is presented in Algorithm 3.6.

Input: image I, a threshold σ_r σ, remapping function r
Output: Enhanced image
    compute input Gaussian pyramid {G [I]}
    for all (x, y, l) do
        g =G_l [I](x, y)
        determine the local neighborhood R_l to evaluate $L_l[r(R_l)](x, y)$
        apply the remapping function: $r(R_l)$
        compute sub-pyramid {$L_l[r(R_l)]$}
        update output pyramid: L_l [O](x, y)= L_l [r(R_l)](x, y)
    end for
    collapse output pyramid: O=collapse ({L_l [O]})

Algorithm 3.6: Edge-aware local contrast Laplacian image enhancement [69].

3.2.3 Image Binarization

Binarization plays an important role in digital image processing. The thresholding method is an effective technique in binarization, thereby used to automatically detect and segment high contrast objects using gray-level images. The result is a binary image containing two classes of pixels following a bimodal histogram (background and foreground pixels) [40].

Image Binarization Using Otsu's Threshold Method

Thresholding is used in image processing to separate an object's pixel from the background pixels. Thresholding converts a multi-gray-level image into a binary image containing two gray-level values. The threshold operation is defined as follows in equation 3.3 [11].

$$g(x, y) = \begin{cases} Go & if\ f(x, y) > T \\ Gb & if\ f(x, y) \leq T \end{cases}$$ (3.3)

Where f (x, y) is the original image, g (x, y) is the binary image, T is the threshold value, Go is the object gray-level value after the thresholding operation, and Gb is the background gray-level value after the thresholding operation. Algorithm 3.7 presents the Otsu's method algorithm as follows.

Input: *Enhanced coronary artery grayscale histogram image.*
Output: *Returns the optimal threshold value or -1 if no threshold is found*
K- Size (h) ▷ *number of intensity levels*
(μ_0, μ_1, N) ◁ *Make mean*
$\sigma_{bmax}^2 \leftarrow 0$
$q_{max} \leftarrow -1$
$n_0 \leftarrow 0$
for $q \leftarrow 0, ..., K - 2$ **do** ▷ *examine all possible threshold values q*
    $n_0 \leftarrow n_0 + h(q)$
    $n_1 \leftarrow N - n_0$
    if $(n_0 > 0) \wedge (n_1 > 0)$ **then**
        $\sigma_b^2 \leftarrow \frac{1}{N^2} \cdot n_0 \cdot n_1 \cdot [\mu_0(q) - \mu_1(q)]^2$
        if $\sigma_b^2 > \sigma_{bmax}^2$ **then** ▷ *maximize* σ_b^2
            $\sigma_{bmax}^2 \leftarrow \sigma_b^2$
            $q_{max} \leftarrow q$
    return q_{max} ▷ *return -1 if the for loop is unsuccessful*

Algorithm 3.7: Image Binarization using Otsu's threshold method [45].

Image Binarization Using Adaptive Threshold Method

To further enhance the estimated edges and generate a binary edge image we perform adaptive thresholding previously enhanced grayscale image. The steps followed details of the adaptive threshold method shown on Algorithm 3.8.

Algorithm 3.8: Image Binarization using the Adaptive threshold method [45].

3.3 Segmentation

Image segmentation is one of the most important tasks in medical image analysis. It is the process of partitioning an image into parts having features and properties. The main aim of segmentation is to simplify the image by presenting in an easily analyzable way and use it to isolate the ROI in an image.

In this proposed research, the image segmentation is applied for partitioning a CTA image into multiple segments or regions and identify the ROI, the coronary artery. The objective of this segmentation process is to label each pixel in the CTA images and locate the coronary artery boundaries. In this research region-based segmentation and edge detection, based image segmentation have experimented.

3.3.1 Region-based segmentation method

Region-based segmentation algorithm operates iteratively by grouping together pixels that are neighbors and have similar values and splitting groups of pixels that are dissimilar in value. The segmentation technique that finds the regions directly from the given image, based on the concept of region growing procedure, is presented in Algorithm 3.9.

Inputs: *Edge thinned image I of size r × c, Largest connected*
component L in the image I
Output*: Segmented image*
Phase I Choose an initial seed point p(x, y).
      for i =1: r
        for j=1: c
            if *I(xi, yj) ∈ L*
                p(x, y)=I(xi, yj)
                Return p(x,y)
            end if
        end for
      end for
Phase II Find the threshold value (T).
      Avg = (Sum of all the pixel intensity values in the
      image) ÷ (Total no. of pixels in the image)
      T = Avg ÷ 2
Phase III Growing the region by comparing it with the neighboring pixels.
      neigb = [-1,0; 0,-1; 1,0; 0,1; -1,-1; 1,-1; 1,1; -1,1]
      count = 1
      reg_size = 1
      cl=number of pixels in L
      while *(count<=cl)*
        for j = 1:8
            xn = x + neigb (j, 1)
            yn = y + neigb (j, 2)
            dist = | I (yn, xn) - P (x, y)|
            if *(dist<=T)*
                reg_size = reg_size+1
            end if
            count = count+1
        end
      end while

Algorithm 3.9: Region-based segmentation using the region-growing algorithm [70].

There are three phases in the region growing based segmentation. Phase I choose an initial seed point p (x, y). Phase II finds the threshold value (T). Phase III growing the region by comparing it with the neighboring pixels.

3.3.2 Image Segmentation by Edge Detection

Segmentation based on edge detection attempts to resolve image segmentation by detecting the edges or pixels between different regions that have a rapid transition in intensity that is

extracted and linked to closed object boundaries [71]. Image segmentation and data extraction can be done using edge detection [72].

The Sobel operator is based on structuring the image with a small, divisible, and integer-valued filter in the horizontal and vertical direction and is therefore relatively not costly in terms of computations [72]. There order in Algorithm 3.10 the steps followed using Sobel operator edge detection techniques.

Input: image w, h (w and h are the width and height of the image respectively)
Output: Segmented image
  G_x = new double[w][h];
  G_y = new double[w][h];
  Gradient = new double[w][h];
  for (x=0;x<w;x+=3)
      for (y=0;y<h;y+=3)
        if(x=0||x=w-1||y=0||y=h-1)
          G_x[x][y]=G_y[x][y]=Gradient[x][y]=0 //Image boundary
        end if
        else
          G_x[x][y]=image[x+1][y-1]+2* image[x+1][y]+image[x+1][y+1]-image[x-1][y-1]-2*image[x-1][y]-image[x-1][y+1]
          G_x[x][y]=image[x-1][y+1]+2* image[x][y+1]+image[x+1][y+1]-image[x-1][y-1]-2*image[x][y-1]-image[x+1][y-1]
          Gradient[x][y]=abs(G_x[x][y])+abs(G_y[x][y])
        end else
      end for
end for

Algorithm 3.10: Edge detection techniques using Sobel operator algorithm [73]

3.4 Feature Extraction

Feature extraction is a method of capturing the visual content of images. Image analysis is the process of extracting meaningful information from images that are used to describe the feature such as its length, regional descriptors, relational descriptor, and boundary descriptor. Feature extraction is responsible for the descriptive features of the coronary CTA image. In this study, statistical features extraction and CNN based feature extraction are used.

3.4.1 Statistical Feature Extraction

Statistical techniques of discriminate analysis, to perform automatic classification of families of random shapes. The following statistical features are used in this study.

- **Mean**

For a random variable vector A made up of N scalar observations, the mean is defined as:

$$\mu = \frac{1}{N}\sum_{i=1}^{N} A_i \tag{3.4}$$

- **Standard Deviation**

For a random variable vector, A made up of N scalar observations, the standard deviation is defined as:

$$S = \sqrt{\frac{1}{N-1}\sum_{i=1}^{N} |A_i - \mu|^2}, \tag{3.5}$$

where μ is the mean of A:

The standard deviation is the square root of the variance. Some definitions of standard deviation use a normalization factor of N instead of $N-1$, which you can specify by setting w to 1.

3.4.2 CNN Based Feature Extraction

A convolutional neural network (CNN) is a multi-layered neural network. CNN has the ability to perform both feature extraction and classification. CNN has been a powerful learning ability due to the use of multiple feature extraction stages that can automatically learn feature representations from the data [74].

The attractive feature of CNN is its ability to exploit the spatial or time correlation of the data. The topology of CNN is divided into multiple learning stages composed of a combination of the convolutional layers, non-linear processing units, and subsampling layers [74]. CNN's are feedforward multilayered hierarchical networks that are similar to a fully connected neural network where each layer, using a bank of convolutional kernels, performs multiple transformations. Convolution operation extracts useful features from locally correlated data points. The output of the convolutional kernels is assigned to the non-linear processing unit (activation function), which not only helps in learning abstractions but also embeds non-

linearity in the feature space. This non-linearity generates different patterns of activations for different responses and thus facilitates in learning of semantic differences in images. The output of the non-linear activation function is usually followed by subsampling, which helps in summarizing the results and also makes the input invariant to geometrical distortions. CNN, with the automatic feature extraction ability, reduces the need for synthesizing a separate feature extractor. Thus, CNN with diminutive processing can learn good internal representation from raw pixels. Important attributes of CNN are hierarchical learning, automatic feature extraction, multi-tasking, and weight sharing [74]. In this study, we use the pre-trained CNN model *ResNet-50* using the *add-16* features layer, *DenseNet-201* using *fc1000* features layers, and a bag of the feature for the feature extraction process.

3.5 Classification

In this step, the image is classified as either coronary artery stenosis present or normal according to the features. There are lots of classifier techniques, such as linear discriminate analysis (LDA), convolutional neural network (CNN), and support vector machines (SVM). In this study, we use SVM and the CNN classifiers.

3.5.1 SVM Image Classification

The SVM classification technique is used to obtain the classification under two categories, coronary artery stenosis, either present or normal of the coronary CTA images. Algorithm 3.11 shows the SVM algorithm.

Input*: training dataset D*

       Minimum number of individuals `minobj` *for a split to be tried*

       hyper-parameter of RBF kernel function γ

       C for tuning margin and errors of SVMs

Output:

       tSVM model

       /*Decision tree algorithm partitions the full dataset D;*/

       learning a tree t for splitting the full dataset D into k partitions

       denoted by $D_1, D_2,..., D_k$ (using the early stopped parameter main obj)

       #pragma `omp` *parallel for*

       for *i ← 1 to k* **do**

          if *Di is impurity* **then**

              /*learning a local SVM model from the impurity terminal-node

              Di;*/

> $lSV\ M_i = SVM(D_i,\ \gamma,\ C)$
> **else**
> > $lSVMi\ isassignedthepluralitylabelin\ Di\ withoutanytraining$
> **end if**
> **end for**
> **return** $tSVM - model = tree\ t\ and\ \{lSV\ M1, lSV\ M2, ..., lSV\ Mk\}$

Algorithm 3.11: SVM algorithm [56].

3.5.2 CNN Image Classifier

Artificial Neural Network (ANN) has been studied for many years to solve complex classification problems including image classification. The distinct advantage of a neural network is that the algorithm could be generalized to solve different kinds of problems using similar designs. Convolutional Neural Network (CNN) is a successful implementation of ANN. CNN has been proved very successful in solving image classification problems. CNN significantly improved the best performance for many image databases [75].

Phase I of the Algorithm 3.12 is the training of CNN. A gradient method is used to update the weights in all the layers [76].

> **Phase I   Conventional Phase**
> > *Initialize all weights and biases of the CNN to a small value.*
> > *Set learning rate Ω such that $0 < \Omega < 1$*
> > *n= 1*
> > *repeat*
> > **for** *m=1 to M do*
> > *propagate pattern x_m through the network*
> > > **for** *k= 1 to the number of neurons in the output layer*
> > > > *Find error*
> > > **end for**
> > > **for** *layers L-1 to 1 do*
> > > > **for** *maps j = 1 to J do*
> > > > *find error factor to be back propagated*
> > > > **end for**
> > > **end for**
> > > **for** *i=1 to L do*
> > > > **for** *j=1 to J do*
> > > > > *for all weights of map, j do*
> > > > > *Find Δw*
> > > > > *Update weights and biases*
> > > > > *w(new) = w(old) + Δw*

> *end for*
>
>   *end for*
>
>   *end for*
>
>   *n = n + 1*
>
>   *Find Mean Square Error (MSE1)*
>
>   *Until MSE1< or n > maximum bounds*
>
> **Phase II** **Transfer Knowledge Phase**
>
>   *repeat*
>
>   **for** *tk= 1 to TK (number of new training samples)*
>
>   *propagate pattern x_{tk} through the network*
>
>   **for** *z= 1 to the number of neurons in the last convolutional*
>
>   *layer(Z)*
>
>   *find output O^z of last layer of the convolutional layer.*
>
>   *$O^z = (O^1, O^2, O^3 \ldots O^Z)$*
>
>   *Find O^{ztk} using TSL framework*
>
>   **end for**
>
>   **end for**
>
> **Phase III** **Weight Update learning phase for transfer learning phase**
>
>   *n=1*
>
>   *repeat*
>
>   **for** *tk= 1 to TK*
>
>   *Train the feedforward layers (Layers after last convolutional layer) using O^{ztk}*
>
>   *available in Phase II. Gradient Descend algorithms can be used.*
>
>   **end for**
>
>   *n = n+1*
>
>   *Find MSE2*
>
>   *Until MSE2< ϵ or n > maximum bounds*

Algorithm 3.12: Three-phase training algorithm for CNN architecture [76].

$$W(new) = W(old) - \alpha(\partial\, E(W)/\partial W) + O, \qquad\qquad (3.6)$$

Phase II of the algorithm is only used when new training samples are available. The issue is to incorporate the information available. The issue to incorporate the information available from the new samples into the trained network [76]. This issue is solved by the Phase II step of the algorithm. In this phase output, O^z of the last CNN layer is tapped and reweighted or updated using equation (3.6) to get a new vector O^{ztk} for each training sample. In Phase III step of the algorithm, is trained with O^{ztk} as training vectors for the classification task [76].

3.6 Stenosis Shape Description

If the classification results show the presence of stenosis, further processing is performed to detect and quantify the area of stenosis. To this ends the following tasks are performed.

3.6.1 Centerline Extraction

After selecting the ROI (blocked area of the vessel), extract the centerline. Centerline approaches have been widely applied to analyze images of *tubular structures* in the human body such as blood vessel analysis, stenosis detection. The vessel centerline extraction is an essential step for the quantitative analysis of coronary artery stenosis. Centerline extraction provides information about the location and shape of the coronary artery by marking its center points, which allows measuring several shape features. The centerline extraction of the arteries from the segmented surface obtained in the segmented coronary artery image is the most popular and fast marching based method [31], [3]. The gradient vector flow field and fast marching based method for centerline computation of coronary arteries is used which is an optimized fast marching algorithm. The approach utilizes the Gradient Vector Flow (GVF) filed based speed image of the vessel model and implements a wave front propagation technique for centerline branch tracking [77]. The details of centerline extraction for the coronary artery are shown in Algorithm 3.13.

Input: *Region of interest result I*
Output: *Final centerline S_f.*
 $S_f = \emptyset$, linelength $= \infty$
$P_s = arg\ max_x \xleftarrow{k}(x)$
$i = 0$
while *linelength $> L$* ***do***
        $T = FastMarching(P_s, F)$
        $m_i = x \mid T(x) \geq T(y)\ \forall x,y \in O$
        $S = backtrace(m_i, P_s)$
        $linelength = length(S)$
        $P_s = P_s + S,\ S_f = S_f + S$
        $i = i + 1$
 end while

Algorithm 3.13: Centerline extraction [77]

3.6.2 Coronary Artery Cross-Section Diameter Computation

The diameter calculation process is performed for the cross-section center point. At first, the plane-fitting procedure is done, and then the cross-sectional diameter calculated. Finally, the expected diameter is calculated, based on centerline points.

The purpose of the plane fitting is obtaining the area of the cross-section that is estimated by the intersection of plane and centerline. Hence, those voxels satisfying equation (3.7) are considered. If (x_c, y_c, z_c) is a centerline point coordinate, and (n_x, n_y, n_z) is the orthogonal vector to the plane, and (x, y, z) is a point equation is given by [78]:

$$n_x(x - x_c) + n_y(x - y_c) + n_z(x - z_c) = 0 \tag{3.7}$$

To calculate the orthogonal vector to plane, the mean of vectors, which is orthogonal to the plane in a centerline point neighborhood is calculated using [78].

$$VN = \frac{\sum_{i=1}^{n_v} V_i}{n_v}, V_i. V_c \neq 0 \tag{3.8}$$

Where VN is the mean of orthogonal vectors to the plane, n_v is the number of points in the neighborhood of the centerline point, v_i is the eigenvector corresponding to the smallest eigenvalue for the ith element on artery, and v_c is the eigenvector of the smallest eigenvalue for centerline point voxel. As the plane is not completely perpendicular, a threshold (T) is used using and equation (3.7) convert to equation (3.9) as follows[78]:

$$n_x(x - x_c) + n_y(x - y_c) + n_z(x - z_c) \leq T \tag{3.9}$$

The estimation of cross-sectional diameter (D) is calculated (using).

$$D = 2 X \frac{\sum_{i=1}^{n_v} \sqrt{(x_i - x_c)^2 + (y_i - y_c)^2 + (z_i - z_c)^2}}{n_v} \tag{3.10}$$

Where (x_i, y_i, z_i) is the coordinates of a point on vessel cross-section, (x_c, y_c, z_c) is the coordinates of the centerline point on vessel cross-section, n_v is the number of voxels neighboring to the centerline point on vessel cross-section.

3.6.3 Coronary Artery Disease (Stenosis) Amount

Using the obtained diameter and the expected diameter from the previous stage, the percentage of coronary artery stenosis is calculated using equation 3.11. The difference between the

obtained diameter and the expected diameter is estimated. The coronary stenosis is confirmed if there is greater than or equal to 50% narrowing in the vessel cross-sectional diameter [31], [3], [78],

$$Stenosis\ amount = [1 - \frac{DS}{Dn}]\ X\ 100 \qquad (3.11)$$

Where, *DS* is the expected vessel diameter, and *Dn* is the obtained diameter with the help of equation 3.11.

3.7 Evaluation

There are several evaluation tools to assess a classifier; amongst them, the accuracy, error rate, sensitivity, specificity, false-positive rate, false-negative rate, and precision are based on the confusion matrix.

3.7.1 The confusion matrix

The confusion matrix contains information about actual and predicted classification done by a classification system. The confusion matrix is a specific table visualizing the performance of the proposed algorithm of the classifier. A decision for the detected result can be either correct (true) or incorrect (false). As described in section 1.4.2, the decision will be one of four possible categories: true positive (TP), true negative (TN), false positive (FP), and false-negative (FN). The correct decision is the diagonal of the confusion matrix. Table 3.1 provides an example of the confusion matrix for two (stent absent or present) classes classification.

Table 3.1: A confusion matrix example.

		Predicted class label	
		Absent	**Present**
Actual class label	**Absent**	True Negative (TN)	False Negative (FN)
	Present	False Positive (FP)	True Positive (TP)

Accuracy (AC)

The accuracy is the total number of all correct predictions, TP and TN divided by the total number of the dataset. The best accuracy rate is 1.0, and 0.0 is the worst rate.

$$accuracy\ (AC) = \frac{TP + TN}{TN + FP + FN + TP} \tag{3.12}$$

Error Rate (ERR)

The error rate is the number of all incorrect predictions, FP and FN divided by the total number of the dataset. The best error rate is 0.0, and 1.0 is the worst rate.

$$ERR = \frac{FP + FN}{TN + FP + FN + TP} \tag{3.13}$$

Sensitivity

Sensitivity also called True Positive Rate (TPR) is the number of TP divided by the total number of positives in the data set, which is a TP and FN.

$$sensitivity = \frac{TP}{TP + FN} \tag{3.14}$$

Specificity

Specificity also called True Negative Rate (TNR) is the number of correct negative predictions divided by the total number of negatives, TN and FP.

$$specificity = \frac{TN}{TN + FP} \tag{3.15}$$

False Positive Rate (FPR)

The false-positive rate is the number of incorrect negative predictions divided by the total number of negatives, FP and TN. The ideal false positive rate is 0.0, and the worst is 1.0.

$$FPR = \frac{FP}{TN + FP} \tag{3.16}$$

False Negative Rate (FNR)

The false-negative rate is the number of incorrect positive predictions divided by the total number of negatives, FN and TN. The best false negative rate is 1.0, and the worst is 0.0.

$$FNR = \frac{FN}{FN + TP} \tag{3.17}$$

Precision

Precision positive prediction is the number of correct positive predictions divided by the total number of positive predictions, TP and FP. The best precision is 1.0, and the worst is 0.0.

$$precision = \frac{TP}{TP + FP} \tag{3.18}$$

3.8 Summary

In this chapter, the proposed framework is discussed in detail. The detection from coronary CTA images identifies either the normal or present of coronary artery stenosis with the image. In addition, we present the way to identify which parts of the coronary artery are infected by the disease and measure the coronary stenosis attribute of the coronary CTA images using vessel image and have the analysis. The analysis of CTA images is detected by the concern of adapting secondary treatments such as vessel attributes to extract information of interest. In the next chapter, the experimentation and its procedure are presented.

Chapter Four
Experimentation of CAD Detection and Quantification

4.1 Overview

This chapter shows the experiments carried out to construct a model with their analysis. This experimental evaluation ensures the realization of the proposed framework architecture of CAD detection and quantification. The experiments were carried out using the prototype developed and tested with MATLAB R2019a on a PC of Intel (R) Core (TM) i5-7200U CPU with 2.50GHz, 2.60GHz speed, 4 GB of RAM, 1TB of Hard Disk capacity, with 64-bit Windows 7 operating system.

In the subsequent, the procedures and the results are discussed as follows. First preprocessing and selecting the best filtering and enhancement algorithm. Secondly, using a filtered image with the selected filter and enhancement algorithms, run segmentation algorithms and select the best one. Thirdly, based on the result of better segmentation algorithm extract features for classification. Again, select the best features for classifications purpose. Finally, compare classification algorithms and select the best model.

4.2 Dataset Preparation

Sample coronary artery image data are taken from Digital Imaging and Communications in Medicine (DICOM) header of coronary CTA images. The coronary CTA image is collected from the MCM General Hospital, Gesund Cardiac and Medical Center, and St. Peter Specialized Hospital. The images were selected from each coronary CTA scan and save in the "JPG" image format using a Philips DICOM viewer. Thus, images consist of 123 with stenosis present and 123 without stenosis present (normal). Using the reference standard for stenosis detection. Lesions with a diameter reduction of 50% or more were considered representative of automatically significant stenosis [3]. Artery images without or with an increment of 50% were considered representative of an automatically normal artery. Thus, physician reading and labels each image as stenosis present and normal and quantify the stenosis attributes for a 10-sample image.

The data were partitioned randomly into training and testing sets. For training classifiers, 70% of the data is used. The remaining 30% were used for testing. As this is a supervised

effort, the training data is labeled into coronary artery stenosis present (1) or normal (0). These classes and the number of images used for each in the training process are shown in Table 4.1.

Table 4.1: Description of a data set

No.	Source	Resolution	Image format	Number of Patients	Image type		Quantity
					Stenosis present	Normal	
1	MCM Genera Hospital	Horizontal 96 dpi x Vertical 96 dpi	jpg	37	80	80	160
2	Gesund Cardiac and Medical Center	Horizontal 96 dpi x Vertical 96 dpi	jpg	11	24	24	48
3	St. Peter Specialized Hospital	Horizontal 96 dpi x Vertical 96 dpi	jpg	9	19	19	38
Total				57	123	123	246

4.3 Image Preprocessing

The noisy images first need to be cleaned by using some preprocessing steps including image filtering, enhancement, and binarization techniques. In this part, we describe each part of the pre-processing procedure that is applied at the initial stage of the proposed methods. To select the best contribution of pre-processing techniques four experimental scenarios are conducted as presented in Table 4.2.

Table 4.2: Four experimental scenarios of pre-processing tasks.

Scenario	Preprocessing tasks
1	Image filtering and image enhancement
2	Image filtering, image enhancement, and image filtering
3	Image enhancement and image filtering
4	Image filtering, image enhancement, and image binarization

4.3.1 Image Filtering

MATLAB is used to apply image filtering techniques in order to enhance the quality of each image by removing noises. As an example, Figure 4.1 shows a sample input image read by MATLAB using the built-in *imread()* function for image filtering.

(A)   (B)
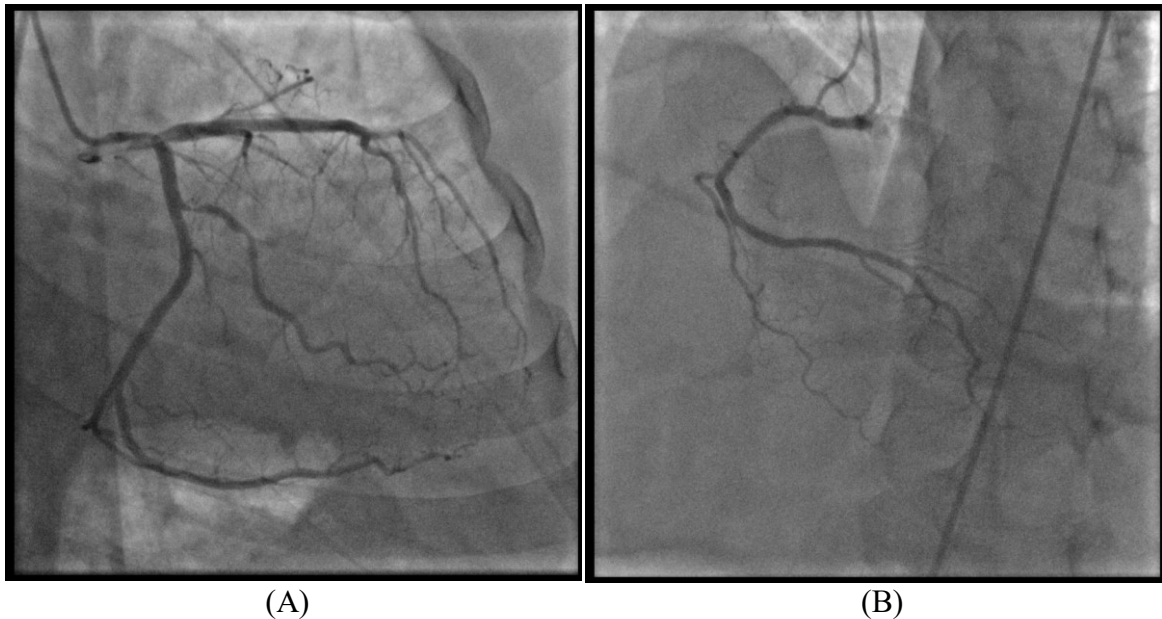
Figure 4.1: Examples of input: (A) Left and, (B) Right coronary artery image.

(A)   (B)
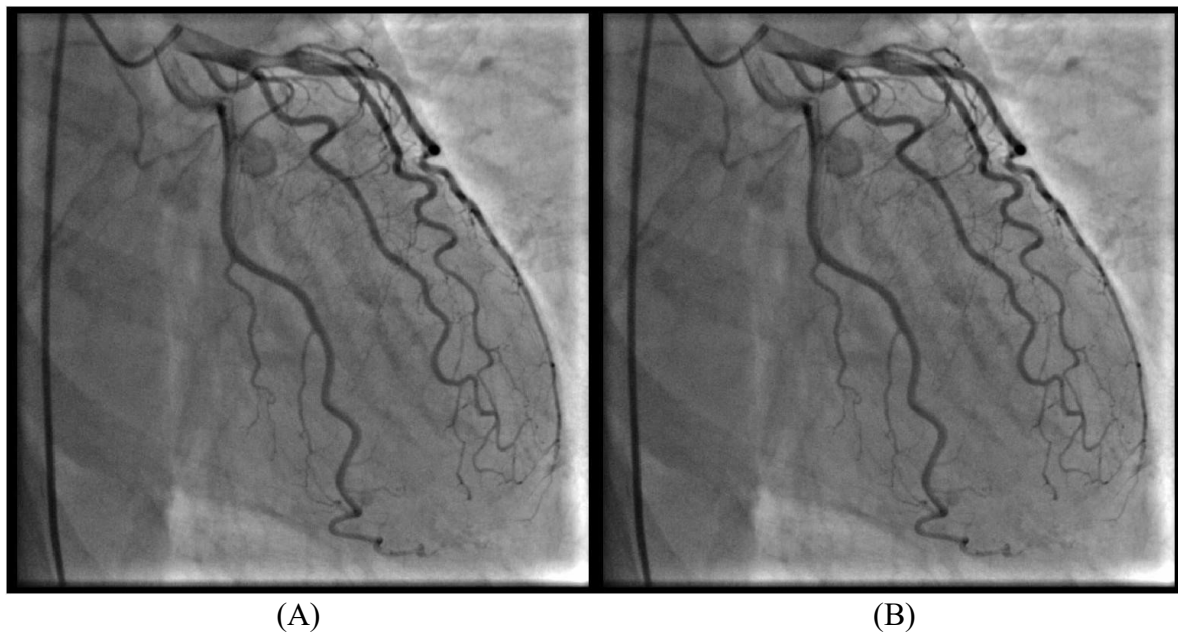
Figure 4.2: (A) Input, original image, (B) Output, Non-local Means filtered image.

The performance of image filtering is evaluated by estimating quality metric parameters such as Peak Signal to Noise Ratio (PSNR), Perception-Based Image Quality Evaluator (PIQE), Entropy, and Mean-Squared Error (MSE). Peak Signal to Noise Ratio (PSNR) is used to measure the quality of a reconstructed image. PIQE calculates the no-reference image quality score for the image using a perception-based image quality evaluator. PIQE can measure the quality of images with arbitrary distortion [79]. Entropy is a statistical measure of randomness that can be used to characterize the texture of the input image. MSE measures the average squared difference between actual and ideal pixel values. This metric is simple to calculate but might not align well with the human perception of quality [79].

We have experimentally compared, the different edge-preserving filtering such as bilateral filtering, guided filtering, and non-local filtering method are used (see Annex A for implementation detail). All experiments have been simulated on five sample images. The objective is to compare the quality of the restored images. Finally, Table 4.3 shows the image quality metric parameters for denoising experiments.

Table 4.3: Comparative performance of edge-preserving filtering on five samples.

Sample image	Original image		Bilateral Filtering Method				Guided Filtering Method				Non-local Means Filtering Method			
	PIQE	Entropy	PSNR	PIQE	Entropy	MSE	PSNR	PIQE	Entropy	MSE	PSNR	PIQE	Entropy	MSE
Image 1	24.702	7.099	42.244	55.021	7.104	3.878	36.251	64.791	7.126	15.416	71.512	24.589	7.094	0.004
Image 2	22.735	7.230	42.286	41.150	7.227	3.841	37.063	62.965	7.217	12.787	75.138	22.693	7.229	0.002
Image 3	18.788	6.406	42.633	48.492	6.384	3.546	37.104	69.683	6.412	12.664	69.131	18.365	6.400	0.007
Image 4	24.688	6.868	42.677	45.447	6.852	3.510	36.980	65.843	6.889	13.033	74.245	25.034	6.867	0.002
Image 5	17.922	6.943	42.400	38.972	6.906	3.741	36.661	73.439	6.868	14.026	76.950	17.922	6.943	0.001

From the table, it is found that the image quality metric parameters of non-local means filtering achieve better quality images compared to the other edge-perspective filtering. As shown in Figure 4.2 thus filtering applies a non-local mean to the original image.

4.3.2 Image Enhancement

The image enhancement technique produces better image quality values for an enhanced image. Image enhancement was done using histogram equalization, adaptive histogram equalization, and enhancing local contrast by transforming the grayscale image. We employ image enhancement using different scenarios, the first scenario (scenario 1) is on the original image and the second scenario (scenario 3) on the filtered image.

| (A) | (B) |
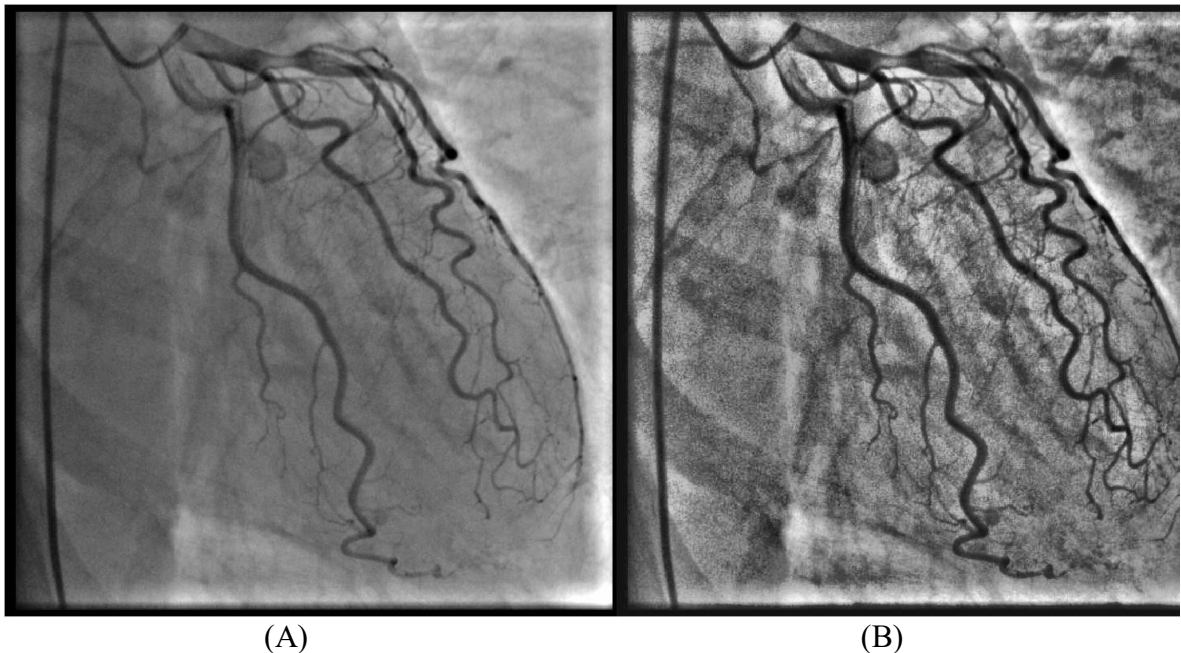
Figure 4.3: (A) Input, Filtered image, (B) Output, Enhanced image using AHE

Experimental results of the image enhancement method on the original image are compared using Perception-based Image Quality (PIQE) and Blind/Reference-less Image Spatial Quality Evaluator (BRISQUE). The algorithm and quality metric parameters estimation are figured out in Annex C. The summary of coronary CTA image enhancement results in the original image is presented in Table 4.4.

Table 4.4: Comparative performance of image enhancement in five samples.

Sample image	Original Image		Histogram Equalization		Adaptive Histogram Equalization		Edge-aware local contrast	
	PIQE Score	BRISQUE	PIQE Score	BRISQUE	PIQE Score	BRISQUE	PIQE Score	BRISQUE
Image 1	23.7023	32.6771	21.8450	26.5232	21.2179	10.5657	16.6608	25.4551
Image 2	21.9913	21.7876	17.9467	20.6143	17.6041	11.6711	16.4171	14.6711
Image 3	12.1512	15.0851	15.2819	18.7622	15.5016	28.5362	12.0645	27.2443
Image 4	17.9942	33.8825	17.1561	17.2821	11.8410	25.0407	14.1734	22.5373
Image 5	11.0768	16.4308	13.7305	16.3355	15.4663	24.1236	9.3523	26.7296

As shown in the above Table 4.4 adaptive histogram equalization gives better results.

We also experimented with image enhancement methods after applying non-local mean filtering. For detailed of the algorithm and quality metrics parameters estimation, one can refer to Annex A. The quality estimation metrics on five sample images are shown in Table 4.5.

Table 4.5: Comparative performance of image enhancement after filtering in five samples.

Sample image	Original Image		Non-Local mean filtering			Image Enhancement								
						Histogram Equalization			Adaptive Histogram Equalization			Edge-aware Local Contrast Enhance		
	PIQE Score	BRIS QUE	PIQE	BRIS QUE	PSNR	PIQE	BRIS QUE	PSNR	PIQE	BRIS QUE	PSNR	PIQE	BRIS QUE	PSNR
Image 1	24.702	19.726	24.590	30.664	71.513	22.834	14.362	15.444	21.864	8.719	18.110	18.322	17.573	33.059
Image 2	22.736	24.423	22.694	24.901	75.138	18.566	20.299	14.715	18.563	14.007	16.129	17.763	10.148	32.771
Image 3	18.789	16.831	18.365	19.416	69.131	17.132	20.246	13.099	14.777	25.263	19.581	15.356	13.496	33.700
Image 4	24.688	26.977	25.034	27.505	74.246	19.272	12.853	14.766	19.921	43.006	18.608	20.101	19.159	33.340
Image 5	17.922	26.749	17.923	26.064	76.951	17.141	16.034	15.836	12.242	23.176	16.776	14.420	27.043	33.655

As shown in Table 4.5 above, each image enhancement method has its own importance in evaluating quality. Adaptive histogram equalization has been giving much better results than the existing ones as shown in Table. Figure 4.3 shows the enhanced image using adaptive histogram equalization on the filtered image.

The classification accuracy of scenario 1 image filtering and image enhancement pre-processing is evaluate using SVM and CNN classifier. The classification result of the SVM classifier using the statistical feature is 0.472 (47%) and a bag of features is 0.71 (71%). CNN classifier result using "ResNet-50" pre-trained network layers and "add-16" features is 0.713 (71%) and using the "DenseNet-201" pre-trained network layers and "fc1000" features is 0.658 (65%).

In scenario 2 after non-local mean filtering and adaptive Histogram Equalization, we experimented with Wiener Filtering, Median Filtering, and Non-local Means Filtering (see Annex B). The quality estimation metrics on five sample images are shown in Table 4.6.

Table 4.6: Comparative performance of image filtering after filtering and enhancement.

Sample image	Original Image		Non-local Means Filtering Method		Adaptive Histogram Equalization		Image Filtering					
							Wiener Filtering		Median Filtering		Non-local Means Filtering	
	PIQE	Entropy	PIQE	Entropy	PIQE	Entropy	PIQE	Entropy	PIQE	Entropy	PIQE	Entropy
Image 1	24.702	7.099	24.589	7.094	21.864	7.449	68.785	7.421	33.163	7.404	25.306	7.456
Image 2	22.735	7.230	22.693	7.229	18.563	7.562	62.777	7.510	28.474	7.522	22.943	7.564
Image 3	18.788	6.406	18.365	6.400	14.777	7.140	65.008	7.081	21.992	7.062	15.075	7.153
Image 4	24.688	6.868	25.034	6.867	19.921	7.244	58.428	7.188	28.934	7.169	22.173	7.254
Image 5	17.922	6.943	17.922	6.943	12.241	7.259	51.967	7.140	17.919	7.184	13.685	7.258

As shown in the above Table 4.6 non-local means filtering gives better results.

The classification accuracy of Scenario 3 image filtering, enhancement, and filtering preprocessing is evaluate using SVM and CNN classifier. The classification result of the SVM classifier using the statistical feature is 0.472 (47%) and a bag of features is 0.723 (72%). CNN classifier result using "ResNet-50" pre-trained network layers and "add-16" features is

0.694 (69%) and using the "DenseNet-201" pre-trained network layers and "fc1000" features is 0.608 (60%).

In scenario 3, we experimented with the image filtering method after applying adaptive histogram equalization. The adaptive histogram is selected image enhancement technique after comparing image enhancement on the original image as shown in Table 4.4. Table 4.7 shows the quality estimation metrics of image filtering after image enhancement on five sample images.

Table 4.7: Comparative performance of image filtering after enhancement in five samples.

Sample image	Original Image		Adaptive Histogram Equalization		Image Filtering					
					Wiener Filtering		Median Filtering		Non-local Means Filtering	
	PIQE Score	Entropy	PIQE Score	Entropy	PIQE Score	Entropy	PIQE Score	Entropy	PIQE Score	Entropy
Image 1	24.702	7.100	22.511	7.453	67.795	7.430	33.100	7.407	25.548	7.463
Image 2	22.736	7.231	18.8338	7.563	62.957	7.510	28.706	7.523	22.851	7.566
Image 3	18.789	6.407	14.766	7.149	64.014	7.088	22.862	7.067	15.792	7.167
Image 4	24.688	6.868	19.654	7.245	58.917	7.190	29.200	7.169	21.594	7.259
Image 5	17.922	6.944	12.256	7.259	52.297	7.140	18.086	7.185	13.733	7.259

The classification accuracy of Scenario 4 image enhancement and filtering pre-processing is evaluate using SVM and CNN classifier. The classification result of the SVM classifier using the statistical feature is 0.472 (47%) and a bag of features is 0.727 (72%). The result of the CNN classifier using "ResNet-50" pre-trained network layers and "add-16" features is 0.696 (69%) and using the "DenseNet-201" pre-trained network layers and "fc1000" features is 0.635 (63%).

Table 4.8: Summary of three image pre-processing scenarios classification result.

Scenarios	SVM Classifier		Convolutional Neural Network (CNN) Classifier	
			ResNet-50	DenseNet-201
	Statistical Features	CNN Features	add-16	fc1000
Scenario 1	0.472	0.710	0.713	0.658
Scenario 3	0.472	0.723	0.694	0.608
Scenario 4	0.472	**0.727**	0.696	0.635

To perform image binarization we use selected non-local means filtering and adaptive histogram equalization based on the estimating quality metric parameters and classification performance as shown in Table 4.8.

4.3.3 Image Binarization

A binary image is an image whose pixel values are changed to 1 and 0 or white and black. In this work, the blood vessels are extracted by assigning 0 to the blood vessels pixels and 1 to the non-vessel pixel. For image binarization, we applied global Otsu's thresholding and Local adaptive thresholding methods.

Otsu's threshold method computes a global threshold using the following MATLAB syntax, $T = otsuthresh(counts)$, where the global threshold T can be used with *imbinarize ()* to convert a grayscale image to a binary image, and *counts,* specified as a vector of non-negative numbers. Figure 4.4 shows the result of Otsu's thresholding method.
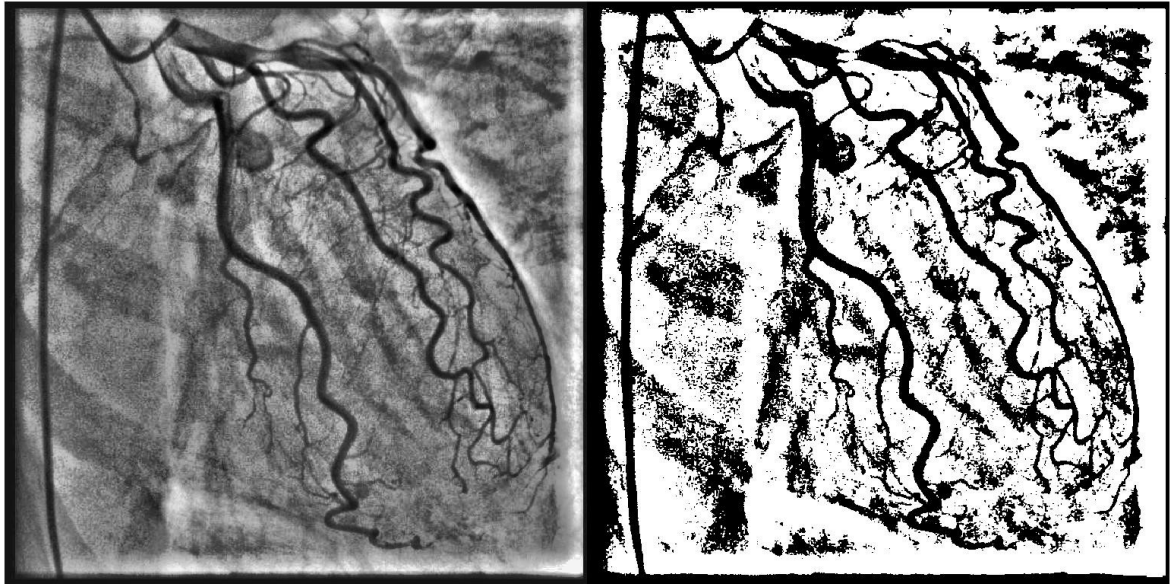
(A)   (B)

Figure 4.4: (A) Input, Filtered and enhanced image, (B) Output, Otsu's threshold image

The adaptive thresholding method computes a locally adaptive threshold for a 2-D grayscale image or 3-D grayscale volume using the syntax, $T = adaptthresh(I)$. The $adaptthresh$ function chooses the threshold based on the local mean intensity (first-order statistics) in the neighborhood of each pixel. The threshold T can be used with the *imbinarize (),* function to convert the grayscale image to a binary image. Further details of the algorithm and quality metric parameters estimation could be shown in Annex D. The output of the adaptive thresholding (0.6 sensitivity) method is shown in Figure 4.5 below.
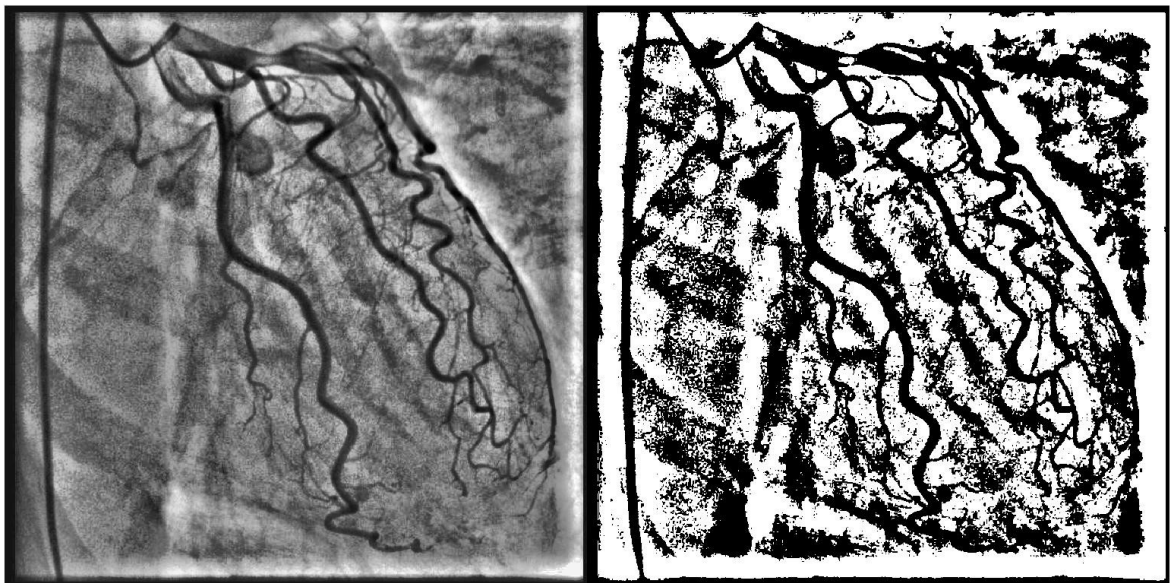
(A)   (B)

Figure 4.5: (A) Input, Filtered and enhanced and, (B) Output, Adaptive threshold image

In this study, image binarization is applied after performing image filtering and image enhancement. Otsu's thresholding and adaptive thresholding method are compared for image binarization based on visual analysis; it is observed binary image using Otsu's thresholding method loses some contents of the artery. As can be observed from Figure 4.4 and Figure 4.5, the adaptive thresholding method has full contents of the artery and have better performance in coronary CTA image binarization.

The classification accuracy of Scenario 2 image filtering, enhancement, and binarization is evaluate using SVM and CNN classifier. The classification result of the SVM classifier using the statistical feature is 0.513 (51%) and a bag of features is 0.67 (67%). The result of the CNN classifier using "ResNet-50" pre-trained network layers and "add-16" features is 0.617 (61%) and using the "DenseNet-201" pre-trained network layers and "fc1000" features is 0.586 (58%).

*Table 4.9: Summary of four image pre-processing scenarios classification results.*

Scenarios	SVM Classifier		Convolutional Neural Network (CNN) Classifier	
			ResNet-50	DenseNet-201
	Statistical Features	CNN Features	add-16	fc1000
Scenario 1	0.472	0.710	0.713	0.658
Scenario 2	0.513	0.670	0.617	0.586
Scenario 3	0.472	0.723	0.694	0.608
Scenario 4	0.472	**0.727**	0.696	0.635

The image segmentation is implemented on selected pre-processing steps, scenario 3 (image enhancement and image filtering) pre-processing task is selected based on the estimating quality metric parameters and classification performance. The summary of the image pre-processing classification result is shown above Table 4.9.

4.4 Image Segmentation

Image segmentation is used to divide an image into parts having similar features and properties. Segmentation has been performed on 246 coronary CTA Images. Thus, the identified ROI using image segmentation is considered as artery structures. Effective treatment for vascular disease is done based on the visualization of the vessels. For many clinical procedures like bypass surgery and stenting, require the visualization of vessels [3]. In order to segment the arteries from the coronary CTA image, we use region-based segmentation method and gradient magnitude as the segmentation function.

4.4.1 Region Growing Artery Segmentation

One of the segmentation algorithms applied in this study is segmentation by growing a region from seed point using a mean measure. The region is iteratively growing by comparing all unallocated neighboring pixels to the region. To illustrate the region growing segmentation we use the next an M-function, called *regiongrow*. The syntax for this function is

J= regiongrowing(I,x,y,reg_maxdist)

Where *I* is an image to be segmented, *J* logical output image of the region, *x* and *y* are the positions of the seed point, and *reg_maxdist* is the maximum intensity distance. Figure 4.6 (B) shows that the region growing segmentation result with 0.4 maximum intensity distance.

<center>(A)   (B)</center>
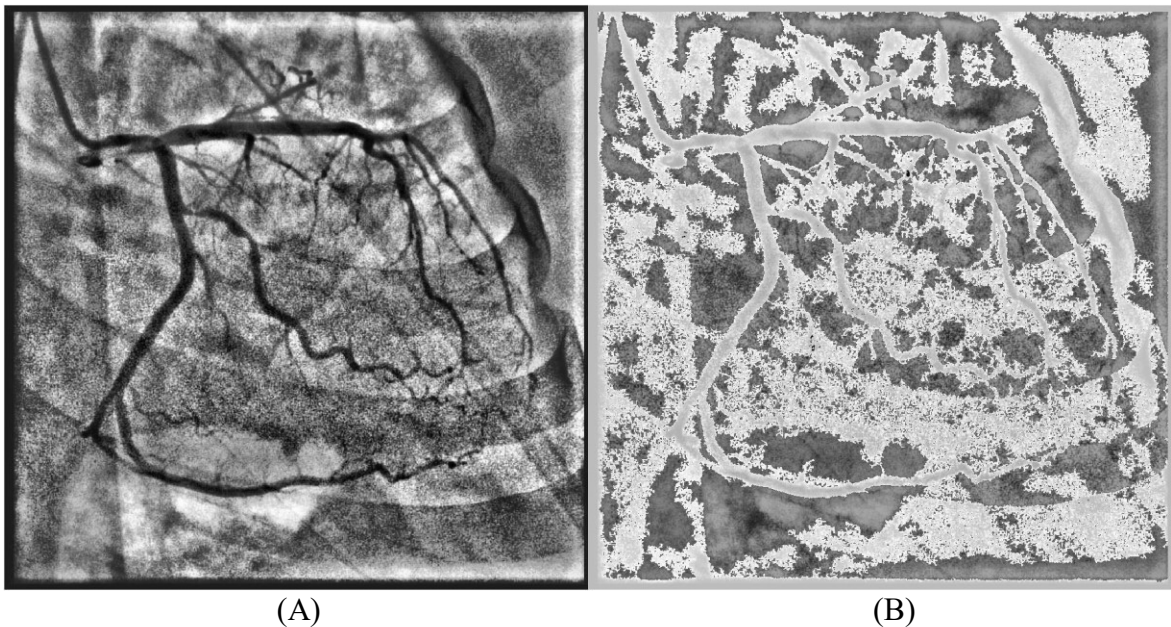
Figure 4.6: (A) Input, enhanced and filtered (B) Output, Segmented image

4.4.2 Artery Segmentation Using Gradient Magnitude Edge Detection

The study also uses the gradient magnitude as the segmentation function to split the image into objects that are identical. The gradient is high at the borders of the objects and low (mostly) inside the object. Gradient magnitude using *gmag = imgradient(I);* returns the gradient magnitude, *gmag,* of the grayscale or binary image *I*. Figure 7.4 (A) shows segmented image using a gradient magnitude edge detection method and Figure 4.7 (B) shows the segmentation result using a Sobel gradient magnitude.

(A)   (B)
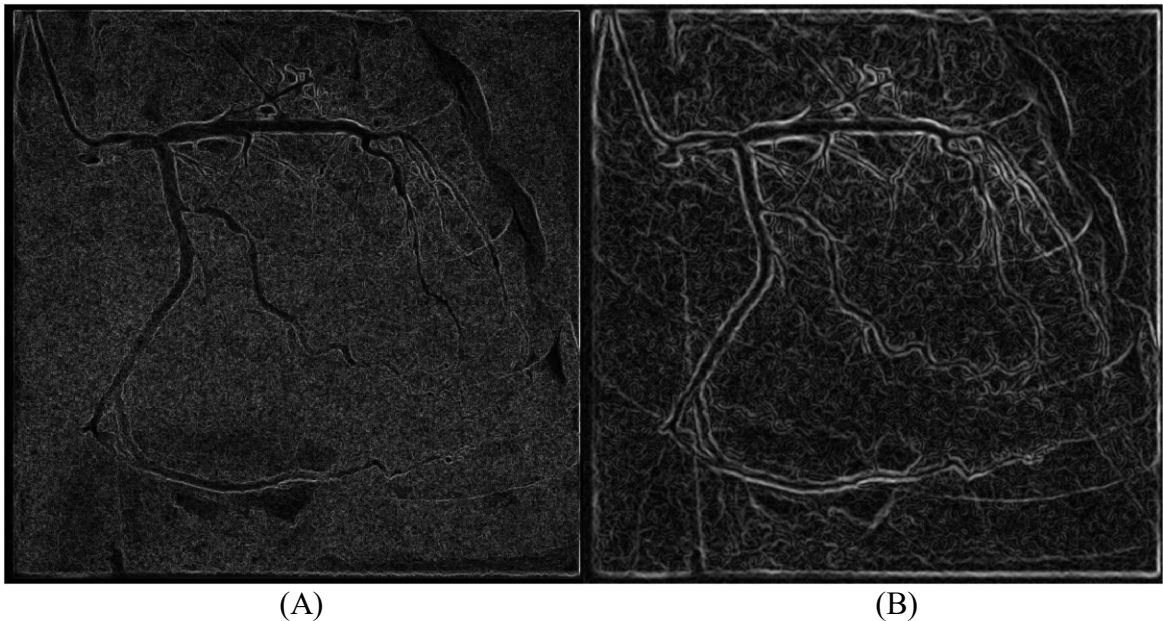
Figure 4.7: (A) Segmented image using a gradient and (B) Sobel-gradient magnitude

The accuracy of segmenting coronary CTA images is done through the help of comparison by visual inspection. For the experimental evaluation, five sample images are used. The selection of samples was based on the criteria that enabled to ensure how the proposed algorithm is an accurate estimator of coronary stenosis present or normal. The samples are chosen considering the images stenosis are present and normal.

Hence, region growing segmentation and Sobel-gradient magnitude edge detection-based segmentation are compared. Sobel-gradient magnitude edge detection based coronary CTA image segmentation achieve better ROI segmentation relative to the region growing

Scenario 5 uses image enhancement, image filtering pre-processing, and image segmentation steps and implement on both SVM and CNN classifier using the following feature extraction. The classification result of the SVM classifier using the statistical feature is 0.567 (56%) and

a bag of features is 0.703 (70%). In addition, the classification result of the CNN classifier using "ResNet-50" pre-trained network layers and "add-16" features is 0.608 (60%) and using "DenseNet-201" pre-trained network layers and "fc1000" features is 0.581 (58%).

4.5 Feature Extraction of Coronary CTA Image

There are many techniques for the feature extraction step. In this study, for SVM classifier we use statistical feature and bag of feature and convolutional neural network (CNN) based feature extraction. Some layers within a CNN are suitable for image feature extraction. The layers at the beginning of the network capture basic image features, such as edges and blobs [80]. In this study, the following CNN based feature extractions are compared with statistical feature extractions. The *ResNet-50* pre-trained network using the *add-16* features layer as shown in Figure 4.8 and *DenseNet-201* pre-trained network using *fc1000* features layers shown in Figure 4.9 was retrained to distinguish between two classes and its parameters which were changed to classify coronary CTA image.

	1	2	3	4	5	6	7	8	9	10	11	12	13	14
1	-0.6134	-1.5036	-2.8456	-0.6372	-0.1714	0.0168	-1.6627	-3.6242	-1.7481	-0.3609	-3.1667	-1.2620	-0.4091	
2	-0.9464	-1.4011	-3.1275	-0.5434	0.1036	-0.3694	-1.3565	-3.5632	-2.1693	0.0278	-2.4718	-1.2530	0.3280	
3	-1.6063	-1.4259	-4.0359	-1.2787	-0.3532	-1.2828	-1.2727	-1.8583	-2.1059	0.4995	-2.9547	-1.5961	-0.5551	
4	-1.8543	-1.3906	-3.3128	-1.5128	-1.2327	-1.9080	-1.0688	-1.8325	-1.5810	-0.1916	-2.0697	-1.6060	-0.7354	
5	-1.8782	-1.8875	-2.1934	-1.4327	-1.7230	-1.9948	-1.5163	-1.9122	-1.5921	-0.8869	-1.9394	-1.7948	-0.8507	
6	-2.6894	-1.7114	-1.9721	-1.7753	-1.7750	-1.2100	-1.6355	-2.0739	-1.3767	-1.7681	-2.4624	-1.3956	-0.9143	
7	-2.1657	-0.8401	-1.4185	-1.6770	-1.6584	-1.3111	-1.7105	-2.1595	-1.6511	-2.2279	-2.5678	-0.9922	-1.3421	
8	0.9282	-1.7533	-2.3028	-0.2432	0.3761	-0.3328	-0.8657	-2.8257	-1.3583	0.6117	-1.8217	-0.9550	-0.0584	
9	-0.2275	-0.9864	-3.0457	-0.3028	-0.6105	-0.2494	-0.3939	-2.3024	-1.2325	0.7198	-1.1482	-0.0991	0.2565	
10	-1.6457	-1.1405	-3.2383	-0.4331	0.1902	-1.7985	-0.4756	-0.6901	-1.7891	1.6090	-1.1818	-1.4606	-0.0528	
11	-2.2014	-0.4181	-2.1816	-1.1753	-1.5661	-2.5804	-1.0914	-1.8112	-1.3558	1.4155	-1.6433	0.3006	0.2844	
12	-1.8668	-0.4630	-1.7224	-1.1165	-1.5164	-1.9348	-1.2864	-2.0441	-1.0824	0.2938	-1.7099	-1.5076	-0.4938	
13	-2.2843	-1.0834	-1.4814	-1.5164	-2.0721	-1.4141	-1.4402	-2.0452	-1.2396	-1.2666	-2.4267	-1.0304	-0.9047	
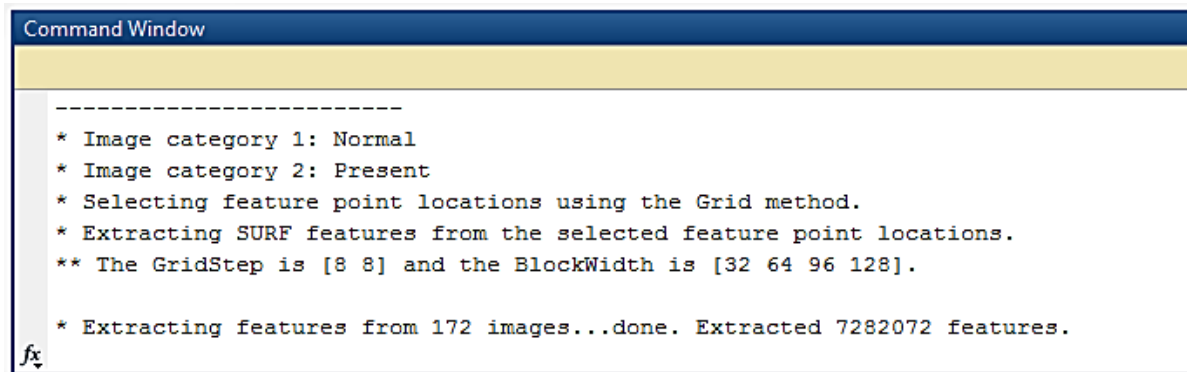
Figure 4.8: Sample screenshot results of the add-16 *features layer.*

	1	2	3	4	5	6	7	8	9	10	11	12	13	14
1	-1.4918	-1.6211	-1.3995	-0.2311	-0.4684	-0.4512	-1.3018	0.2630	-1.4133	-0.3329	-2.4127	-1.1003	-1.5143	-1.3
2	-1.7382	-1.9760	-1.3594	-0.4527	-1.2891	-1.7276	-2.6474	-1.9645	-1.6051	-2.2800	-1.0561	-2.0185	-3.3411	-3.1
3	-1.3392	-1.5151	-0.8566	-1.8572	-1.1415	-1.6143	-0.3527	-1.7926	-0.9547	-2.2128	-1.2997	-1.7555	0.0357	-1.7
4	0.5596	-0.5585	0.2524	0.0949	-0.7991	-0.4760	0.2467	0.2659	1.1734	0.3422	-1.0891	-0.1088	0.6391	0.8
5	0.3251	-0.9534	-0.5905	0.3810	-0.7345	-1.0456	-0.1032	0.2070	0.2477	-0.3955	-1.0545	-0.8262	1.0974	0.5
6	1.1858	-0.5282	-0.4945	-0.8650	-3.1651	-2.2966	-0.8394	-0.1347	0.2363	-0.2868	-0.4209	-0.6853	-0.1108	-0.4
7	-0.2409	-1.5338	-0.4746	-0.1329	-1.4670	-1.5729	-1.5094	-0.8826	-0.8396	-1.2236	-0.6752	-0.8631	-0.7790	0.8
8	-0.2768	0.2967	-0.4346	0.3678	-0.7396	-0.1288	-0.9262	0.2654	0.2690	0.0171	0.5107	0.1202	0.7437	-0.3
9	-1.6909	-0.9129	-1.2305	0.3872	-0.6775	0.1252	-1.5337	-0.0926	-1.0313	-0.7160	0.2336	0.0860	-0.4771	-1.1
10	-0.3232	1.4827	1.7135	2.4973	2.1762	2.2918	0.0975	1.2661	1.3239	1.1656	-0.3111	0.1223	1.3147	2.5
11	-3.6946	-3.2162	-3.3604	-1.7032	-4.2237	-3.7345	-4.1863	-2.7727	-2.7514	-3.6791	-2.2380	-2.7788	-4.2181	-5.0
12	-3.6724	-2.0790	-3.3153	-2.0547	-3.0997	-2.7813	-3.6696	-3.8226	-2.8870	-4.1347	-1.4071	-2.8008	-3.8115	-4.3
13	-3.0216	-2.7711	-3.6373	-2.4008	-2.6517	-2.6001	-2.8363	-3.2645	-2.5331	-3.7918	-2.0179	-3.0313	-3.0960	-4.7

Figure 4.9: Sample screenshot results of the fc1000 *features layer.*

4.5.1 Bag of Features

In this step, we use a bag of features approach for image category classification. This technique is also often referred to as a bag of words. Visual image categorization is a process of assigning a category label to an image under test. Categories contain images representing of coronary CTA image stenosis present and normal. The cardiologist reading each of coronary CTA images and label (normal as category 1 and stenosis present as category 2) was concatenated as shown in Figure 4.10, as an input to differentiate the two classes of the coronary CTA images.

```
Command Window

    ------------------------
    * Image category 1: Normal
    * Image category 2: Present
    * Selecting feature point locations using the Grid method.
    * Extracting SURF features from the selected feature point locations.
    ** The GridStep is [8 8] and the BlockWidth is [32 64 96 128].

    * Extracting features from 172 images...done. Extracted 7282072 features.
fx
```

Figure 4.10: Sample screenshot of the bag of features (BOF)

4.6 Coronary CTA Image Classification

In the previous section, the pre-processing and segmentation steps were described in detail. Then the classification was proceeded using a feature extraction method. In addition to these features, the cardiologist evaluates each of the coronary CTA images and labels (Normal as 0, and Stenosis present as 1).

There are two basic phases of pattern classification. They are training and testing phases. We have used the SVM and CNN classifiers, which uses a well-known algorithm to determine whether the coronary CTA image is normal or stenosis present membership in a given group, based on training data. Hence, we need to design the classifier by partitioning the data set into training and testing dataset. From the total dataset for both classifier SVM and CNN, 70% was used for training and to build a classification model and the remaining 30% of the total testing data was used for evaluation, which was selected randomly.

4.6.1 SVM Classifier

Support Vector Machines (SVMs) are widely used for classification tasks due to their excellent generalization properties and their computational efficiency. In this step, the coronary CTA image is classified as either normal or present stenosis according to the features. For SVM classifier we use statistical features extraction and using SVM trained with CNN features extracted from the images, bag of features is extracted using a CNN, we use these feature extractions for all scenarios.

Among the different types of SVM, we have used multiclass linear SVM classifiers for this study on the detection of CAD. The experimentation was conducted under the following five scenarios. As mentioned before, 70% of these datasets were used for training and 30% was used for testing purpose for each scenario.

The SVM Classification performance is evaluated based on the quality parameters such as Accuracy (AC), Error Rate (ERR), Sensitivity, Specificity, False Positive Rate (FPR), False Negative Rate (FNR), and Precision. The confusion matrix used to compute the quality parameter is defined in terms of combination of **number of stenosis present images correctly detected** (TP), **number of stenosis normal images correctly detected** (TN), **number of stenosis normal images wrongly detected** (FP), and **number of stenosis present images wrongly detected** (FN).

Table 4.10: The performance measure of the SVM classifier with BOF for all scenarios.

Scenarios	Ground Truth		Predicted class label				Performance Measure						
	Normal	Present	TN	TP	FP	FN	AC	ERR	Sensitivity	Specificity	FPR	FNR	Precision
1	37	37	0.43	0.93	0.07	0.57	0.68	0.32	0.62	0.86	0.14	0.38	0.93
2	37	37	0.50	0.92	0.08	0.50	0.71	0.29	0.65	0.87	0.13	0.35	0.92
3	37	37	0.66	0.77	0.23	0.34	0.72	0.27	0.66	0.85	0.14	0.33	0.90
4	37	37	0.71	0.62	0.38	0.29	0.66	0.34	0.68	0.65	0.35	0.32	0.62
5	37	37	0.40	0.96	0.04	0.60	0.68	0.32	0.61	0.90	0.10	0.39	0.96

All scenarios are computed accuracy measures for coronary CTA image-based classification using an SVM classifier. The experiments that were validated using a confusion matrix are shown in Table 4.10. The overall accuracy of a maximum accuracy is 72.7 %.

Table 4.11: The summary of SVM classifier accuracy with statistical and bag of features

Scenarios	SVM Classifier	
	Statistical Features	**CNN Features**
Scenario 1	0.472	0.710
Scenario 2	0.472	0.723
Scenario 3	0.472	**0.727**
Scenario 4	0.513	0.670
Scenario 5	0.567	0.703

When we using the statistical features the maximum accuracy of all scenarios was only 56%. This was achieved when scenario 5 image filtering, image enhancement, and image segmentation image processing tasks. Whereas, when using the CNN features extraction technique, the SVM classification accuracy reached 72.7%. This was achieved when scenario 3 image enhancement and image filtering image pre-processing tasks. A comparison between statistical features and CNN features of the SVM classifier on all scenarios are illustrated in Table 4.11.

We calculate the Accuracy (AC), Error Rate (ERR), sensitivity, specificity, false-positive rate (FPR), false-negative rate (FNR), and precision for scenario 3 image enhancement and image filtering pre-processing tasks, it was proved that the highest accuracy has all the other scenarios. The confusion matrix and the performance measure of scenario 3 shown in Table 4.12 and Table 4.13, respectively.

Table 4.12: The confusion matrix of scenario 3 SVM classification accuracy with BOF.

		Predicted class label		Total
		Normal	**Present (Stenosis)**	
Actual class label	**Normal (37)**	0.55	0.45	1
	Present (37)	0.10	0.90	1
Total		0.65	1.35	

Table 4.13: The performance measurement of scenario 3.

Performance Measure	Index
Accuracy (AC) = (0.90+0.55)/ (0.55+0.10+0.45+0.90)	0.727
Error Rate (ERR) = (0.10+0.45)/ (0.55+0.10+0.45+0.90)	0.273
Sensitivity = 0.90/ (0.90+0.45)	0.667
Specificity = 0.55/ (0.55+0.10)	0.851
False Positive Rate (FPR) = 0.10/ (0.55+0.10)	0.149
False Negative Rate (FNR) = 0.45/ (0.45+0.90)	0.333
Precision = 0.90/ (0.90+0.10)	0.903

For the image filtering, image enhancement, and image segmentation when using SVM image classification using CNN feature extraction achieved the highest values compared to the other image processing. Achieved the accuracy of 72.7%. Moreover, performance measurement is shown in Table 4.13.

4.6.2 Classification Using Deep Learning Convolutional Neural Network (CNN)

A Convolutional Neural Network (CNN) is a powerful machine learning and the most common neural network model from the field of deep learning. CNN's can learn rich feature representations for a wide range of images.

In this study, we evaluated two popular, widely used CNN architectures (ResNet-50 and DenseNet-201) which we use for training and transfer learning from coronary CTA image classification.

Table 4.14: Summary of all scenarios using CNN classifier

Scenarios	Pre-trained network (Architecture) and feature layer	
	ResNet-50	DenseNet-201
	add-16	fc1000
Scenario 1	**0.713**	0.658
Scenario 2	0.694	0.608
Scenario 3	0.696	0.635
Scenario 4	0.617	0.586
Scenario 5	0.608	0.581

The CNN classification technique with the pre-trained network ResNet-50 and DensNet-201 accuracy reached only 71.3 % maximum. This was achieved when extracting and classifying for all scenarios are illustrated in Table 4.14. Whereas, when attaching the CNN feature to the SVM obtain a better result, the accuracy with SVM was 72.7 %.

4.7 Stenosis Detection and Quantification

After completing the coronary CTA image classification, if the image was classified as present stenosis, the stenosis quantification process to be used. In this study, we proposed a semi-automatic detection and quantification of coronary artery stenosis from CTA images. For stenosis detection and quantification, we use the better one image pre-processing method stated previously. This process uses image enhancement and image filtering pre-processing. After completing the pre-processing and classification, we can introduce the following stenosis detection and quantification approach using image preprocessing techniques in the below steps.

- Select ROI by drawing a rectangle
- Extract ROI by cropping
- Draw centerline based on existing centerline
- Calculate angle θ
- Rotate by θ
- Measure stenosis length, maximum diameter (Dn), and minimum diameter (Ds)

- Calculate stenosis

## 4.7.1 Selecting and Extracting Region of Interest (ROI)

The stenosis quantification process starts by manually drawing a rectangle box on around the ROI (blocked area) of the vessel. A cropping rectangle is automatically drawn by assuming the initial point $P_1(x, y)$ and endpoint $P_2(x, y)$ are the left upper and right lower corners of the rectangle respectively. Then the centerline is extracted automatically based on the better centerline extraction method as discussed in the following section.

4.7.2 Extract Centerline of Artery

Identifying the center of the artery is for calculating the artery diameter in order to detect stenosis. Several techniques have been proposed for the centerline extraction of the skeleton of blood vessels. In this study, we used methods that are based on skeletonization and distance transformation for centerline extraction.

Centerline Extraction Based on Skeletonization Method

A skeletonization method extracts the centerline while preserving the topology and Euler number of the objects by reducing all objects to lines in a 2-D binary image. It reduces all objects in the binary image to 1-pixel wide curved lines, without changing the essential structure of the image. Skeletonization requires a binary image in which foreground pixels are 1 (white) and the background is 0 (black). To make the original image suitable for skeletonization, take the complement of the artery image so that the artery is light and the background is dark. Then, we perform skeletonization of the binary image using MATLAB function *bwskel ()*. The binarization is followed by pruning. Pruning small spurs that appear on the skeleton using *out=bwskel(BW, 'MinBranchLength', N);* where. The minimum branch length is specified as a non-negative integer. $bwskel$ () function prunes branch shorter than N as shown in Figure 4.11 (A). Finally, the skeleton (centerline) employs over the original image by using the $labeloverlay$ function as shown in Figure 4.11 (B).
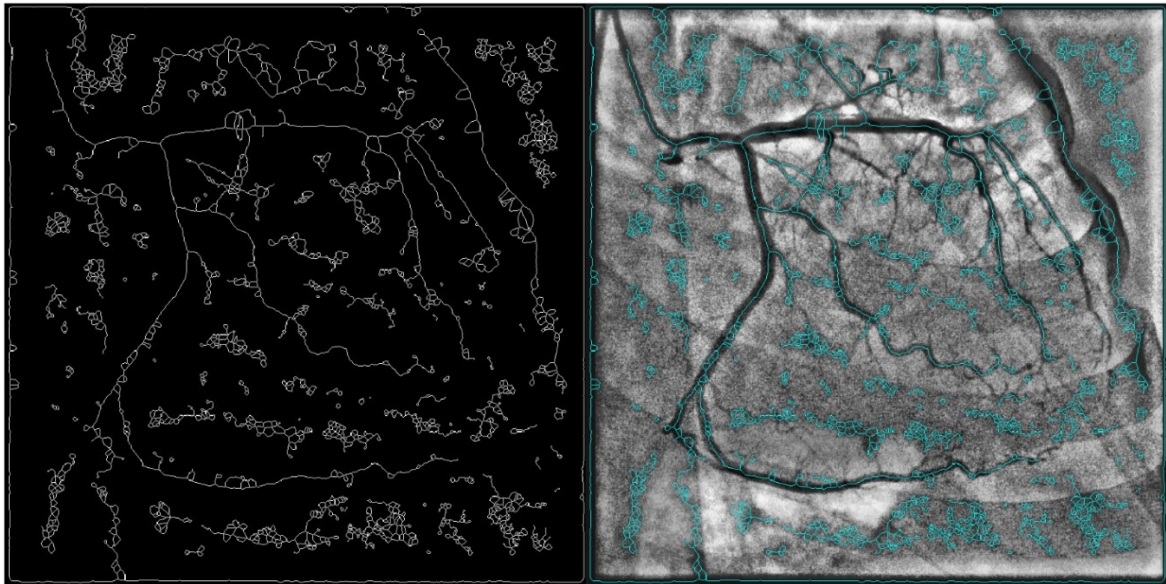
(A)   (B)

Figure 4.11: (A) Centerline, (B) Centerline over input image.

Centerline Extraction Based on Distance Transformation

The distance transform provides a metric or measure of the separation of points in the image. The *bwdist* function calculates the distance between each pixel that is set to off (0) and the nearest nonzero pixel for binary images.
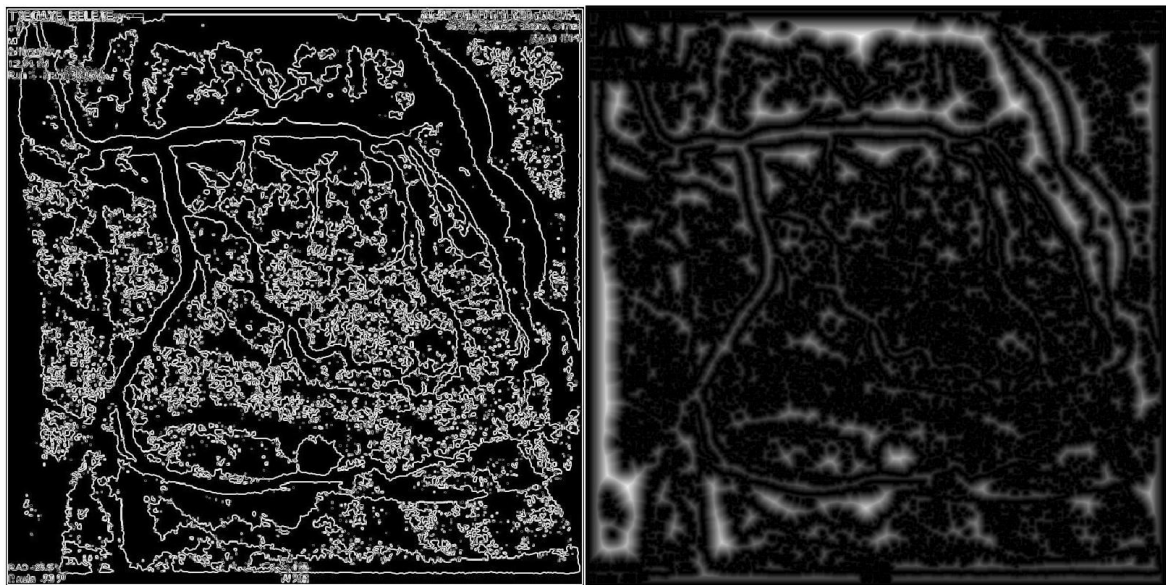
(A)   (B)

Figure 4.12: (A) Input, Segmented image, (B) Output, Euclidean distance transform.

| (A) | (B) |
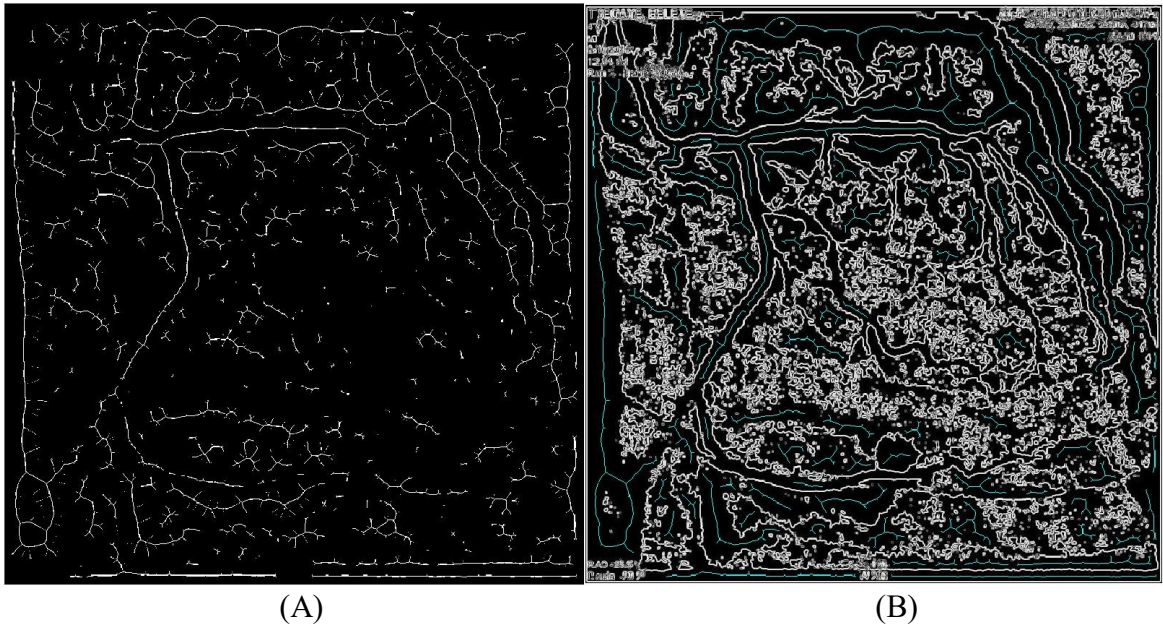
Figure 4.13: (A) Centerline, (B) Centerline over a segmented image.

The experimental results of the centerline extraction methods are compared between skeletonization and distance transformation methods. The skeletonization method gives better results over distance transformation method centerline extraction. In the distance transformation method, the centerline is not continuous. This is clear in Figure 4.13 (B) and the skeletonization method is shown in Figure 4.11 (B)

4.7.3 Line of Interest (LOI)

After cropping the ROI and centerline extraction, we draw a line on a blocked area of the vessel. The selection of LOI helps us calculate the angle in order to rotationally normalize. Select two sides of points for LOI over the centerline approximately the same distance from the center of the line.

Once the image displayed and appears on your screen, the program allows you to draw a line through the blocked vessel based on the centerline by locating two points using the mouse.

Let $P_1(x_1, y_1)$ and $P_2(x_2, y_2)$ are the beginning and ending points of selected LOI. Figure 4.14 (A) shows $P_1(x_1, y_1)$ which is the starting point between blockage point and normal size of the vessel.

Then select the second point on the blockage vessel between blockage point and normal size of the vessel. Figure 4.14 (B) shows $P_2(x_2, y_2)$ is selected.

(A)   (B)
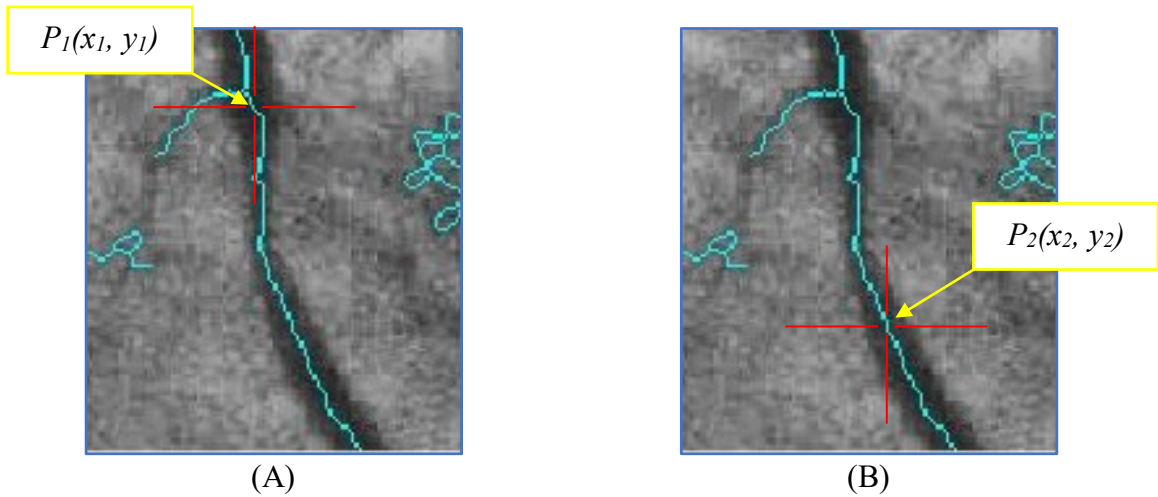
Figure 4.14: (A) Starting points for LOI, (B) Ending points for LOI.

4.7.4 Rotation Normalization

We calculate the angle that would rotate the LOI to be rotationally normalized, where the LOI becomes horizontally oriented. The angle of the required rotation, θ, can be calculated as follows:

$$\theta = (tan^{-1})\frac{y_2 - y_1}{x_2 - x_1} \tag{4.1}$$

Where:

y_2 = Vertical ending point $P_2(y_2)$

y_1 = Vertical ending point $P_1(y_1)$

x_2 = Horizontal ending point $P_2(x_2)$

x_1 = Horizontal ending point $P_1(x_1)$

In Figure 4.15, we can see the normalized coronary CTA image with LOI centerline in a horizontal orientation.
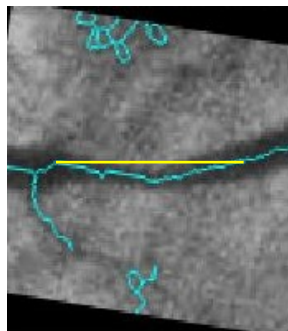
Figure 4.15: Rotationally Normalized LOI.

81

4.7.5 Calculate Stenosis Amount

Finally, we performed a standard calculation of the stenosis process through measure the maximum and minimum vessel diameter using equation 4.2.

$$Stenosis\ Persentage = [1 - \left(\frac{Ds}{Dn}\right)] * 100 \qquad (4.2)$$

where **Ds** is the diameter of the stenosis portion, **Dn** is normal vessel diameter.

We start our measurement by stenosis length horizontally by selecting two points from left to right on the blockage vessel between blockage point and normal size of the vessel. Then we measure **Dn** (normal vessel diameter) vertically by selecting two points from top to bottom on the normal vessel diameter. Finally, **Ds** (stenosis diameter) is computed vertically by selecting two points from top to bottom on the blockage vessel diameter. Figure 4.16 (A) and Figure 4.16 (B) show the approximate stenosis measurements and results respectively.

(A)   (B)
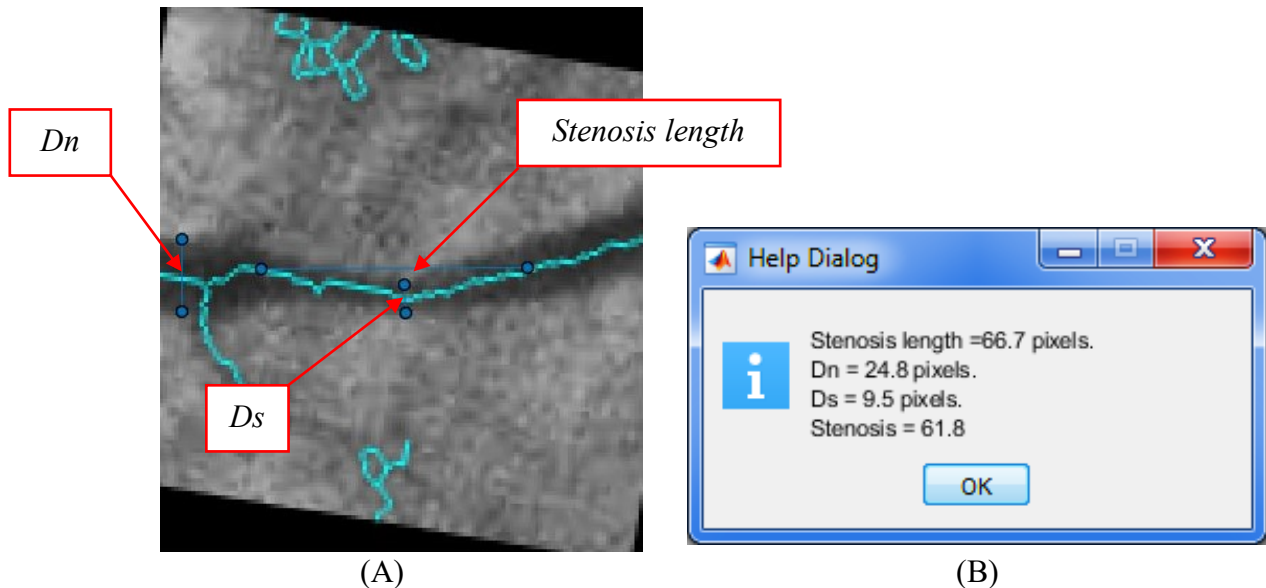
Figure 4.16: (A) Stenosis measurements, (B) Stenosis measurements result

To analyze the performance, we can comparison methods according to the reference results of the Doctor's opinion and the results in Table 4.15. The accuracy and mean percentage error or relative error (MRE) was calculated to assess the overall performance of quantifying stenosis using the ground truth.

Table 4.15: Evaluation of stenosis for coronary CTA in ten samples.

| Samples	Doctor's Opinion	Proposed Method	
	Stenosis (Percentage)	Stenosis (Percentage)	Stenosis length (pixels)
Sample 1	59	61.8	66.7
Sample 2	50	51.2	60.2
Sample 3	73	72	70.3
Sample 4	58	58.3	60.4
Sample 5	61	62.1	67.7
Sample 6	71	74.5	75.2
Sample 7	55	56.8	60.2
Sample 8	53	53.3	58.4
Sample 9	70	70.7	66.2
Sample 10	65	65.5	68.8
Mean (%) Error		1.32	

The MRE is computed using equation (4.3).

$$MRE = \frac{100\%}{n} \sum_1^n (x_{ia} - x_{im}) \qquad (4.3)$$

where n represents the number of samples, x_{ia} represents the ith proposed method value in the ith image and x_{im} represents the ith Doctor's opinion value in the ith image.

The overall sample image quantification of stenosis resulted in an accuracy of **97%**. As can be seen from the results, the measuring means the percentage error of counting using the proposed algorithm was **1.32**.

4.8 Experimental Results

We conduct experiments under five scenarios for the purpose of achieving better classification and an experiment for stenosis quantification. The classification experiment conducted on both SVM and CNN classifiers using different pre-trained network layers and features were shown over the five image processing steps scenarios. Thus, image processing steps are compared based on the results of the classification and quality metrics parameters estimation. The summary of all scenarios of classification performance is summarized in Table 4.16.

Table 4.16: Summary of all scenarios on SVM and CNN classifier

Scenarios	SVM Classifier		Convolutional Neural Network (CNN) Classifier	
			ResNet-50	DenseNet-201
	Statistical Features	CNN Features	add-16	fc1000
Scenario 1	0.472	0.710	0.713	0.658
Scenario 2	0.472	0.723	0.694	0.608
Scenario 3	0.472	**0.727**	0.696	0.635
Scenario 4	0.513	0.670	0.617	0.586
Scenario 5	0.567	0.703	0.608	0.581

The total number of datasets was 246 images out of these, 70% were used for training and the remaining 30% were used for testing using percentage splitter. The cardiologist's reading and label of each image as normal and stenosis present.

Finally, the highest classification performance (accuracy) of the proposed method becomes **72.7%** as shown in Table 4.16 using the SVM classifier and CNN feature (bag of feature) on scenario 3 (image normalization and filtering pre-processing).

4.9 Discussion of Results

This study presented detection and quantifying CAD. To overcome the diagnosis of CAD we have proposed a computer-aided diagnosis system that can be applied to coronary CTA image. Classification methods for coronary CTA images classifier as normal and stenosis present as detection. The detection and quantification of stenosis were tested using sample data selected from the ground truth. Our applied statistical approach to test the performance of the proposed system and compare the performance with respect to the ground truth. As we have discussed so far, this proposed work achieves 72.7 % classification accuracy for the detection of coronary artery disease on the local database.

Regarding stenosis quantification, 10 composite images were tested to check stenosis quantification performance. An error measure was used to check the accuracy of the proposed

quantification algorithm. The mean percentage error to stenosis quantification was 1.32 from the ground truth which is found to be a good result.

Table 4.17: The comparison of the proposed method with others

Authors, Year	No. of Patient	No. of Images	Stenosis Quantification	No. of Stenosis Quantification sample image	Stenosis Detection			Stenosis Quantification
					Accuracy (%)	Sensitivity (%)	Specificity (%)	Accuracy (%)
Chi *et al.,* 2017 [31].	6	Not mentioned	Yes	3	Not mentioned	82	95	89
Kang *et al.,* 2013 [59].	42	62	No	-	Not mentioned	93	81	-
Mohan and Vishnukumar, 2016 [3].	Not mentioned	15	No	-	86	Not mentioned	Not mentioned	-
Proposed method	57	246	Yes	10	72	66	85	97

In the above Table 4.18, the results we obtained are compared to previous researchers. Through those related works, [31], [59], and [3]*,* claim that they could achieve better results than this work, theirs are constrained as they focused is CAD detection on stenosis presented images only, they didn't consider the CAD classification of stenosis as normal and present stenosis. Which this study considered a higher level of accuracy. Moreover, when we comparing with other research work with respect to quantification of stenosis the accuracy in this study recorded the highest value as well.

However, the challenges are still reflected, one of the challenges is image quality; the accuracy is impaired when image quality is reduced. In addition to this, the size of the datasets, for the experiment, we collected the datasets from MCM General Hospital, Gesund Cardiac and Medical Center, and St. Peter Specialized Hospital. However, some of these images were not sufficient in amount and variety. Hence, our stenosis classifies the algorithm was trained and tested using available sample data only.

Chapter Five
Conclusions and Future Works

5.1 Conclusions

The goal of this work was to detect CAD and quantify stenosis to coronary CAT images. That will provide valuable information for computer-assisted surgery planning and navigation.

The diagnosis and treatment of CAD on coronary CTA images are dependent on the skill, experience, and motivation of a physician. The use of a computer-aided diagnosis system would allow making diagnosis and treatment of CAD with a high degree of certainty.

This proposed study conducts experiments on four pre-processing scenarios and selects the image enhancement followed by image filtering for image cleaning and quality enhancement. For image enhancement, adaptive histogram equalization technique is selected. Then, for image filtering, the non-local mean filtering method was used for noise removal by edge-preserving. In addition, we used the segmentation method, Sobel gradient magnitude and region growing segmentation algorithm for identifying the ROI.

In the feature extraction and classification step, the statistical features and CNN based feature extraction was used. The accuracy of the CNN based feature extraction using the CNN classifier was higher than that of the statistical features using the SVM classifier. To achieve better accuracy, the statistical features were replaced by CNN based feature extraction using the SVM classifier, which achieves a promising result, with an accuracy of **72.7** %. In stenosis, quantification resulted in an accuracy of **97 %**.

The proposed study could be used to quantify the stenosis using stenosis length, diameter, and percentage using image processing techniques that allow physicians to advance in computer-assisted diagnostics, treatment, and follow-up of stenosis.

5.2 Future Works

This study attempts to apply image processing to classify the coronary CTA image into normal and present of stenosis and quantify the stenosis. Based on the finding of the study, we recommend the following as a feature research direction.

- The need for improving the accuracy of the classification model. This requires testing classification algorithm with the feature extraction techniques.

- The need for denoising an effective and more advanced segmentation algorithm that works to identify ROI from such complex coronary CTA images.

- The stenosis quantification approach has to be extended to automatically find ROI and quantify the stenosis attribute.

References

[1]   C. K. Chow, K. K. Teo, and S. Yusuf, "Risk Factors Predicting Nonfatal Myocardial Infarction: The Interheart Study," in *Acute Coronary Syndromes*, 2nd ed., vol. 298, no. 7, Pierre Theroux, Ed. Saunders, an imprint of Elsevier Inc., 2011, pp. 14–20.

[2]   J. A. de and T. O. Lemos, *Chronic Coronary Artery Disease: A Companion to Braunwald's Heart Disease*. London: Elsevier, 2018.

[3]   N. Mohan and S. Vishnukumar, "Detection and localization of coronary artery stenotic segments using image processing," *Proc. IEEE Int. Conf. Emerg. Technol. Trends Comput. Commun. Electr. Eng. ICETT 2016*, pp. 1–5, 2016.

[4]   P. Chinmayi, L. Agilandeeswari, and M. Prabukumar, "Survey of Image Processing Techniques in Medical Image Analysis: Challenges and Methodologies," in *Advances in Intelligent Systems and Computing*, 2018, vol. 614, no. 10.1007/978-3-319-60618–7_45, p. 12.

[5]   E. Escolar, G. Weigold, A. Fuisz, and N. J. Weissman, "New imaging techniques for diagnosing coronary artery disease Esteban," *CMAJ*, vol. 174, no. 4, 2006.

[6]   S. Keevil, C. Lewis, M. Lewis, V. McMillan, and A. Pascoal, *CT scanners for coronary CT angiography (CCTA) in challenging patient groups*, vol. 44. London: KiTEC - King's Technology Evaluation Centre Department of Medical Engineering and Physics King's College Hospital NHS Foundation Trust, 2014.

[7]   M. Schaap *et al.*, "Coronary lumen segmentation using graph cuts and robust kernel regression," *Springer-Verlag Berlin Heidelb.*, vol. 5636 LNCS, pp. 528–539, 2009.

[8]   M. J. Budoff and J. S. Shinbane, Eds., *Cardiac CT Imaging: Diagnosis of Cardiovascular Disease*, 2nd ed. London: Springer-Verlag, 2010.

[9]   L. K. Lee and S. C. Liew, "A survey of medical image processing tools," *2015 4th Int. Conf. Softw. Eng. Comput. Syst. ICSECS 2015 Virtuous Softw. Solut. Big Data*, vol. 2, no. October, pp. 171–176, 2015.

[10]   J. Thirumaran and S. Shylaja, "Medical Image Processing – An Introduction," *Int. J. Sci. Res.*, vol. 4, no. 11, 2017.

[11] R. C. Gonzalez and R. E. Woods, *Digital Image Processing*, 3rd ed., no. September. Upper Saddle River, New Jersey: Pearson Education, Inc, 2015.

[12] M. Petrou and C. Petrou, *Image Processing: The Fundamentals*, 2nd ed. Wiley, 2011.

[13] J. Narmadha, S. Ranjithapriya, and T. Kannaambaal, "Survey on image processing under image restoration," *Proc. - 2017 IEEE Int. Conf. Electr. Instrum. Commun. Eng. ICEICE 2017*, vol. 2017-Decem, pp. 1–5, 2017.

[14] Geoff Dougherty, *Digital Image Processing for Medical Applications*, 1st ed. Channel Islands: Cambridge University Press, 2009.

[15] T. S. Huang and K. Aizawa, "Image processing: Some challenging problems," in *Proceedings of the National Academy of Sciences of the United States of America*, 1993, vol. 90, no. 21, pp. 9766–9769.

[16] E. Miranda, M. Aryuni, and E. Irwansyah, "A survey of medical image classification techniques," *Proc. 2016 Int. Conf. Inf. Manag. Technol. ICIMTech 2016*, no. November, pp. 56–61, 2017.

[17] WHO, "WHO | Cardiovascular diseases (CVDs)," *WHO*, 2018. [Online]. Available: https://www.who.int/cardiovascular_diseases/en/. [Accessed: 01-Feb-2020].

[18] Zhonghua Sun, *Coronary Computed Tomography Angiography in Coronary Artery Disease: A Systematic Review of Image Quality, Diagnostic Accuracy and Radiation Dose*. New York, 2013.

[19] S. G. Abdissa, K. Oli, Y. Feleke, D. Y. Goshu, D. M. Begna, and A. Tafese, "Spectrum of cardiovascular diseases among Ethiopian patients at Tikur Anbessa Specialized University Teaching Hospital, Addis Ababa.," *Ethiop. Med. J.*, vol. 52, no. 1, pp. 9–17, 2014.

[20] World Health Rankings, "Ethiopia : Coronary Heart Disease." [Online]. Available: https://www.worldlifeexpectancy.com/ethiopia-coronary-heart-disease. [Accessed: 01-Feb-2020].

[21] D. S. Baim, "Diagnostic Cardiac Catheterization And Angiography," in *Harrison's Cardiovascular Medicine*, 17th ed., vol. 19, no. 2, J. Loscalzo, Ed. The McGraw-Hill

Companies, Inc., 2010, pp. 112–119.

[22]   S. Banik, R. M. Rangayyan, and G. S. Boag, *Landmarking and Segmentation of 3D CT Images*, vol. 4, no. 1. Morgan & Claypool All, 2009.

[23]   D. A. Dowe, M. Fioranelli, and P. Pavone, Eds., *Image Coronary Arteries*, 2nd ed. Rome: Springer, 2013.

[24]   C. Wang, "Computer-assisted coronary CT angiography analysis: From Software Development to Clinical Application," Linköping University, 2011.

[25]   M. Gerhard-Herman, J. A. Beckman, and M. A. Creager, "Vascular Laboratory Testing," in *Vascular Medicine: A Companion to Braunwald's Heart Disease*, and J. L. Creager, Victor Dzau, Ed. Eds. Elsevier Inc., 2006, pp. 146–165.

[26]   Marco A. Gutierrez, M. S. R. Ramon, R. A. Moreno, A. G. Santiago, and M. M. G. Macedo, "CAD of Cardiovascular Diseases," in *Medical Image Analysis and Informatics: Computer-Aided Diagnosis and Therapy*, P. M. de Azevedo-Marques, A. Menchattini, M. Sameri, and R. M. Rangayyan, Eds. CRC Press, 2018, pp. 145–171.

[27]   C. A. Karlo, S. Leschka, P. Stolzmann, N. Glaser-Gallion, S. Wildermuth, and H. Alkadhi, "A systematic approach for analysis, interpretation, and reporting of coronary CTA studies," *Insights Imaging*, vol. 3, no. 3, pp. 215–228, 2012.

[28]   I. O. Macia, "Medical Image Analysis for the Detection, Extraction and Modelling of Vascular Structures," University of the Basque Country, 2012.

[29]   X. Ji, J. Zheng, R. Yang, W. Kainz, and J. Chen, "Evaluations of the MRI RF-Induced Heating for Helical Stents under a 1.5T MRI System," *IEEE Trans. Electromagn. Compat.*, vol. 61, no. 1, pp. 57–64, 2019.

[30]   H. Sofian, J. T. C. Ming, and N. M. Noor, "Detection of the lumen boundary in the coronary artery disease," *2015 IEEE Int. WIE Conf. Electr. Comput. Eng. WIECON-ECE 2015*, vol. 3, pp. 143–146, 2016.

[31]   Y. Chi *et al.*, "Stenosis detection and quantification on cardiac CTCA using panoramic MIP of coronary arteries," in *Proceedings of the Annual International Conference of the IEEE Engineering in Medicine and Biology Society, EMBS*, 2017, pp. 4191–4194.

[32] P. Mirunalini and C. Aravindan, "Automatic Segmentation of Coronary Arteries and Detection of Stenosis," *IEEE*, vol. 25, no. 2, pp. 1–4, 2013.

[33] O. Blakstad, "Experimental research," *Researching Translation and Interpreting*, 2008. [Online]. Available: https://explorable.com/experimental-research. [Accessed: 01-Feb-2020].

[34] A. Bryman, "Experimental research," *Research Methods and Organization Studies*, 2010. [Online]. Available: https://explorable.com/experimental-research. [Accessed: 01-Feb-2020].

[35] R. Freitas, "Scientific Research Methods and Computer Science," *MAPI Semin. Work.*, pp. 1–6, 2009.

[36] R. Maxion, "Experimental Methods for Computer Science Research," in *Fourth Latin-American Symposium on Dependable Computing*, 2009, pp. 136–136.

[37] MathWorks, "MathWorks ™ Products," *The MathWorks, Inc.*, 2019. [Online]. Available: https://www.mathworks.com/company/aboutus/products.html. [Accessed: 01-Feb-2020].

[38] Mayo Clinic, "Coronary artery disease - Symptoms and causes - Mayo Clinic." [Online]. Available: https://www.mayoclinic.org/diseases-conditions/coronary-artery-disease/symptoms-causes/syc-20350613. [Accessed: 01-Feb-2020].

[39] C. T. Lee, G. H. Williams, and L. S. Lilly, *Pathophysiology of Heart Disease: A Collaborative Project Of Medical Students And Faculty*, 6th ed. 2016.

[40] Lambros S. Athanasiou, D. I. Fotiadis, and L. K. Michalis, *Atherosclerotic Methods Based On Characterization Plaque Coronary Imaging*. London: ElsevierInc., 2017.

[41] S. M. Chang, S. Bhatti, and F. Nabi, "Coronary computed tomography angiography," *Current Opinion in Cardiology*, vol. 26, no. 5. pp. 392–402, 2011.

[42] C. Smuclovisky, Ed., *Coronary Artery CTA: A Case-Based Atlas*, 2nd ed. South Florida: Springer International Publishing AG, 2018.

[43] Atam P. Dhawan, *Medical Image Analysis*, 2nd ed. New Jersey: IEEE Press, 2011.

[44] P. Vasuki, J. Kanimozhi, and M. B. Devi, "A survey on image preprocessing techniques for diverse fields of medical imagery," *Proc. - 2017 IEEE Int. Conf. Electr. Instrum. Commun. Eng. ICEICE 2017*, vol. 2017-Decem, pp. 1–6, 2017.

[45] W. Burger and M. J. Burge, *Priciples of Digital Image Processing: Advanced Methods*, 3rd ed. London: Springer-Verlag, 2013.

[46] H. R. Myler and A. R. Weeks, *The Pocket Handbook of Image Processing Algorithms in C*. New Jersey: Prentice Hall PTR, 1993.

[47] A. P. Dhawan, "Image Segmentation and Feature Extraction," in *Principles And Advanced Methods In Medical Imaging And Image Analysis*, Singapore: World Scientific Publishing Co. Pte. Ltd., 2008, pp. 197–228.

[48] S. K. Zhou, *Medical Image Recognition, Segmentation and Parsing: Machine Learning and Multiple Object Approaches*. London: Elsevier, 2016.

[49] M. Sonka, V. Hlavac, and R. Boyle, *Image Processing, Analysis, and Machine Vision*, 1st ed. Chapman & Hall, 1993.

[50] M. C. Bakkay, S. Chambon, H. A. Rashwan, C. Lubat, and S. Barsotti, "Automatic detection of individual and touching moths from trap images by combining contour-based and region-based segmentation," *IET Comput. Vis.*, vol. 12, no. 2, pp. 138–145, 2018.

[51] S. S.Patil and A. V. Dusane, "Use of Color Feature Extraction Technique based on Color Distribution and Relevance Feedback for Content based Image Retrieval," *Int. J. Comput. Appl.*, vol. 52, no. 17, pp. 9–12, 2012.

[52] T. H. Le and H. Tran, "Image Classification using Support Vector Machine and Artificial Neural Network," *I.J. Inf. Technol. Comput. Sci. 2012, 5, 32-38*, no. May 2012, p. 8, 2012.

[53] D. Soni, "Supervised vs. Unsupervised Learning," *Towards Data Science*. [Online]. Available: https://towardsdatascience.com/supervised-vs-unsupervised-learning-14f68e32ea8d?gi=afda760d8182. [Accessed: 01-Feb-2020].

[54] S. Khan, H. Rahmani, S. A. A. Shah, and M. Bennamoun, "A Guide to Convolutional

Neural Networks for Computer Vision," *Synth. Lect. Comput. Vis.*, vol. 8, no. 1, pp. 1–207, 2018.

[55] A. Yadav, "Support Vector Machines (SVM)," *Towards Data Science*. [Online]. Available: https://towardsdatascience.com/support-vector-machines-svm-c9ef22815589. [Accessed: 01-Feb-2020].

[56] T. N. Do and F. Poulet, "Parallel learning of local SVM algorithms for classifying large datasets," *Lect. Notes Comput. Sci. (including Subser. Lect. Notes Artif. Intell. Lect. Notes Bioinformatics)*, vol. 10140 LNCS, pp. 67–93, 2017.

[57] P. Soille, *Morphological Image Analysis : Principles and Applications*, 2nd ed. Berlin Heidelberg: Springer-Verlag, 2004.

[58] P. K.Ghosh and K. Deguchi, *Mathematics Of Shape Description: A Morphological Approach to Image Processing and Computer Graphics*. John Wiley & Sons (Asia) Pte Ltd, 2008.

[59] D. Kang *et al.*, "Automated knowledge-based detection of nonobstructive and obstructive arterial lesions from coronary CT angiography," *Med. Phys.*, vol. 40, no. 4, pp. 1–10, 2013.

[60] R. Goldenberg, D. Eilot, G. Begelman, E. Walach, E. Ben-Ishai, and N. Peled, "Computer-aided simple triage (CAST) for coronary CT angiography (CCTA)," *Int. J. Comput. Assist. Radiol. Surg.*, vol. 7, no. 6, pp. 819–827, 2012.

[61] H. Sofian, A. Ng, J. Than, S. Mohamad, and N. M. Noor, "Calcification boundary detection in coronary artery using intravascular ultrasound images," *IEEE Reg. 10 Annu. Int. Conf. Proceedings/TENCON*, vol. 2017-Decem, pp. 2835–2839, 2017.

[62] Y. Jia, C. Rong, C. Wu, and Y. Yang, "Research on the decomposition and fusion method for the infrared and visible images based on the guided image filtering and Gaussian filter," in *3rd IEEE International Conference on Computer and Communications, ICCC*, 2017, pp. 1797–1802.

[63] K. He, J. Sun, and X. Tang, "Guided image filtering," *IEEE Trans. Pattern Anal. Mach. Intell.*, vol. 35, no. 6, pp. 1397–1409, 2013.

[64] K. He, J. Sun, and X. Tang, "Guided image filtering," *IEEE Trans. Pattern Anal. Mach. Intell.*, vol. 35, no. 6, pp. 1397–1409, 2013.

[65] J. V. Manjón, J. Carbonell-Caballero, J. J. Lull, G. García-Martí, L. Martí-Bonmatí, and M. Robles, "MRI denoising using Non-Local Means," *Med. Image Anal.*, vol. 12, no. 4, pp. 514–523, 2008.

[66] H. Zhu *et al.*, "A parallel Non-Local means denoising algorithm implementation with OpenMP and OpenCL on Intel Xeon Phi Coprocessor," *J. Comput. Sci.*, vol. 17, pp. 591–598, 2016.

[67] S. Muniyappan, A. Allirani, and S. Saraswathi, "A novel approach for image enhancement by using contrast limited adaptive histogram equalization method," *2013 4th Int. Conf. Comput. Commun. Netw. Technol. ICCCNT 2013*, 2013.

[68] C. W. Kurak, "Adaptive histogram equalization: A parallel implementation," 1991, pp. 192–199.

[69] S. Yu and W. Yiquan, "An improved local Laplacian filter based on the relative total variation," *Digit. Signal Process. A Rev. J.*, vol. 78, pp. 56–71, 2018.

[70] Z. Mishra, G. Ramu, and B. Acharya, *Architecture for LEA Encryption Algorithm*. Springer Singapore.

[71] P. Mishra, S. Agarwal, and U. Kiran, "Survey Paper Based on Medical Image Segmentation and Clustering Techniques," vol. 2, no. 12, pp. 3191–3194, 2013.

[72] V. P. Kulkarni and C. A. M. D. S. T, "A Survey on image processing techniques," *Iaetsd J. Adv. Res. Appl. Sci.*, vol. 5, no. 1, pp. 373–376, 2018.

[73] G. L. Smitha and E. Baburaj, "Sobel edge detection technique implementation for image steganography analysis," *Biomed. Res.*, pp. S487–S493, 2018.

[74] A. Khan, A. Sohail, U. Zahoora, and A. S. Qureshi, "A Survey of the Recent Architectures of Deep Convolutional Neural Networks," pp. 1–69, 2019.

[75] Q. Li, W. Cai, X. Wang, Y. Zhou, D. D. Feng, and M. Chen, "Medical image classification with convolutional neural network," *2014 13th International Conference on Control Automation Robotics and Vision, ICARCV 2014*. pp. 844–848, 2014.

[76] A. Anuse and V. Vyas, "A novel training algorithm for convolutional neural network," *Complex Intell. Syst.*, vol. 2, no. 3, pp. 221–234, 2016.

[77] H. Cui and Y. Xia, "Automatic Coronary Centerline Extraction Using Gradient Vector Flow Field and Fast Marching Method from CT Images," *IEEE Access*, vol. 6, pp. 41816–41826, 2018.

[78] A. Khedmati, A. Nikravanshalmani, and A. Salajegheh, "Semi-automatic detection of coronary artery stenosis in 3D CTA," *IET Image Process.*, vol. 10, no. 10, pp. 724–732, 2016.

[79] MathWorks, "Image Quality Metrics." [Online]. Available: https://www.mathworks.com/help/images/image-quality-metrics.html. [Accessed: 01-Feb-2020].

[80] MathWorks, "Image Category Classification Using Deep Learning - MATLAB & Simulink Example." [Online]. Available: http://www.mathworks.com/help/vision/examples/image-category-classification-using-deep-learning.html. [Accessed: 01-Feb-2020].

Glossary

Angina	Angina is a type of chest pain or discomfort caused by reduced blood flow to the heart. Angina (an-JIE-nuh or AN-juh-nuh) is a symptom of coronary artery disease. Angina, which may also be called angina pectoris, is often described as squeezing, pressure, heaviness, tightness or pain in your chest.
Angiography	Roentgen graphic examination of blood vessels after injection of a radiopaque contrast medium; produces an angiogram
Atherosclerotic	A stage of arteriosclerosis involving fatty deposits (atheromas) inside the arterial walls, thus narrowing the arteries.
Calcifications	Tissue hardened by deposition of lime salts
Catheter	A thin flexible tube inserted into the body to permit the introduction or withdrawal of fluids or to keep the passageway open.
Catheterization	The operation of introducing a catheter into the body.
DICOM	(Digital Imaging and Communications in Medicine) is a standard for handling, storing, printing, and transmitting information in medical imaging.
Emboli	An abnormal particle (e.g. an air bubble or part of a clot) obstructing a blood vessel.
Hyperlipidemia	Presence of excess lipids in the blood.
Ischemia	Local anemia in a given body part sometimes resulting from vasoconstriction, thrombosis or embolism.
Lesions	Any localized abnormal structural change in a bodily part
Lumen	In biology, a lumen is the inside space of a tubular structure, such as an artery or intestine. It comes from the Latin lumen, meaning 'an opening'. It can refer to, The interior of a vessel, such as the central space in an artery or vein through which blood flows.

Myocardial Infarction	Destruction of heart tissue resulting from obstruction of the blood supply to the heart muscle.
Myocardium	The middle muscular layer of the heart wall.
Plaques	(Pathology) a small abnormal patch on or inside the body. (Medicine) a small, distinct, typically raised patch or region on or within the body resulting from local damage or deposition of material, such as a fatty deposit on artery wall in atherosclerosis or a site of localized damage of brain tissue in Alzheimer's disease.
Stenosis	A narrowing of the arteries leading to a reduction in blood flow. Maybe due to the build-up of atherosclerotic deposits of fibrous and fatty tissue or maybe a congenital defect.
Stent	A slender tube inserted inside a tubular body part (as a blood vessel) to provide support during and after surgical anastomosis.
Thrombosis	The formation or presence of a thrombus (a clot of coagulated blood attached at the site of its formation) in a blood vessel.

Annexes

Annex - A: Image Pre-processing (Scenario 1) MATLAB Code.

```matlab
clear all;
%% Taking an Image
% Reading input images for the dataset
% ImagePath='C:\CCTA\Grouped CTA Image data\New Labeled
CTA\Normal';
ImagePath='C:\CCTA\Grouped CTA Image data\New Labeled
CTA\Present';
% [fname, path]=uigetfile('.jpg','provide an Image for
testing');
d=dir([ImagePath '\*.jpg']);
for i=1:length(d)
%% Image Filtering
%    I=im2double(imread([ImagePath '/' d(i).name]));
     I=imread([ImagePath '/' d(i).name]);%Origional image
%        score = piqe(I);
%        fprintf('***PIQE score for the Origional image is
%0.4f.\n',score)
%        J = entropy(I)
%    IB=imbilatfilt(I); % Applies an edge-preserving Gaussian
bilateral filter to the grayscale or RGN image, I.
%        [peaksnr, snr] = psnr(I, IB);
%        fprintf('\n Bilateral mens Peak-SNR value is
%0.4f\n', peaksnr);
%        score = piqe(IB);
%        fprintf('PIQE score for  Bilateral image is
%0.4f\n',score)
%        J = entropy(IB)
%        err = immse(I, IB);%The lower the value of MSE, the
lower the error.
%        fprintf('\n Bilateral mean-squared error is
%0.4f\n', err);
%    ID=imguidedfilter(I); % Guided filtering of images
%        [peaksnr, snr] = psnr(I, ID);
%        fprintf('\n Guided mens Peak-SNR value is %0.4f\n',
peaksnr);
%        score = piqe(ID);
%        fprintf('PIQE score for Guided image is
%0.4f.\n',score)
%        J = entropy(ID)
%        err = immse(I, ID);%The lower the value of MSE, the
lower the error.
%        fprintf('\n Guided mean-squared error is %0.4f\n',
err);
  IN=imnlmfilt(I);% Non-local means filtering of image
```

```matlab
%          [peaksnr, snr] = psnr(I, IN);
%          fprintf('\n Non-local mens Peak-SNR value is
%0.4f\n', peaksnr);
%          score = piqe(IN);
%          fprintf('PIQE score for Non-local image is
%0.4f.\n',score)
%          J = entropy(IN)
%          err = immse(I, IN);%The lower the value of MSE, the
lower the error.
%          fprintf('\n Non-local mean-squared error is
%0.4f\n', err);
%    IG=imgaussfilt(I);% Gaussian filtering
%    imshowpair(I,IN,'montage')
%% Image Enhancement
  IG=rgb2gray(IN);%Convert non-local menas filtered RGB
image to gray scale image.
%    IG=rgb2gray(I);%Convert origional RGB image to gray
scale image.
%    IH=histeq(IG);%Apply Histogram equalization
%          score = piqe(IH);
%          fprintf('PIQE score for Histogram image is
%0.4f.\n',score)
%          brisqueI =brisque(IH);
%          fprintf('BRISQUE %0.4f.\n',brisqueI)
%          [peaksnr, snr] = psnr(IG, IH);
%          fprintf('\n Histogram mens Peak-SNR value is
%0.4f', peaksnr);
IAH=adapthisteq(IG,'clipLimit',0.02,'Distribution','rayleigh
');%Apply Adaptive histogram equalization
%          score = piqe(IAH);
%          fprintf('PIQE score for Adaptive Histogram image is
%0.4f.\n',score)
%          brisqueI =brisque(IAH);
%          fprintf('BRISQUE %0.4f.\n',brisqueI)
%          [peaksnr, snr] = psnr(IG, IAH);
%          fprintf('\n Adaptive Histogram mens Peak-SNR value
is %0.4f', peaksnr);
%    IC=localcontrast(IG);%Edge-aware Local Contrast Enhance
%          score = piqe(IC);
%          fprintf('PIQE score for Edge-aware image is
%0.4f.\n',score)
%          brisqueI =brisque(IC);
%          fprintf('BRISQUE %0.4f.\n',brisqueI)
%          [peaksnr, snr] = psnr(IG, IC);
%          fprintf('\n Edge-aware mens Peak-SNR value is
%0.4f', peaksnr);
% %    imshowpair(IN,IAH,'montage')
imwrite(IAH, [d(i).name])
```

```
end
```

Annex - B: Image Pre-processing (Scenario 2) MATLAB Code.

```matlab
clear all;
%% Taking an Image
% % Reading an input images for the dataset
% ImagePath='C:\CCTA\Grouped CTA Image data\New Labeled
CTA\Normal';
ImagePath='C:\CCTA\Grouped CTA Image data\New Labeled
CTA\Present';
% [fname, path]=uigetfile('.jpg','provide an Image for
testing');
d=dir([ImagePath '\*.jpg']);

for i=1:length(d)
% %      Image Filtering Using Bilateral Filtering with
Gaussian Kernels
%      I=im2double(imread([ImagePath '/' d(i).name]));
    I=imread([ImagePath '/' d(i).name]);
        score = piqe(I);
        fprintf('****PIQE Origional image is
%0.4f.\n',score)
        J = entropy(I)
    IN=imnlmfilt(I);% Non-local means filtering of image
        score = piqe(IN);
        fprintf('PIQE Non-local image is %0.4f.\n',score)
        J = entropy(IN)
%% Image Enhancement
IG=rgb2gray(IN);
% IG=rgb2gray(I);
IH=adapthisteq(IG,'clipLimit',0.02,'Distribution','rayleigh'
);
    score = piqe(IH);
    fprintf('PIQE Adaptive image is %0.4f.\n',score)
    J = entropy(IH)
%% Image Filtering
K = wiener2(IH,[5 5]);
    score = piqe(K);
    fprintf('PIQE Wiener image is %0.4f.\n',score)
    J = entropy(K);
M = medfilt2(IH);
    score = piqe(M);
    fprintf('PIQE Median image is %0.4f.\n',score)
    J = entropy(M)
IN1=imnlmfilt(IH); %48.7537 PSNR 0.0000 MSE Applies an edge-
preserving Gaussian bilateral filter to the grayscale or RGN
image, I.
```

```matlab
    score = piqe(IN1);
    fprintf('PIQE Non-loca image is %0.4f.\n',score)
    J = entropy(IN1)
imwrite(IN1, [d(i).name])
end
```

Annex - C: Image Pre-processing (Scenario 3) MATLAB Code.

```matlab
clear all;
%% Taking an Image
% ImagePath='C:\CCTA\Grouped CTA Image data\New Labeled
CTA\Normal';
% ImagePath='C:\CCTA\Grouped CTA Image data\New Labeled
CTA\Present';
ImagePath='C:\CCTA\Grouped CTA Image data\Evaluation
sample';
% [fname, path]=uigetfile('.jpg','provide an Image for
testing');
d=dir([ImagePath '\*.jpg']);

for i=1:length(d)
%% Image Filtering
%     I=im2double(imread([ImagePath '/' d(i).name]));
    I=imread([ImagePath '/' d(i).name]);
    score = piqe(I);
    fprintf('PIQE *******Origional image is
%0.4f.\n',score)
    brisqueI = brisque(I);
    fprintf('BRISQUE score for original image is
%0.4f.\n',brisqueI)
    J = entropy(I)
%% Image Enhancement
% IG=rgb2gray(IN);
IG=rgb2gray(I);
IH1=histeq(IG);
    score = piqe(IH1);
    fprintf('PIQE Histogram image is %0.4f.\n',score)
    brisqueI =brisque(IH1);
    fprintf('BRISQUE %0.4f.\n',brisqueI)
IH=adapthisteq(IG,'clipLimit',0.02,'Distribution','rayleigh'
);
    score = piqe(IH);
    fprintf('PIQE, Adaptive Histogram image is
%0.4f.\n',score)
    brisqueI =brisque(IH);
    fprintf('BRISQUE %0.4f.\n',brisqueI)
    J = entropy(IH)
IC=localcontrast(IG);
```

```matlab
    score = piqe(IC);
    fprintf('PIQE score Contrust image is %0.4f.\n',score)
    brisqueI =brisque(IC);
    fprintf('BRISQUE %0.4f.\n\n',brisqueI)
    J = entropy(IC)
%% Image Filtering
K = wiener2(IH,[5 5]);
    score = piqe(K);
    fprintf('PIQE Wiener image is %0.4f.\n',score)
    J = entropy(K)
M = medfilt2(IH);
    score = piqe(M);
    fprintf('PIQE Median image is %0.4f.\n',score)
    J = entropy(M)
IN=imnlmfilt(IH);
    score = piqe(IN);
    fprintf('PIQE Non-loca image is %0.4f.\n',score)
    J = entropy(IN)
imwrite(IN, [d(i).name])
end
```

Annex - D: Image Pre-processing (Scenario 4) MATLAB Code.

```matlab
clear all;
%% Taking an Image
%% Reading an input images for the dataset
%% New Label
% ImagePath='C:\CCTA\Grouped CTA Image data\New Labeled
CTA\Normal';
ImagePath='C:\CCTA\Grouped CTA Image data\New Labeled
CTA\Present';
% [fname, path]=uigetfile('.jpg','provide an Image for
testing');
d=dir([ImagePath '\*.jpg']);

for i=1:length(d)
%% Image Filtering Using Bilateral Filtering with Gaussian
Kernels
%     I=im2double(imread([ImagePath '/' d(i).name]));
    I=imread([ImagePath '/' d(i).name]);
%     score = piqe(I);
%     fprintf('PIQE score for the Origional image is
%0.4f.\n',score)
%     brisqueI = brisque(I);
%     fprintf('BRISQUE score for original image is
%0.4f.\n',brisqueI)
%    IB=imbilatfilt(I); % Applies an edge-preserving Gaussian
bilateral filter to the grayscale or RGN image, I.
```

```
%    ID=imguidedfilter(I); % Guided filtering of images
     IN=imnlmfilt(I);% Non-local means filtering of image
%      score = piqe(IN);
%      fprintf('PIQE score for the filterd image is
%0.4f.\n',score)
% imshowpair(I,J,'montage')

%% Image Enhancement
IG=rgb2gray(IN);
% IG=rgb2gray(I);
%Apply Histogram equalization
% IH=histeq(IG);
IH=adapthisteq(IG,'clipLimit',0.02,'Distribution','rayleigh'
);
%      score = piqe(IH);
%      fprintf('PIQE score for the Histogram image is
%0.4f.\n',score)
%      score = piqe(IH1);
%      fprintf('PIQE score for the Histogram1 image is
%0.4f.\n',score)

%% Image Threshold Using Otsu's Method MATLAB Code
[counts,x] = imhist(IH,16);
stem(x,counts)
T = otsuthresh(counts);
BW = imbinarize(IH,T);

%% Image Threshold Using Adaptive Thresholding MATLAB Code.
% % [counts,x] = imhist(J,16);
T=adaptthresh(IH,0.6);
BW1=imbinarize(IH,T);
% % figure, imshow(BW);
% figure, imshowpair(BW,BW1,'montage')
imwrite(BW, [d(i).name])
end
```

Annex - E: SVM Classifier, Training MATLAB Code.

```
clc;
clear;
close all;
%% Taking an Image
% % Reading an input images for the dataset
ImagePath='C:\CCTA\Grouped CTA Image data\New Labeled
CTA\Normal';
% ImagePath='C:\CCTA\Grouped CTA Image data\New Labeled
CTA\Present';
d=dir([ImagePath '\*.jpg']);
```

```matlab
% d=dir([ImagePath '\*.png']);%Segmented Image Readng

for i=1:length(d)
% %      Image Filtering Using Bilateral Filtering with
Gaussian Kernels
%      I=imread([ImagePath '/' d(i).name]);
    I=imread([ImagePath '/' d(i).name]);

%% Scenario 1

    IN=imnlmfilt(I);%Non-local means filtering of image
    IG=rgb2gray(IN);

Im=adapthisteq(IG,'clipLimit',0.02,'Distribution','rayleigh'
);

%% Scenario 2

%      IN=imnlmfilt(I);%Non-local means filtering of image
%      IG=rgb2gray(IN);
%
IH=adapthisteq(IG,'clipLimit',0.02,'Distribution','rayleigh'
);
%      T=adaptthresh(IH,0.6);%T = adaptthresh(I,sensitivity)
computes a locally adaptive threshold with sensitivity
factor specified by sensitivity. sensitivity is a scalar in
the range [0,1] that indicates sensitivity towards
thresholding more pixels as foreground.
%      Im=imbinarize(IH,T);

%% Scenario 3

%      IN=imnlmfilt(I);%Non-local means filtering of image
%      IG=rgb2gray(IN);
%
IH=adapthisteq(IG,'clipLimit',0.02,'Distribution','rayleigh'
);
%      Im=imnlmfilt(IH);%Non-local means filtering of image

%% Scenario 4

%      IG=rgb2gray(I);
%
IH=adapthisteq(IG,'clipLimit',0.02,'Distribution','rayleigh'
);
%      Im=imnlmfilt(IH);%Non-local means filtering of image

%% Scenario 5
```

```matlab
% Im=rgb2gray(I);

end

c=input('Enter the Class(Number for Stenosis(1) Present or
for Normal(0))');
%% Feature Extraction
F=FeatureStatistical(Im);
try
    load db;
    F=[F c];
    db=[db; F];
%      db=[db; obj];
    save db.mat db
catch
    db=[F c]; % 10 12 1
    save db.mat db
end
```

Annex - F: SVM Classifier, Testing MATLAB Code.

```matlab
clear all;
%% Taking an Image
% % Reading an input images for the dataset
ImagePath='C:\CCTA\Grouped CTA Image data\New Labeled
CTA\Normal';
% ImagePath='C:\CCTA\Grouped CTA Image data\New Labeled
CTA\Present';

% [fname, path]=uigetfile('.jpg','provide an Image for
testing');
d=dir([ImagePath '\*.jpg']);
% d=dir([ImagePath '\*.png']);%Segmented Image Readng

for i=1:length(d)
% %      Image Filtering Using Bilateral Filtering with
Gaussian Kernels
    I=imread([ImagePath '/' d(i).name]);
%% Scenario 1

    IN=imnlmfilt(I);%Non-local means filtering of image
    IG=rgb2gray(IN);

Im=adapthisteq(IG,'clipLimit',0.02,'Distribution','rayleigh'
);
%% Scenario 2
```

```matlab
%       IN=imnlmfilt(I);%Non-local means filtering of image
%       IG=rgb2gray(IN);
%
IH=adapthisteq(IG,'clipLimit',0.02,'Distribution','rayleigh'
);
%       T=adaptthresh(IH,0.6);%T = adaptthresh(I,sensitivity)
computes a locally adaptive threshold with sensitivity
factor specified by sensitivity. sensitivity is a scalar in
the range [0,1] that indicates sensitivity towards
thresholding more pixels as foreground.
%       Im=imbinarize(IH,T);

%% Scenario 3

%       IN=imnlmfilt(I);%Non-local means filtering of image
%       IG=rgb2gray(IN);
%
IH=adapthisteq(IG,'clipLimit',0.02,'Distribution','rayleigh'
);
%       Im=imnlmfilt(IH);%Non-local means filtering of image

%% Scenario 4

%       IG=rgb2gray(I);
%
IH=adapthisteq(IG,'clipLimit',0.02,'Distribution','rayleigh'
);
%       Im=imnlmfilt(IH);%Non-local means filtering of image

%% Scenario 5

% Im=rgb2gray(I);

% end
%% Find the class the test image belongs
Ftest=FeatureStatistical(Im);
%% Compare with the feature of training image in the
database
load db.mat
Ftrain=db(:,1:2);
Ctrain=db(:,3);
for (i=1:size(Ftrain,1));
    dist(i,:)=sum(abs(Ftrain(i,:)- Ftest));
end
m=find(dist==min(dist),1);
det_class=Ctrain(m);
msgbox(strcat('Detected Class=',num2str(det_class)));
end
```

Annex - G: Stenosis Quantification MATLAB Code.

```matlab
clear all;
%% Taking an Image
I = imread('442603L2.jpg');%Example
%% Centerline Extraction
T=adaptthresh(I,0.6);
BW=imbinarize(I,T);
se = strel('disk', 2)
BW2 = imclose(BW,se);
% figure, imshowpair(BW,BW2,'montage')
Ic=imcomplement(BW2);
out=bwskel(Ic,'MinBranchLength',200);
c=labeloverlay(I,out,'Transparency',0)
% figure, imshowpair(out, c, 'montage')
%% Draw crop rectangle
figure, imshow(I), title('Draw crop rectangle')
Re = drawrectangle('SelectedColor','yellow','LineWidth',
0.5);
Re.Position
Repoint1 = Re.Position;
rx1 = Repoint1(1);
rx2 = Repoint1(2);
ry1 = Repoint1(3);
ry2 = Repoint1(4);
%% Draw Stenosis Center
croped = imcrop(c,'Position',[rx1,rx2,ry1,ry2]);
%% Draw Stenosis Center line
figure, imshow(croped), title('Draw Stenosis Center line')
hs = drawline('SelectedColor','yellow','LineWidth',
0.5);%,'LineWidth', 2

point1 = hs.Position;
x1 = point1(1);
x2 = point1(2);
y1 = point1(3);
y2 = point1(4);
%% Finding the angle of inclination from two ends of a line.
%%%%%%%%%%%Slope and Rotate
slope = (y2 - y1) ./ (x2 - x1);
angle = atand(slope);
J = imrotate(croped,angle,'bilinear', 'crop');
imshow(J),title('Measure Horizontal, Dn, and Ds Distance')
%% Draw Horizontal line
hs2 = drawline('SelectedColor','yellow','LineWidth',
0.5);%,'LineWidth', 2
point2 = hs2.Position;
x1 = point2(1);
```

```matlab
x2 = point2(2);
y1 = point2(3);
y2 = point2(4);

hline = images.roi.Line(gca,'Position',[x1 y1; x2
y2],'LineWidth', 0.5);%x1 x2 y1 y2
% setLabelTextFormatter(hline,'%02.0f Cm');

%% Draw Dn
hs3 = drawline('SelectedColor','red','LineWidth',
0.5);%,'LineWidth', 2
point3 = hs3.Position;
Dnx1 = point3(1);
Dnx2 = point3(2);
Dny1 = point3(3);
Dny2 = point3(4);
% hline = imdistline(gca, [Dnx1 Dnx2], [Dny1 Dny2]);%x1 x2
y1 y2
hline = images.roi.Line(gca,'Position',[Dnx1 Dny1; Dnx1
Dny2],'LineWidth', 0.5);
% setLabelTextFormatter(hline,'%02.0f Cm');
%% Draw Ds
hs3 = drawline('SelectedColor','red','LineWidth',
0.5);%,'LineWidth', 2
point3 = hs3.Position;
Dsx1 = point3(1);
Dsx2 = point3(2);
Dsy1 = point3(3);
Dsy2 = point3(4);
% hline = imdistline(gca, [Dsx1 Dsx2], [Dsy1 Dsy2]);%x1 x2
y1 y2
hline = images.roi.Line(gca,'Position',[Dnx1 Dny1; Dnx1
Dny2],'LineWidth', 0.5,'LineWidth', 0.5);
% setLabelTextFormatter(hline,'%02.0f Cm');
%% Calculate Stenosis % = [1-(Ds/Dn)]*100
SL= x2-x1;
Ds=Dsy2-Dsy1;
Dn=Dny2-Dny1;
Stenosis = [1-(Ds/Dn)]*100;
message = sprintf('Stenosis length =%.1f pixels.\nDn = %.1f
pixels.\nDs = %.1f pixels.\nStenosis = %.1f %',...
  SL, Dn, Ds, Stenosis);
uiwait(helpdlg(message));
```